USGS
science for a changing world

Prepared in cooperation with Washington State Department of Ecology

Simulated Seasonal Loads of Total Nitrogen and Total Phosphorus by Major Source from Watersheds Draining to Washington Waters of the Salish Sea, 2005 through 2020

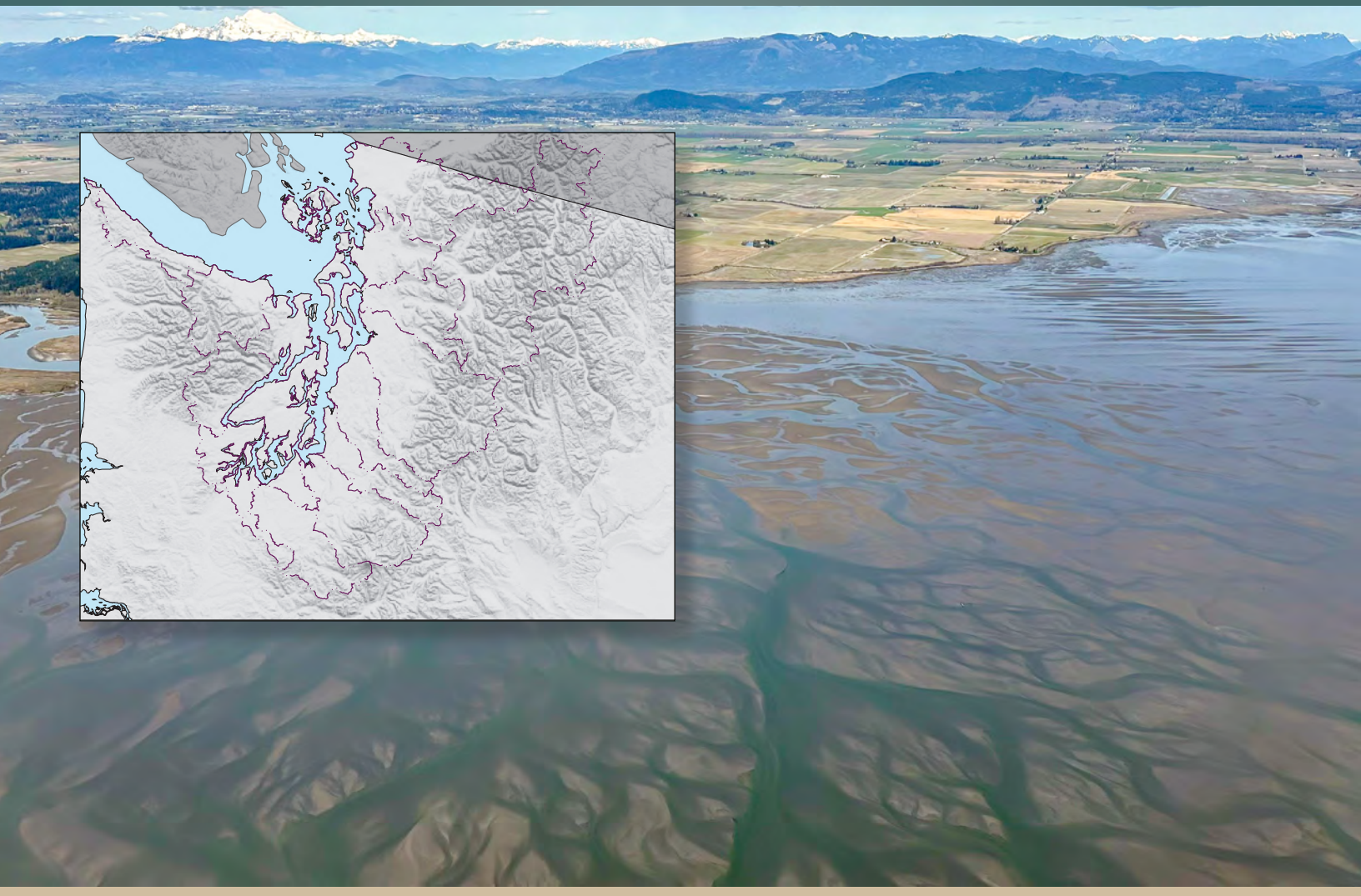

Scientific Investigations Report 2026–5001

Supersedes preprint https://doi.org/10.22541/essoar.173878059.92247480/v1

U.S. Department of the Interior
U.S. Geological Survey

Cover. Inset: Map showing SPAtially Referenced Regressions On Watershed attributes (SPARROW) Puget Sound model region, Washington. Background: Photograph showing braided tidal channels, Skagit Bay, Washington, Eyes Over Puget Sound Surface Conditions Report, April 4, 2025. Photograph from Washington State Department of Ecology (available online at https://gis.ecology.wa.gov/portal/apps/storymaps/collections/8f990a7682cc4bed94366c51de63b9b8.) Used with permission.

Simulated Seasonal Loads of Total Nitrogen and Total Phosphorus by Major Source from Watersheds Draining to Washington Waters of the Salish Sea, 2005 through 2020

By Noah M. Schmadel, Cristiana Figueroa-Kaminsky, Daniel R. Wise, Jamie K. Wasielewski, Zachary C. Johnson, and Robert W. Black

Prepared in cooperation with Washington State Department of Ecology

Scientific Investigations Report 2026–5001
Supersedes preprint https://doi.org/10.22541/essoar.173878059.92247480/v1

U.S. Department of the Interior
U.S. Geological Survey

U.S. Geological Survey, Reston, Virginia: 2026
Supersedes preprint https://doi.org/10.22541/essoar.173878059.92247480/v1

Suggested citation:
Schmadel, N.M., Figueroa-Kaminsky, C., Wise, D.R., Wasielewski, J.K., Johnson, Z.C., and Black, R.W., 2026, Simulated seasonal loads of total nitrogen and total phosphorus by major source from watersheds draining to Washington waters of the Salish Sea, 2005 through 2020: U.S. Geological Survey Scientific Investigations Report 2026–5001, 66 p., https://doi.org/10.3133/sir20265001. [Supersedes preprint https://doi.org/10.22541/essoar.173878059.92247480/v1.]

Associated data for this publication:
Schmadel, N.M., Figueroa-Kaminsky, C., Wise, D.R., Wasielewski, J.K., Gala, J., and Johnson, Z.C., 2025, Model application and calibration load data for seasonally dynamic total nitrogen and total phosphorus SPARROW models developed for watersheds draining to Washington waters of the Salish Sea, 2005 through 2020: U.S Geological Survey data release, https://doi.org/10.5066/P9LY1PQF.

ISSN 2328-0328 (online)

Acknowledgments

Special thanks to John Gala at Washington State Department of Ecology for help with retrieving and harmonizing water-quality data. And thanks to many other staff at Washington State Department of Ecology Environmental Assessment Program for providing expertise and for helping to make other datasets and products available.

Contents

Figures

Tables

Conversion Factors

International System of Units to U.S. customary units

Multiply	By	To obtain
	Length	
millimeter (mm)	0.03937	inch (in.)
meter (m)	3.281	foot (ft)
kilometer (km)	0.6214	mile (mi)
	Area	
square kilometer (km^2)	247.1	acre
square kilometer (km^2)	0.3861	square mile (mi^2)
square meter (m^2)	10.76	square foot (ft^2)
	Volume	
liter (L)	0.2642	gallon (gal)
cubic meter (m^3)	35.31	cubic foot (ft^3)
cubic meter (m^3)	264.2	gallon (gal)
	Flow rate	
meter per second (m/s)	3.281	foot per second (ft/s)
cubic meter per second (m^3/s)	35.31	cubic foot per second (ft^3/s)
cubic meter per day (m^3/d)	35.31	cubic foot per day (ft^3/d)
	Mass	
gram (g)	0.03527	ounce, avoirdupois (oz)
kilogram (kg)	2.205	pound avoirdupois (lb)
metric ton (t)	1.102	ton, short [2,000 lb]
metric ton (t)	0.9842	ton, long [2,240 lb]

U.S. customary units to International System of Units

Multiply	By	To obtain
	Length	
foot (ft)	0.3048	meter (m)
	Flow rate	
cubic foot per second (ft^3/s)	0.02832	cubic meter per second (m^3/s)

Temperature in degrees Celsius (°C) may be converted to degrees Fahrenheit (°F) as follows:

$°F = (1.8 \times °C) + 32$.

Datums

Vertical coordinate information is referenced to the North American Vertical Datum of 1988 (NAVD 88).

Horizontal coordinate information is referenced to the North American Datum of 1983 (NAD 83).

Elevation, as used in this report, refers to distance above the vertical datum.

Supplemental Information

Inputs and outputs of the seasonally dynamic nutrient models of the Puget Sound region watersheds are available at https://doi.org/10.5066/P9LY1PQF.

Simulated loads, yields, and source contributions are presented in this report and can be interactively accessed or downloaded via a mapper at https://apps.usgs.gov/sparrow/sparrow-puget-sound/.

Abbreviations

BMP	best management practice
DO	dissolved oxygen
Ecology	Washington State Department of Ecology
EIM	Environmental Information Management
ET	evapotranspiration
ML	machine learning
MS4	municipal separate stormwater sewer systems
MSE	mean square error
NADP	National Atmospheric Deposition Program
NLCD	National Land Cover Database
NOAA	National Oceanic and Atmospheric Administration
NPDES	National Pollutant Discharge Elimination System
NSE	Nash-Sutcliffe efficiency
NuGIS	Nutrient use Geographic Information System
NWIS	National Water Information System
PSNSRP	Puget Sound Nutrient Source Reduction Project
RBEROST	River Basin Export Reduction Optimization Support Tool
RMSE	root mean square error
SPARROW	SPAtially Referenced Regressions On Watershed attributes
SSM	Salish Sea Model
STORET	Storage and Retrieval Data Warehouse
TMDL	total maximum daily load
TN	total nitrogen
TP	total phosphorus
USGS	U.S. Geological Survey
VIF	variance inflation factor
WQP	Water Quality Portal
WQX	Water Quality Exchange
WRIA	Water Resource Inventory Area
WRTDS_K	Weighted Regressions on Time, Discharge, and Season model with Kalman filtering
WSDA	Washington State Department of Agriculture

Simulated Seasonal Loads of Total Nitrogen and Total Phosphorus by Major Source from Watersheds Draining to Washington Waters of the Salish Sea, 2005 through 2020

By Noah M. Schmadel,[1] Cristiana Figueroa-Kaminsky,[2] Daniel R. Wise,[1] Jamie K. Wasielewski,[2] Zachary C. Johnson,[1] and Robert W. Black[1]

Abstract

The U.S. Geological Survey and the Washington State Department of Ecology (Ecology) have developed watershed models of seasonal load estimates of total nitrogen (TN) and total phosphorus (TP) discharging into the Washington State waters of the Salish Sea from 2005 through 2020. The modeling approach used was dynamic SPARROW (SPAtially Referenced Regressions On Watershed attributes), a statistical-physical watershed modeling technique, initially applied at large spatial scales to represent long-term average stream loads throughout a stream network, refined here to estimate seasonal TN and TP loads across watersheds.

Upstream contributing sources included permitted treated wastewater facilities, crop fertilizer, animal feeding operations, septic systems, urban land and stormwater, atmospheric deposition (TN only), nitrogen fixation by *Alnus rubra* Bong. (red alder) trees (TN only), and background geologic material (TP only). Instream load magnitudes and their source compositions varied across watersheds, and even within each watershed, yet the largest loads typically occurred in the large rivers during winter and fall when streamflow was highest. Likewise, instream loads were typically lowest in summer during low streamflow, yet the relative instream aquatic decay was highest. The seasonal storage lag component of all nonpoint sources was estimated to contribute a quarter of the seasonal instream load during winter and fall high streamflow and sometimes half of the instream load during summer low streamflow.

Simulated seasonal loads carried by streams to a few hundred river mouth marine discharge points ranged by several orders-of-magnitude for TN and TP due to the spatial and seasonal differences in hydrologic flows, magnitude and timing of contributing sources, and instream decay. The Snohomish and Skagit Rivers discharged the largest TN and TP loads, yet the Samish River was shown to have some of the highest TN and TP yields and concentrations. Additionally, a reference scenario estimate developed of the pre-industrial local and regional TN loads suggests that red alder tree density has increased in lower riparian areas and that treated wastewater is the dominant source in some watersheds that has led to increases in TN loading to marine waters.

Introduction

Nutrient reduction efforts are underway for the watersheds draining to Washington State waters of the Salish Sea, referred to herein as the Puget Sound region (fig. 1; Figueroa-Kaminsky and others, 2022). The Washington State Department of Ecology's (Ecology) Puget Sound Nutrient Source Reduction Project (PSNSRP) is a collaborative effort with communities and stakeholders to address human sources of nutrients with a restoration plan implemented through Ecology's National Pollutant Discharge Elimination System (NPDES) and 319 nonpoint source programs (Figueroa-Kaminsky and others, 2022). The Salish Sea Model (SSM), a numerical marine model used by the PSNSRP, has indicated that compliance with dissolved oxygen (DO) standards in the bottom layers of marine waters depends on reductions in nutrient loads from wastewater treatment facilities and other nonpoint sources of nutrient pollution in watersheds (Ahmed and others, 2019). This report provides information on nutrient contributions from upstream watershed point and nonpoint sources and pathways to support current and planned efforts to reduce nutrient discharge in the Puget Sound region.

Refinement of the SPARROW (SPAtially Referenced Regressions On Watershed attributes) model to a seasonal temporal scale was chosen to simulate nutrient loads due to its successful application at (1) an annual scale in the Pacific Northwest region by Wise and Johnson (2013) and Wise (2019), and (2) a seasonal temporal scale applied in the northeastern and midwestern regions of the United States (Schmadel and others, 2021, 2024). SPARROW is a statistical-physical watershed modeling technique developed by the U.S. Geological Survey (USGS) for estimating constituent point and nonpoint source contributions and fate

[1]U.S. Geological Survey.

[2]Washington State Department of Ecology.

and transport in surface waters (Schwarz and others, 2006). SPARROW has often been applied at annual timescales for large-scale representation of nutrient sources across entire stream networks (for example, Wise, 2019), but because marine DO can respond more rapidly to dynamic nutrient loads, the approach was refined to clarify seasonal upstream contributions from discernible point and nonpoint sources delivered from watersheds to coasts and estuaries.

This report documents seasonally dynamic SPARROW total nitrogen (TN) and total phosphorus (TP) load models spanning 2005 through 2020 that track major sources and pathways draining watersheds of the Puget Sound region (hereafter, the TN and TP models). The TN and TP models can help to inform a regional assessment of watershed nutrient source contributions and pathways, implementation of nitrogen reduction actions initiated in the PSNSRP, and ongoing implementation in watersheds with established freshwater DO total maximum daily loads (TMDLs). Objectives for this study were to:

- Develop comprehensive nutrient source datasets for model inputs.
- Identify and consolidate water-quality (TN and TP concentration) and quantity (streamflow) datasets for use as dynamic SPARROW model calibration data.
- Expand the SPARROW modeling technique to seasonal timesteps and apply it to the Puget Sound region using local data.
- Estimate TN and TP loads on seasonal timesteps throughout the stream network as represented in the 1:100,000 National Hydrography Dataset.
- Identify and quantify the relative contribution of major TN and TP sources and pathways across the Puget Sound region including loads at the mouths of rivers and streams.

Study Area Description

For this report, the Puget Sound region refers to watersheds draining into the Washington State waters of the Salish Sea (fig. 1). Ecology has grouped all contributing watersheds by Water Resource Inventory Areas (WRIAs) based on information regarding water availability, regulations, and water use (Washington State Department of Ecology, 2019a).

The Puget Sound region includes 19 WRIAs with various land cover patterns that affect the delivery of nutrients to streams. The major land cover types in the Puget Sound region are forested (62 percent), grassland/scrubland (12 percent), and urban land (12 percent) based on the 2019 National Land Cover Database (NLCD; Dewitz and U.S. Geological Survey [2021]; refer to fig. 1.1). Urban land, including major cities and urban areas (for example, the Cities of Seattle and Tacoma), is concentrated along coastal shoreline areas and estuaries, whereas the headwaters are mostly forested. Areas of agricultural land can be found in the northern watersheds, such as the lower Nooksack and Skagit Rivers, and in a few areas in southern watersheds, such as the lower Nisqually and Deschutes Rivers.

Rivers are relatively short and steep from the Cascade Range crest to the coastal lowlands. Streamflow patterns are influenced by several factors, including reservoir storage, wet winters, dry summers, and seasonal snowmelt at higher elevations (refer to Figueroa-Kaminsky and others [2022] for more details).

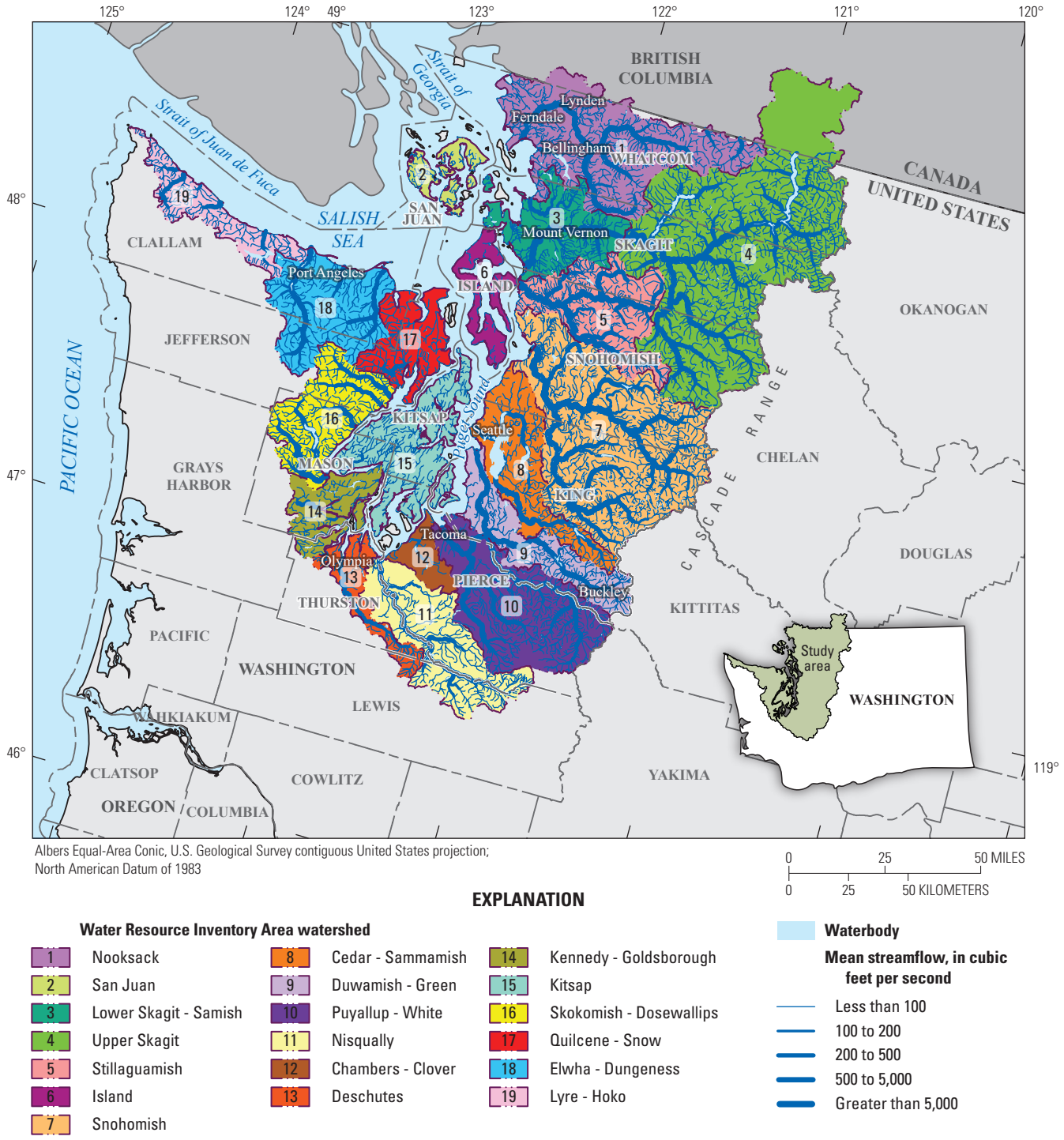

Figure 1. The Puget Sound region and its rivers and waterbodies, that is comprised of 19 Washington State Water Resource Inventory Areas that drain into waters of the Salish Sea.

Methods

The TN and TP models were developed as a collection of stream reaches and their catchments from the National Hydrography Dataset (E2NHDPlusV2; Schwarz, 2019). The models functioned by accumulating incremental seasonal load, which is subject to storage, diversions, and aquatic decay processes downstream from headwaters to shorelines (fig. 2*A-B*). The models produced estimates of seasonal load delivered from each incremental catchment that drained to each reach, accumulated totals at every reach location, and a yield when incremental load is divided by the watershed contributing area. Explanatory variables, together with statistically estimated model coefficients, were required for each reach and incremental catchment to quantify major source pathways and were interpreted to have a physical meaning or as a proxy for a key process. Explanatory variables included a mix of constant and seasonally changing data that were selected to represent (1) the major source inputs, (2) their land-to-water delivery processes, and (3) aquatic decay processes across the stream network (fig. 2*B*).

An initial pool of possible explanatory variables was based on previous models such as findings by Wise (2019) on nitrogen fixation by *Alnus rubra* Bong. (red alder) trees, and on empirical studies (Figueroa-Kaminsky and others, 2022). The TN and TP models were calibrated by minimizing error between the predicted and monitored loads with estimated model coefficients and synchronous explanatory variables. Various configurations of different variables and interactions between the source input and land-to-water variables were specified and tested, yet many failed to return statistically significant model coefficients due to collinearity between certain variables or other factors. Often, re-specifying variables and their interactions may identify statistically significant coefficients and additional source pathways. The final selected list of variables produced models with the lowest overall error, but many test models were required to determine which combination of variables resulted in the lowest error while also representing the major source pathways.

Source input variables used to explain and track the major nonpoint nutrient source pathways across the Puget Sound region were crop fertilizer in kilograms (kg), animal feeding operations (number of animals), on-site treated wastewater (number of households on septic systems), urban land in square kilometers (km^2), atmospheric deposition (TN only, in kg), nitrogen fixation by red alder trees (TN only, in square meters [m^2]), upland geologic material (TP only, in metric tons), and the storage lag of those nonpoint sources, in kg. Those source variables were mediated in their delivery to streams by land-to-water variables of precipitation and evapotranspiration (ET), along with soil properties and density of stormwater outfalls (TN only).

The modeled domain, the Puget Sound region, contained a stream network of 12,314 reaches. The modeled period-of-record was from January 2005 through December 2020 in seasonal timesteps, or 64 periods, with the following seasonal definitions: winter includes January, February, and March; spring includes April, May, and June; summer includes July, August, and September; and fall includes October, November, and December. The goal of seasonal definitions was to represent distinctly different hydrologic and water-quality conditions—in the models, fall started in October and winter ended in March to separate these generally wetter and colder seasons from spring and summer, which are drier and warmer.

Dynamic SPAtially Referenced Regressions On Watershed Attributes Model

The analytical mass-balance framework for the TN and TP models was guided by the approaches and findings in Schmadel and others (2021, 2024) to produce seasonal nutrient load estimates for every E2NHDPlusV2 stream reach across the Puget Sound region. Seasonally varying nutrient loads transported through a reactive river reach were estimated as the summation of load entering from the upstream end of the reach and load generated within the reach's catchment (after Schmadel and others, 2024):

$$L_{out,t,i} = [L_{in,t,i} + L_{I,t,i} + L_{S,t,i}] D_{j,t,i} \quad (1)$$

where

$L_{out,\,t,\,i}$ is the accumulated instream load at the outlet of catchment i (each catchment i has a reach i) at each season t, in units of kilograms per season;

$L_{in,\,t,\,i}$ is the load entering reach i from upstream reaches at each season t, in units of kilograms per season;

$L_{I,\,t,\,i}$ is the load delivered from catchment i to reach i from contemporaneous inputs, I, at each season t, in units of kilograms per season;

$L_{S,\,t,\,i}$ represents the load released from storage repositories, S, in catchment i at each season t due to the retention of previous inputs that have been lagged in their delivery until the current season t, in units of kilograms per season;

$D_{j,\,t,\,i}$ is the aquatic decay function for each reach i at each season t; and

$j = 1$ indicates a stream reach while $j = 2$ indicates a separate function for lakes and reservoirs.

A. **Collection of reach catchments and monitoring stations, from McMahon and others (2003)**

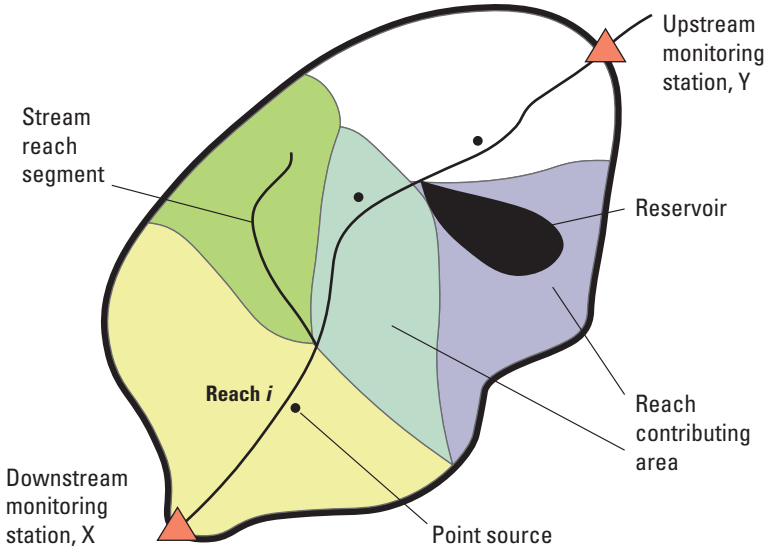

B. **Major nutrient source pathways, modified from Preston and others (2009)**

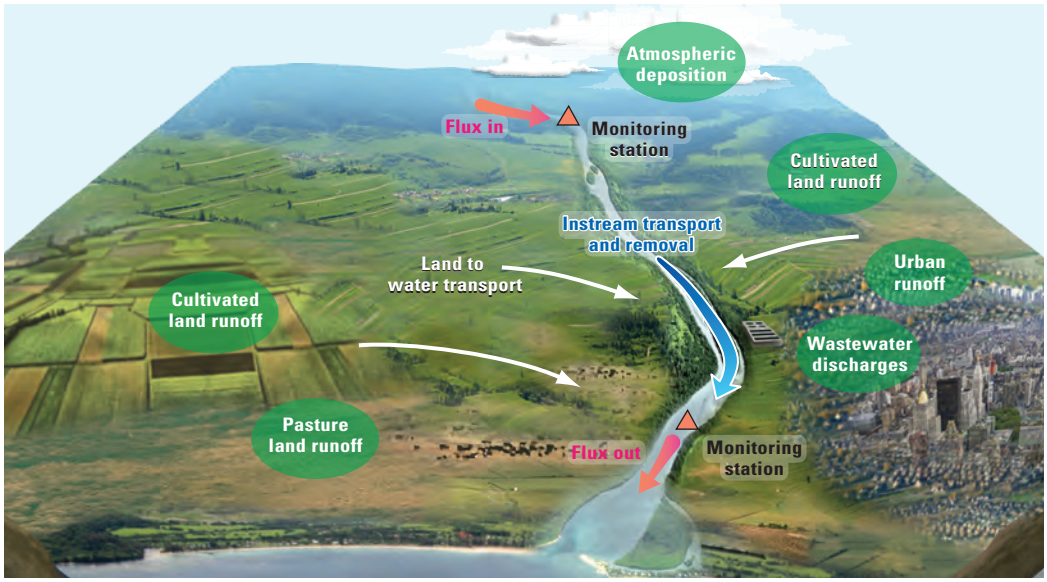

Adapted from The State of the Nation's Ecosystems 2008: Focus on Nitrogen
The H. John Heinz III Center for Science, Economics and the Environment
Graphic by Grabhorn Studios

Figure 2. Conceptual illustration of SPARROW (SPAtially Referenced Regressions On Watershed attributes) model structured (*A*) as a collection of catchments feeding stream and reservoir reaches linked to point-source and monitoring station locations (from McMahon and others [2003]) to quantify (*B*) major nutrient source pathways (modified from Preston and others [2009]). Refer to fig. 1 in Schmadel and others [2024] for dynamic conceptualization.

A net decay of nutrients was estimated each period based on seasonal streamflow. For lakes and reservoirs, hereafter, waterbodies ($j = 2$), the aquatic decay function was:

$$D_{j=2,t,i} = \exp\left(-v_{f,j=2}\frac{A_i}{Q_{t,i}}\right) \quad (2)$$

where

$v_{f,j=2}$ is the uptake velocity model coefficient for waterbody reaches and subscript f denotes a net whole-waterbody mean, in units of meters per day;

A_i is the waterbody wetted surface area with its outlet assigned to reach i, in units of square meters;

$Q_{t,i}$ is the streamflow in reach i at each season t, in units of cubic meters per day; and

$\frac{A}{Q}$ is the reciprocal hydraulic load, a measure of time required to displace a unit volume of water, in units of day per meter;

For a stream reach ($j = 1$), the aquatic decay function was updated to:

$$D_{j=1,t,i} = \exp\left(-v_{f,j=1}\frac{\tau_{t,i}}{d_{t,i}}\right) \quad (3)$$

where

$v_{f,j=1}$ is the uptake velocity model coefficient for stream reaches and subscript f denotes a net whole-stream mean, in units of meters per day;

$\tau_{t,i}$ is time of travel estimate of reach i at each season t, which is halved for catchment inputs assumed to enter at the reach midpoint, in units of day;

$d_{t,i}$ is the seasonal water depth of reach i at each season t, in units of meters; and

$\frac{\tau}{d}$ is the reciprocal hydraulic load, in units of day per meter.

The net unit-area rate of biogeochemical reactions that remove and replenish TN or TP is represented by v_f, in units of meters per day [m/d] and assumes that the load in each reach decreases over time as a constant percentage (first-order decay conditions) in a waterbody (eq. 2) or stream channel (eq. 3; Alexander and others, 2000).

For streams draining watersheds in the Puget Sound region, other factors such as stream temperature, in addition to travel times, may affect decay (Sheibley and others, 2015). Therefore, the hypothesis that the mean uptake velocity (v_0; meters per day [m/d]) varied seasonally and spatially due to water temperature was tested by estimating v_f as (after Schmadel and others [2020, 2021]):

$$v_{f,j=1,t,i} = v_0 + \beta_T\left[\ln(T_{t,i}) - \overline{\ln(T)}\right] \quad (4)$$

where

$v_{f,j=1,t,i}$ is the uptake velocity coefficient for each stream reach i at each season t and subscript f denotes a net whole-stream mean, in units of meters per day;

v_0 is a constant model coefficient that represents the mean or intercept uptake velocity of streams, in units of meters per day;

β_T is a constant model coefficient that represents the effect of temperature, T, on v_0, in units of meters per day; and

$T_{t,i}$ is the mean water temperature in reach i at season t, in units of degrees Celsius.

Mean seasonal water temperature, T, was mean-centered to provide a meaningful estimate of v_0 and log-transformed to add model calibration stability and reduce the dependence on the shape of the distribution. A positive value of β_T, for example, implies an increase in uptake velocity caused by a temperature above the mean temperature.

Load delivered from an incremental catchment to the edge of a stream or waterbody reach was estimated, assuming all mass (except mass from point sources) passed through and completely mix in a storage repository with some fraction retained each season, as (after Schmadel and others, 2024):

$$L_{I,t,i} = \sum_{n=1}^{N}\alpha_n I_{n,t,i} f_{I,n,t,i} \quad (5)$$

$$L_{S,t,i} = \alpha_S L_{t-1,i} f_{S,t,i} \quad (6)$$

where

α_n are positive model coefficients that represent the mean fraction or yield of source input n that is delivered to reach i, in units of fraction or kilograms per square kilometer if a yield;

α_S is a positive model coefficient and represents the mean fraction of inputs that were lagged or retained in the storage repository S in the previous period and therefore not yet released as load to streams until the current or later periods, in units of fraction;

$I_{n,t,i}$ is the input for each n of N sources such as datasets of land-applied fertilizer applied to catchment i in the current season t, in units of kilograms, or square kilometers if areal, per season;

$L_{t-1,i}$ is the combined load delivered to reach i in the previous season t–1 ($L_{I,t-1,i} + L_{S,t-1,i}$) in units of kilograms per season; and

f_I and f_S are the dimensionless land-to-water delivery functions (refer to eqs. 7 and 8).

The α_S coefficient represents the mean strength of storage retention where a value approaching zero implies no storage effects whereas a value approaching one would imply that all inputs are retained and accumulate in storage with little delivery to streams. The amount of mass retained simultaneously depends on the amount released; a higher release fraction leads to an immediate lowering of the storage retention fraction. As mass passes through the storage repository and is delivered to the stream, $\ln(\alpha_S)$ is negative and provides an estimate of the mean storage retention rate each season (and its inverse is a retention timescale) of mass. An estimate of the previous period instream load is required to initiate storage lag in equation 6; the initial condition solution from Schmadel and others (2024) was used to estimate $L_{t=0}$.

The land-to-water delivery functions further mediate seasonal and spatially explicit effects on the delivery of source inputs to streams (after Schmadel and others, 2024):

$$f_{I,t,n,i} = \exp\left(\sum_m \theta_m X_{m,t,i}\right) \quad (7)$$

$$f_{S,t,i} = \exp\left[\sum_m \gamma_m X_{m,t-1,i} + \sum_d \beta_d \left(\frac{X_{d,t,i}}{X_{d,t-1,i}}\right)\right] \quad (8)$$

where

θ_m are model coefficients that mediate m processes on the delivery of source input n to reach i and retain units inverse of each corresponding explanatory variable;

γ_m are model coefficients that mediate the influence of previous period land-to-water delivery variables and retain the units inverse of each explanatory variable;

X_m are explanatory variables such as precipitation centered on their mean value that interactive with source inputs and retain units of each explanatory variable;

β_d are model coefficients that mediate the effects of d changing seasonal processes affecting storage lag and retain units inverse of each corresponding explanatory variable; and

X_d are the explanatory variables expressed as a ratio, or a difference if log-transformed, to quantify the effects of season-to-season change on retention rates and retain units of each explanatory variable.

Data Compilation and Treatment

Stream Network with Diversions

The stream network used in the TN and TP models was defined by the National Hydrography Dataset (E2NHDPlusV2; Schwarz, 2019). The stream network in the model includes 12,314 reaches and 2 more pseudo reaches were added to represent transfer return flows (next paragraph). Using the E2NHDPlusV2 stream network provided a consistent framework for spatial referencing and source pathway tracking from headwaters to shorelines. Navigation through the stream network was based on E2NHDPlusV2 attributes including hydrologic sequencing and to- and from-nodes. All explanatory data were linked to the corresponding NHDPlusV2 catchment polygons provided by the 1:100,000 National Hydrography Dataset (U.S. Environmental Protection Agency, 2019). Waterbodies were defined as lakes and reservoirs from NHDPlusV2 (fig. 1). Ice, estuaries, wetlands, and polygons on large rivers or canals were omitted from the representation of waterbodies in the TN and TP models.

Water diversions through the stream network were represented using the diversion fraction variable (DivFrac) from E2NHDPlusV2 with additional diversion estimates from Wise and others (2021). Throughout the Puget Sound region, 13 withdrawals for agricultural irrigation and municipal water uses along with 2 transfers (Centralia Power Canal Near Mckenna, Washington from the Nisqually River and Lake Tapps Diversion at Dieringer, Washington from the White River) and their returns to downstream reaches were included from Wise and others (2021) (refer to fig. 1.2). Diversions were expressed as a constant fraction (the fraction of seasonal streamflow remaining in the stream after diversion), except for a seasonally dynamic fraction estimated for the Lake Tapps Diversion using the upstream USGS gaging station 12099200 White River above Boise Creek at Buckley, Washington, and the diverted measurement at 12098920 White River Flume at Buckley, Washington for the return flow estimate (U.S. Geological Survey, 2022), calculated as 1 minus DivFrac.

Calibration Load Data

The mass balance solution (eq. 1) was calibrated to observed instream loads to estimate model coefficients and simulate load at every stream and waterbody reach. Seasonal observed instream TN loads were estimated at 49 calibration stations and TP loads were estimated at 47 calibration stations (table 1, fig. 3). More than 50 stations were considered for both models, but some were excluded for various reasons (they degraded model performance at other sites because of factors that were not well-represented by explanatory variables or not commonly observed at other sites). For example, nutrient concentration at one station was affected by a nearby hatchery operation (station KMC-0321; refer to Schmadel and others [2025] for concentrations). More than 80 percent of the stream network representing the Puget Sound region was upstream of a calibration station, and 14 of the 19 WRIAs contained at least one station (fig. 3). Load simulations made downstream of the calibration network were an accumulation of mass from upstream and were, therefore, a reflection of upstream conditions. However, any simulated load that entered from catchments downstream of a calibration station did not affect the calibration results and therefore could not be directly compared to an observed load.

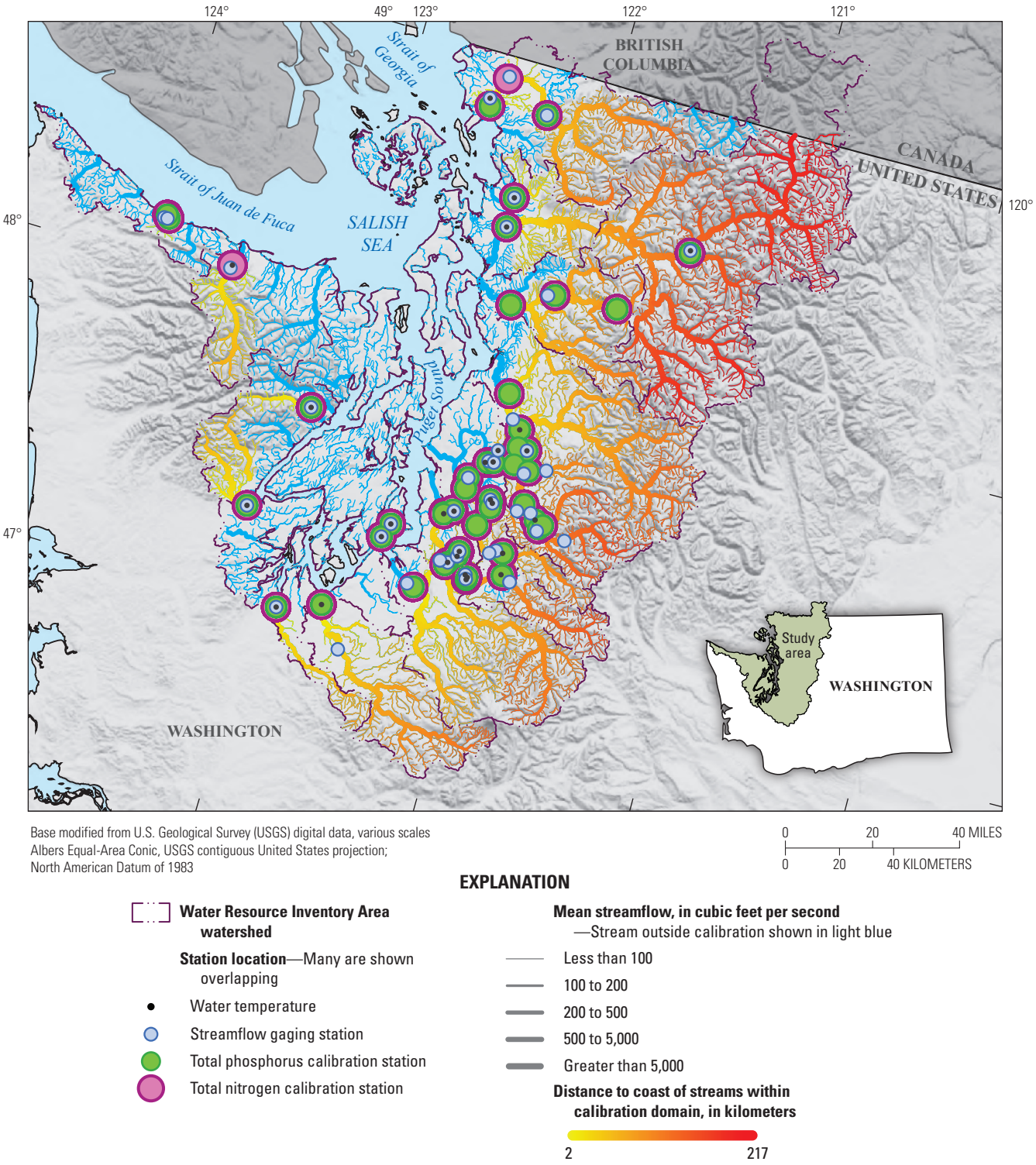

Figure 3. Calibration stations, locations of streamflow gaging stations that were paired with calibration stations, locations of water temperature measurement, streams downstream or outside of the calibration domain, and streams within the calibration domain colored by their distance to their coastal outlet, for the Puget Sound region.

Table 1. Sources of observed water-quality, streamflow, and water-temperature data used to estimate seasonal total nitrogen load, total phosphorus load, streamflow, and water temperature in the Puget Sound region.

Source	Number of total nitrogen stations	Number of total phosphorus stations	Number of streamflow gaging stations	Number of stream-temperature measurement locations
U.S. Geological Survey National Water Information System (NWIS)	0	0	68	4
Washington State Department of Ecology Environmental Information Management (EIM)	24	22	18	2
King County, Washington	18	18	9	5
Pierce County, Washington	3	3	1	0
Thurston County, Washington	3	3	1	0
City of Bellingham, Washington	1	1	3	0
U.S. Department of Agriculture NorWEST	0	0	0	18
Totals	**49**	**47**	**100**	**29**

Estimation of TN and TP seasonal loads used for model calibration required three parts: (1) observed discrete TN and TP instream concentrations, (2) continuous daily streamflow, and (3) a load estimation model. Input data and estimated seasonal loads can be found in Schmadel and others (2025), and the approach is summarized here. Discrete water-quality data (observed TN and TP concentrations) and daily streamflow were retrieved, compiled, and harmonized from several databases including: Ecology's Environmental Information Management (EIM) database (Washington State Department of Ecology, 2019b); USGS's National Water Information System (NWIS; U.S. Geological Survey, 2022); and several individual local entities (City of Bellingham, Washington and King, Pierce, and Thurston Counties in Washington) (King County, 2024; table 1). Often duplicative of the EIM database, other databases checked for any additional water-quality data included the WQP (Water Quality Portal, 2022) and the U.S. Environmental Protection Agency Water Quality Exchange (WQX) (previously known as the Storage and Retrieval Data Warehouse (STORET)) and is where Tribal nations' water-quality data are made available. Discrete concentration data were filtered or combined, if possible, into total forms of nitrogen and phosphorus based on USGS parameter codes (p-codes), or close matches, 00600 for TN and 00665 for TP (refer to Schmadel and others [2025]).

Discrete water-quality observations were paired with the closest continuous streamflow gage (fig. 3). Many discrete samples were collected at a gage location, but many more were collected near a gage. Locations of discrete observation were set as the calibration station location, and streamflow that did not match perfectly in location was scaled by the ratio of drainage areas. Some gages were considered too far away to pair with discrete samples; the differences in drainage areas between the discrete and gage locations were constrained to plus or minus 25 percent (Konrad and Voss, 2012). Many water-quality data collected across the Puget Sound region were not used because there were too few samples or no clear pairing with streamflow. However, all available discrete data and streamflow were considered to develop as many calibration stations as possible. For example, several of the water-quality data station names were different yet similar (such as names KCM-0438 and 0438) for data collected at the same location; therefore, any water-quality data collected at the same location were grouped and renamed to the most frequently used name and any duplicates were removed (Schmadel and others, 2025).

Further manual inspection led to the combination of discrete data at a few more stations with different names, each within about 100 meter (m) reach distance: data from KCM-0438 were combined with 08C070 and data from KCM-0311 were combined with 09A080 (fig. 3; refer to Schmadel and others [2025] for a list of station names that were combined). To extend the number of calibration sites further, sites with simulated daily streamflow from the National Water Model (National Oceanic and Atmospheric Administration, 2022a) were considered as additional gaging stations but only at locations not affected by diversions or reservoirs and with less than 50 percent standard error (5 TN and 5 TP stations added). Compared to previous annual SPARROW applications that were able to develop 22 TN and TP stations for the Puget Sound region (Wise, 2019), consideration of additional discrete and streamflow data allowed for a near doubling of calibration stations.

The discrete TN and TP concentration data paired with daily streamflow were fed into two different flux estimation model approaches to produce seasonally continuous estimates of TN and TP load: the USGS Fluxmaster regression approach (Schwarz and others, 2006) and the Weighted Regressions on Time, Discharge, and Season model with Kalman filtering (WRTDS_K; Hirsch and others, 2010; Hirsch and others, 2015; Lee and others, 2019). Both Fluxmaster and WRTDS_K build regressions of water-quality data on discharge and season. However, Fluxmaster estimation is less sensitive to gaps or fewer samples (Lee and others, 2016). The following criteria were considered for use of WRTDS_K: (1) at least 100 discrete water-quality samples, and (2) gaps less than 2 years between consecutive samples. Fluxmaster produced similar seasonal TN and TP loads compared to WRTDS_K for most cases. However, Fluxmaster estimation extended the number of stations by considering looser criteria: (1) at least 24 samples (but all stations selected had many more), and (2) samples covered the beginning and end of the 16-year period-of-record. Censored concentration data were set to the minimum detection limit for load estimation. Some stations contained a large portion of censored values (for example, TP station 04A100 on the upper Skagit River; refer to Schmadel and others [2025]). Load was re-estimated using Fluxmaster by allowing the censored value to randomly vary between zero and the minimum detection limit, but that re-estimation did not cause a noticeable improvement to the seasonal load estimate.

The overall percentage standard error in WRTDS_K was estimated for each station; stations with more than 100 samples and with over 50 percent standard error were replaced with Fluxmaster values. A seasonal load was further considered inaccurate and excluded if the corresponding standard error of the Fluxmaster estimate was greater than 50 percent of the seasonal load estimate. Based on error estimates from both flux model approaches, loads generated by Fluxmaster were selected for the TP model and a mix of WRTDS_K (n=23) and Fluxmaster (n=26) stations were selected for the TN model. A mixed approach seemed to provide a more accurate TN model, but nearly the same results were produced using only Fluxmaster loads. Calibration datasets for TN and TP stations were mostly complete with 64 seasonal load estimates each. Some stations had missing streamflow yet gaps were small and load estimates still covered most of the period (greater than [>] 80 percent); those load estimates within error constraints were used in calibration. If loads estimated at a station covered less than 10 years (about two-thirds coverage), that station was generally not considered in calibration to prevent any trend bias.

Streamflow and Water Temperature

Seasonal streamflow and water temperature were estimated for all stream reaches to constrain seasonal aquatic losses of TN and TP (no temperature effect) through the stream network (eqs. 2–4). Seasonal streamflow tended to be highest in winter and fall, and lowest in spring and summer (fig. 4). With seasonal streamflow estimated, seasonal stream depth was estimated via power-law scaling (Leopold and Maddock, 1953). Seasonal travel time through each reach was estimated by the length and seasonal velocity (Jobson, 1996) that was estimated using seasonal streamflow with attributes of drainage area and streambed slope from E2NHDPlusV2.

Streamflow Water Balance

Observed streamflow was available from 2005 through 2020 with extensive coverage at 99 locations throughout the Puget Sound region (app. 1, fig. 1.2; Schmadel and others, 2025). Estimates of seasonal streamflow were extended from gages to all stream reaches empirically. A starting base seasonal water balance was adjusted upstream and downstream using the SPARROW framework (tables 1.1 and 1.2). The starting base seasonal water balance—using variables of seasonal precipitation, ET, and previous season ET losses—indicated that a regional mean of 46 percent (0.460 precipitation coefficient; table 1.1) of net precipitation was delivered to streams each season while 40 percent (0.404 storage lag coefficient; table 1.1) was lagged in delivery longer than a season, with a mean net loss or use of 14 percent of water. This base water-balance model still accounted for diversions and seasonal changes in water inputs but may not represent some processes across all space with only three variables. Runoff may be affected by, for example, snow water storage, wildfire effects, reservoir operations, additional water uses, and irrigation return flows (Konrad, 2019), and representing those processes was not performed. Therefore, to arrive at representative seasonal streamflow for the entire model domain, and for the purpose of representing aquatic decay of nutrients, the base water balance was empirically corrected to observed streamflow at gaging stations instead of further trying to quantify additional processes. Moving downstream from a headwater, streamflow was adjusted downstream from the first gage, and that simulated streamflow was accumulated downstream, adjusting at each sequential gage, thus improving the representativeness of all streamflow downstream. Streamflow in reaches upstream of gages was adjusted by the ratio of observed to predicted streamflow calculated at the closest gage (red colored reaches in fig. 1.2; Schmadel and others, 2025).

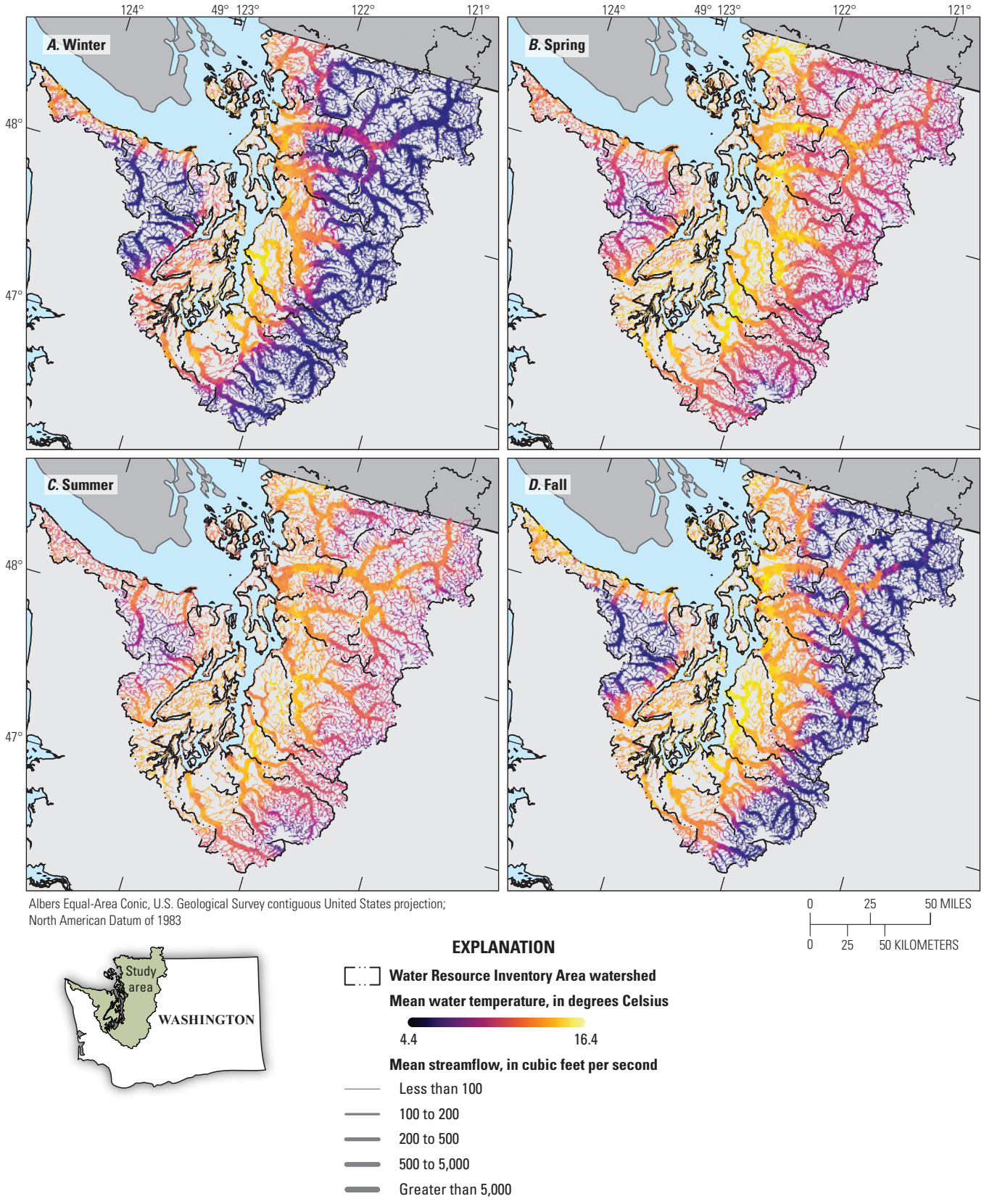

Figure 4. Estimated mean seasonal streamflow and water temperature from 2005 through 2020, Puget Sound region, in (*A*) Winter, January–March; (*B*) Spring, April–June; (*C*) Summer, July–September; and (*D*) Fall, October–December.

Water-Temperature Estimation

Warmer water temperatures tended to occur more in mountain valleys and lower elevations of the Puget Sound region, especially in summer followed by spring (fig. 4). Like streamflow estimation, an empirical approach was taken for water-temperature estimation. A simple 3-variable random forest model trained to observed water temperature at 29 locations provided estimates of seasonal water temperature at every reach (fig. 5). Instead of only using air temperature as a proxy for water temperature (Yearsley, 2009), two random forest models were built for air temperatures above and below 5 °C, or close to the point of maximum water density before freezing where the air-water relationship breaks down, and each model was correlated to air temperature, elevation, and season. The model was trained on 80 percent of the temperature data while the remaining 20 percent was used for testing. The root mean square error (RMSE) of the model for air temperature above 5 °C was 1.01 °C for training and 1.04 °C for testing (training 0.69 and testing 0.61 °C RMSE for less than 5 °C). Observed water temperature was retrieved by Ecology from several databases including NWIS, EIM, and the U.S. Department of Agriculture's NorWEST (U.S. Department of Agriculture, 2024; table 1). These databases included a mix of discrete and continuous measurements. Therefore, observed data had to be filtered and screened for use as training data in the random forest models: at least one season-year pairing containing at least 50 daily mean temperature observations was required for a given seasonal water-temperature estimate, leaving a total of 29 locations of continuous seasonal temperature observations.

Source Input Variables

Variables used to explain and track major nonpoint nutrient sources across the Puget Sound region were crop fertilizer, animal feeding operations, on-site treated wastewater (in other words, household septic systems), urban land, atmospheric deposition (TN only), nitrogen fixation by red alder trees (TN only), and upland geologic material (TP only). The storage lag source was represented as a function of those nonpoint sources applied in previous seasons. TN and TP load from permitted treated wastewater facilities and inflow from Canada were represented as point sources and were therefore assumed to bypass storage and discharge directly to streams. However, inflow from Canada was small relative to other point sources, contributing less than 3 percent of drainage area to the Puget Sound region, and had negligible effects on model calibration, but was included in the models for completeness.

Monthly point-source load data were computed for the Puget Sound region from 2005 through 2020 by Wasielewski and others (2024), and loads were aggregated seasonally for use in the TN and TP models. Across the Puget Sound region, 163 permitted discharging facilities were tracked (97 municipal wastewater treatment facilities, 20 industrial treatment facilities, and 46 fish hatcheries; fig. 1.2). Many permitted outfall locations discharged directly to marine waters and not into streams—marine waters were defined as downstream of the E2NHDPlusV2 terminal stream reaches. Of the 163 permitted point-source outfall locations, the largest discharges were directly into marine waters but were assigned to the nearest E2NHDPlusV2 stream reach for mass balance accounting, and only 60 facilities (37 percent by total number of facilities) were located upstream of TN and TP calibration stations.

The number of households with on-site treated wastewater (septic) systems within the Puget Sound region were tabulated and compiled by Wise and others (2025; fig. 6*A*). Septic systems are often located near areas of urban land and, therefore, can be difficult to identify as an independent source separate from urban land, which is why septic sources are often not identified separately in SPARROW model applications (Wise, 2019).

Ecology also tabulated the number of animals in animal feeding operations for dairy production (Figueroa-Kaminsky and others, 2022). The potential source pathway from animal feeding operations was represented in the models as the estimated number of animals counted per E2NHDPlusV2 catchment (fig. 6*B*).

Seasonal nitrogen and phosphorus fertilizer and manure application to cropland in the Puget Sound region was computed from 2005 through 2020 (available in Schmadel and others [2025]), which used fertilizer data from the Nutrient Use Geographic Information System (NuGIS; Wise and others, 2025) together with agricultural-use polygons produced by the Washington State Department of Agriculture (WSDA; Figueroa-Kaminsky and others, 2022). The NuGIS data were annual county-level estimates of nutrients from fertilizer application and livestock manure, including commercial fertilizers sold by county each year. The NuGIS data were then processed to the seasonal timestep based on Ecology's survey of WSDA crop types grown from 2005 through 2020, and the typical fertilizer amounts needed for each type (refer to Figueroa-Kaminsky and others [2022] and Wise and others [2025] for more details). The computed seasonal application amounts represented combined nutrients from fertilizer and manure but are referred to here as the cropland fertilizer source of nutrients. Fertilizer application to cropland varied seasonally with the highest application rates in spring followed by summer with the least amount applied in fall (figs. 1.3 and 1.4).

Red alder trees grow adjacent to river corridors and waterbodies in many parts of the Puget Sound region and were assumed to provide a large source of TN as they fix nitrogen from the atmosphere and leach it into soils (Compton and others, 2003; Wise, 2019). Basal area of red alder trees was used as a source variable in the TN model, which was estimated within watersheds of the Puget Sound region for 2005 through 2017, updated annually (Wise and others, 2025). Basal area of red alder trees for 2018 through 2020 was estimated by linear interpolation of the available data.

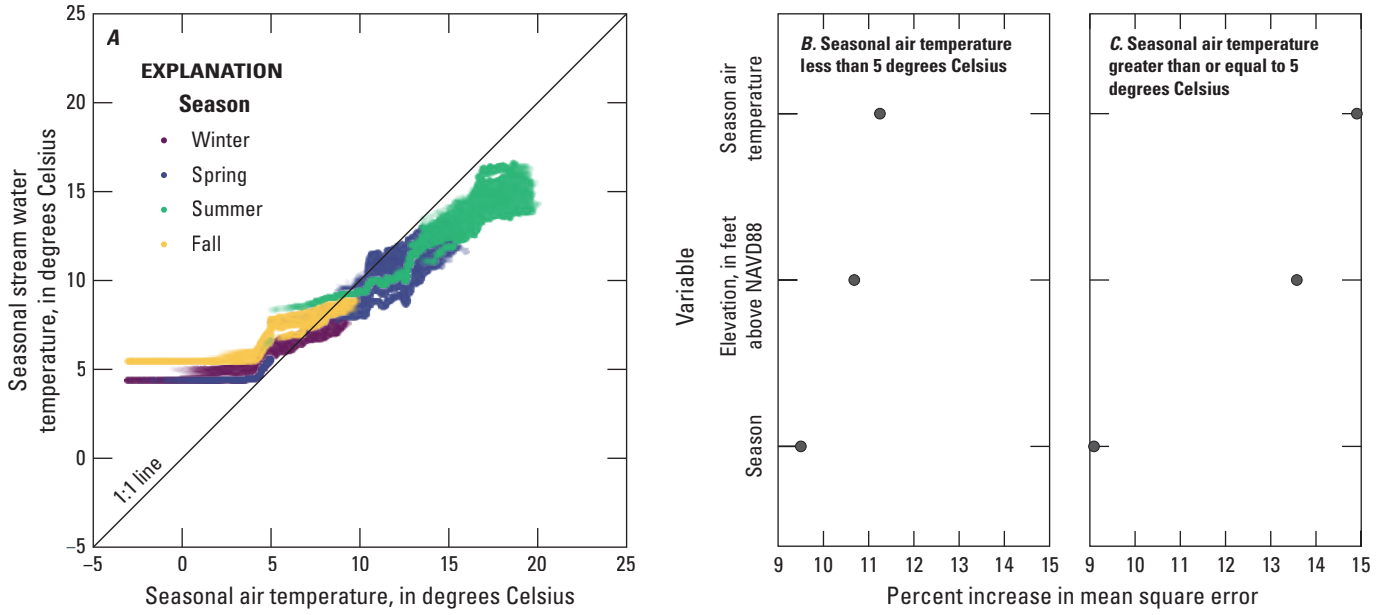

Figure 5. Graphs showing (*A*) estimated seasonal stream water temperature relative to seasonal air temperature from 2005 through 2020, (*B*) relative importance of water-temperature predictor variables for seasonal air temperature less than 5 degrees Celsius, and for (*C*) seasonal air temperature greater than or equal to 5 degrees Celsius. [Winter, January–March; Spring, April–June; Summer, July–September; Fall, October–December.]

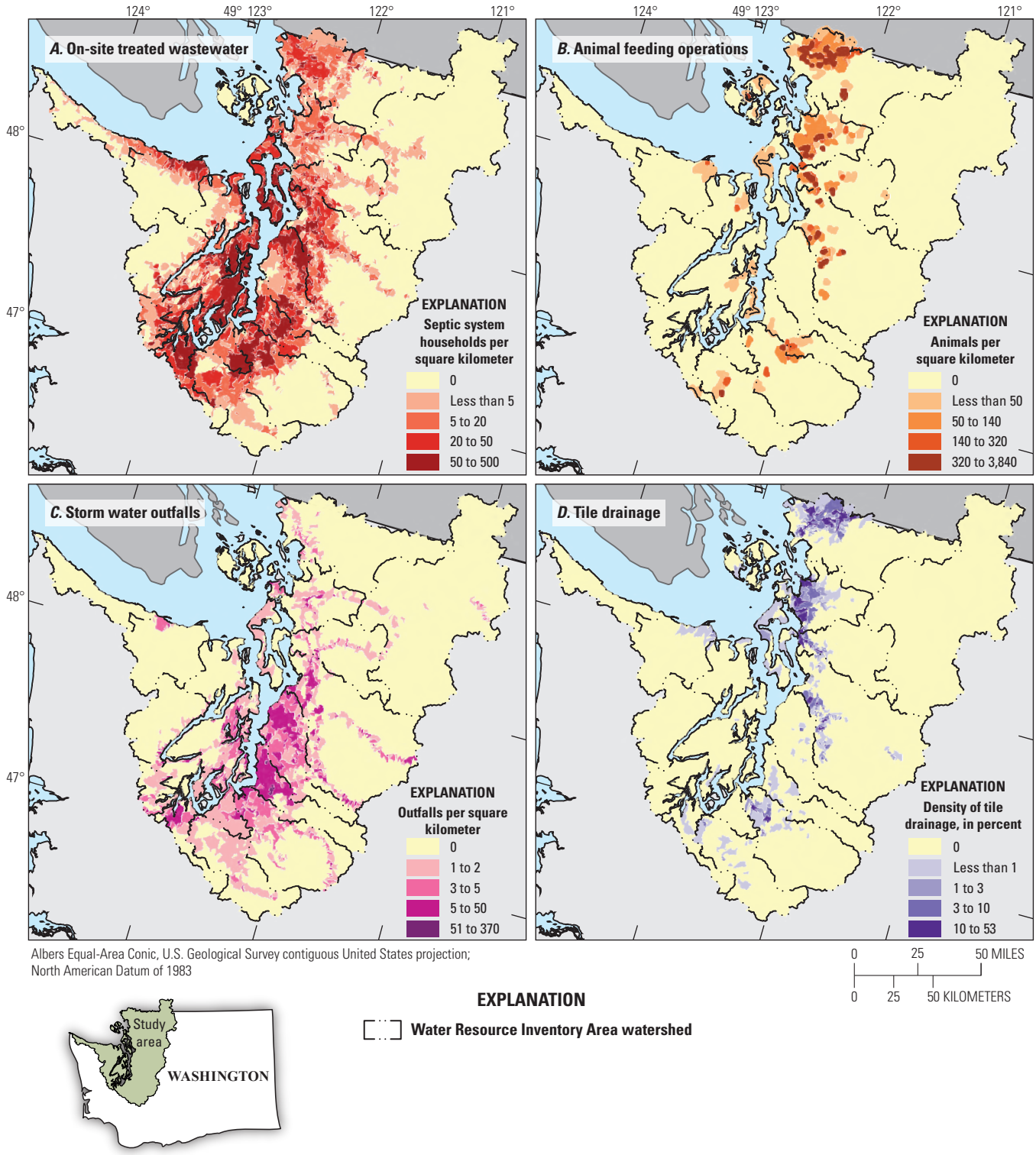

Figure 6. Density of (*A*) households with on-site wastewater treatment (septic) systems, (*B*) animal feeding operations for dairy production, (*C*) storm water outfalls, and (*D*) tile drainage within NHDPlusV2 catchments in the Puget Sound region.

Urban land was represented by NLCD (Wieczorek and others, 2023); it was a constant variable in the TN and TP models but was reset when a new year of data was available between 2004 to 2019 to account for change in urban land. This urban land variable was a lumped nutrient source, representative of many possible urban sources and pathways. The spatial specificity of this source type was improved by interacting with land-to-water variables that mediated delivery (eqs. 7 and 8). Monthly total and wet inorganic nitrogen atmospheric deposition rates were estimated by Wise and others (2025) from National Atmospheric Deposition Program (NADP) monitoring data (National Atmospheric Deposition Program, 2022) and monthly precipitation data from the National Oceanic and Atmospheric Administration (NOAA) ClimGrid database (National Oceanic and Atmospheric Administration, 2022b) and aggregated seasonally for use in the TN and TP models. Background phosphorus available in upland geologic material was estimated following Robertson and Saad (2019) using phosphorus concentration values in the upper 1 meter of soil multiplied by soil bulk density from Wieczorek and others (2018).

Land-to-Water Delivery Variables

Precipitation and ET were dynamic land-to-water climatic variables that drove or attenuated source delivery. Monthly precipitation and air temperature data were from the NOAA ClimGrid database and ET data were from Wieczorek and others (2022). The ET data were based on estimates from a water balance model (McCabe and Wolock, 2011; Wolock and McCabe, 2018). There was a strong seasonal pattern with precipitation with the highest precipitation typically occurring in the fall that continued into winter (fig. 1.5). Spring moisture was still high but was typically in a recession from winter into summer. ET, lower in magnitude compared to precipitation, had a pattern inverse to precipitation with the highest values in the summer, followed by spring (fig. 1.6). In the Puget Sound region, water-balance estimates suggested that moderate ET was still occurring during winter and spring near coastal areas. Nutrient removal processes like crop harvest may not be explicitly identified but were implicitly indicated in the results. For example, a result that ET negatively interacts with crop fertilizer may, in part, represent the effects of crop harvest.

The model also included soil properties, such as organic matter content, clay content, and erodibility factors (attributes from Wieczorek and others [2018]). Those soil properties further interacted with source input variables to adjust their delivery and attenuation spatially. Effects of other human infrastructure were also tested; the density of stormwater outfalls multiplied by rainfall intensity, represented by the ratio of seasonal precipitation to mean annual precipitation, was used as an additional interaction with the urban land source. Those outfalls (municipal separate stormwater sewer systems [MS4]) that carry stormwater to streams in many areas (fig. 6*C*) are relatively stable and reflect locations of stormwater inputs for areas served by MS4 systems in 2016 (Figueroa-Kaminsky and others, 2022). Likewise, tile drainage in croplands from Valayamkunnath and others (2020) was tested as an interaction with crop fertilizer (fig. 6*D*). Many other variables were tested, including permeability, past wildfire extent, mean percentage snow cover, and probability of springs (Rohde and others, 2024), but none were found to provide clear and significant interactions with sources at the regional scale; a lack of significance does not necessarily imply a lack of process or effect, but rather indicates limitations to statistical approaches and challenges of discerning noise that could arise by attempting to use both constant and dynamic datasets.

Calibration Process of Total Nitrogen and Total Phosphorus Models

Model coefficients of the TN and TP models were calibrated through nonlinear weighted least-squares regression using the seasonal loads (kg/season) estimated at 49 TN stations and 47 TP stations (fig. 3). Across 64 seasons, a total of 2,951 TN load observations and 2,834 TP load observations were used in calibration of the TN and TP models, respectively. For every load observation, there was a model residual (calculated as observation minus prediction) used to examine patterns in model error.

Seasonal patterns in model residuals were examined for heteroscedasticity and serial correlation following Schmadel and others (2021, 2024). To examine for heteroscedasticity, squared residuals were regressed against specified binary seasonal variables (one if winter, zero otherwise) to produce predicted squared residuals as a function of season. Models with significant seasonal patterns in the squared residuals were recalibrated by weighting the observations by the inverse of the predicted squared residuals to reduce potential bias due to heteroscedasticity solely caused by seasonality. Once weighted, bootstrap resampling with 100 iterations was then performed to estimate 90 percent confidence intervals on the load predictions.

Serial correlation in the residuals can cause a bias in estimated standard errors of coefficients. Its effects were quantified for improved interpretation of source pathway and uncertainty. Serial correlation can artificially reduce a coefficient *p*-value by indicating significance based on the previous period value instead of by the underlying process that drives nutrient fate and transport. This potential bias may limit the amount of constant explanatory variables possible in a dynamic model, as a constant variable does not change throughout the 64 periods. Following Schmadel and others (2024), standard errors (and associated *t*-values and *p*-values) of the model coefficients were therefore corrected for serial correlation by performing a first-order autoregressive analysis of the model residuals assumed independent across stations.

Another potential validation step considered is a withholding of some calibration data for further assessment of error and the model's ability to simulate loads at unmonitored locations. However, withholding calibration stations is not common practice in SPARROW modeling because each developed model is already limited in the number of stations necessary to represent the gradients across a region. Thus, removal of any stations (for example, 10 percent of stations) may cause a large portion of the model domain to go unrepresented. In the Puget Sound region, of the WRIAs that contained calibration stations, many contained only one station near the basin outlet. Excluding any one single station could result in a different model interpretation because less of the region is represented—withholding stations to test model performance in unmonitored locations is not trivial as each station represents different upstream information. However, each station had a unique leverage on the estimation of coefficients and certain calibration stations were more important to represent gradients across WRIAs than others. For example, some stations more densely packed in urban areas may not necessarily provide new information. It was found, however, that exclusion of any calibration station near urban areas (for example, in King County, Washington; fig. 3) provided a model with higher error in the urban source pathway coefficient. Calibration stations close to one another could be excluded if they provide redundant information; however, stations 09A080 and KCM-3106 on the Green River are located on the same model reach but provided different load values as there is a stormwater outfall in between. Thus, 09A080 was artificially moved to the next upstream reach and both stations were kept in the models.

Model Specifications

The interactions between source inputs and land-to-water delivery variables were assumed and set within the TN and TP models. To set source input coefficients to per-year units for comparison purposes to previous estimates, constant source input variables or variables expressed at an annual timescale (for example, urban land or animal count), were divided by four, or by the number of timesteps in 1 year. Red alder tree coverage was the exception; red alder tree coverage was divided in half under the assumption that deciduous forests fix nitrogen for half of the year and decompose and leach the other half of the year. Precipitation in the TN model was assumed to interact with all nonpoint sources except for atmospheric deposition—precipitation was already used in the calculation of atmospheric deposition and setting an interaction with precipitation could cause a double-counting effect. Precipitation in the TP model was set to interact with all nonpoint sources. ET was tested in both models; the specification set for the TN model (after many test models) was a season-to-season change in ET interacting with the storage lag source. In the TP model, the previous season precipitation and ET variables were set to interact with the storage lag source, but also, the current period ET was set to interact with crop fertilizer and septic. The indication was that precipitation increases TN and TP delivery (positive coefficient) whereas ET represents a loss process (negative coefficient). The additional interaction between ET and septic in the TP model suggested that some of the TP in septic leachate was removed in its transport to streams.

Soil and catchment attribute variables also interacted with source inputs. Clay content was assumed to interact with all source inputs in both models (except for upland geologic material in the TP model because soil properties are already included in that variable calculation). Organic content was included in the TN model and interacted with all nonpoint sources whereas soil erodibility (K-factor) interacted with all nonpoint sources in the TP model (but again did not interact with upland geologic material). Additional soil and catchment variables included only in the TP model were small stream density (Schmadel and others, 2020) and mean catchment slope (Wieczorek and others, 2018) to represent channel erosion processes.

Interaction between atmospheric deposition and urban sources could cause feedback noise in the TN model (Conrad-Rooney and others, 2023), potentially increasing uncertainty in both source terms. Therefore, to break up some collinearity and better isolate the two assumed independent source pathways, the density of stormwater outfalls interacted with the urban source term in the TN model. Furthermore, to represent dynamic effects caused by outfalls, their density was scaled by rainfall intensity expressed as the ratio of seasonal precipitation to long-term mean precipitation.

Point-source data included permitted treated wastewater from municipal and industrial facilities and fish hatchery operations. These point sources were lumped into a single source type in the models, represented by one coefficient. Furthermore, because nearly two-thirds of the point sources discharged into streams and marine waters at locations downstream of calibration stations, the point-source coefficient was set to α_n=1 (eq. 5) to prevent overestimation of this source (after Schmadel and others, 2024). Mass inflow from Canada was treated as its own source, also with its source coefficient set to α_n=1, which was based on the nearest calibration station data scaled by the ratio of drainage areas between the station and the Canadian border.

Aquatic decay in streams was specified with seasonal hydraulic load. All streamflow conditions were represented in the TN aquatic decay expression. Aquatic losses of TP in streams were set to occur only when seasonal streamflow was less than the annual mean, because streams under high flow conditions are hypothesized to not be net sinks of TP (Valett and others, 2022). Water temperature was added as an additional process to TN stream decay (eq. 4) but not for TP.

Simulated Seasonal Total Nitrogen and Total Phosphorus Load Results

Model Performance and Uncertainty

Model quality objectives for this study, defined in more detail by Figueroa-Kaminsky and others (2022), were, in summary, to:

1. Detect nutrient transformation and removal processes at a seasonal scale across the regional gradient of soil and topographic properties.
2. Detect any long-term multi-year and seasonal trends that occurred due to source or pathway changes.
3. Determine if computed instream losses were comparable to field estimates.
4. Compute 90 percent confidence intervals for all simulated loads at similar magnitudes as achieved for other SPARROW studies (Wise, 2019; Schmadel and others, 2021).
5. Achieve a similar overall RMSE as other SPARROW studies (Preston and others, 2009; Wise, 2019; Schmadel and others, 2021).
6. Achieve explanatory variable coefficients with *p*-values of 0.05 or less with limited instances when a slightly (for example, still near 0.10, but less than 0.20) higher *p*-value may be acceptable when a variable can be justified by other evidence.
7. Explain at least 60 percent of the overall variability in the observed loads.

Model results are summarized in this report and accessible and viewable via a mapper (U.S. Geological Survey, 2025).

Regression statistics (tables 2–7) and diagnostic plots (fig. 7*A–H*; figs. 8 and 9) indicated that TN and TP models simulated loads. The RMSE was like that from previous larger-scale static annual models that encompass the Puget Sound region (Wise, 2019). The RMSE of the seasonal TN model in natural logarithmic space was 0.470 (compared to 0.538 in the static model) and RMSE of the seasonal TP model was 0.648 (0.615 in the static model). Overall mean error was interpreted as plus or minus 50 percent and 72 percent of the simulated TN and TP loads, respectively (tables 4 and 7). The TN and TP models were shown to explain 95 percent and 93 percent (82 percent and 71 percent by yield) of the variability in the observed loads, respectively (R^2 in tables 4 and 7). The Nash-Sutcliffe efficiency (NSE) in real space further indicated that the TN model performed efficiently at 88 percent NSE; although the TP model performance was much less at 45 percent NSE, that efficiency is still considered satisfactory (tables 4 and 7; Moriasi and others, 2007).

Residuals of the TN load in natural logarithm space (calculated as ln[observed] minus ln[predicted]) were mostly less than one (as absolute values; fig. 7*C*), which indicated good agreement between prediction and observation. Likewise, residuals remained small for high yields—for example, a large negative residual corresponding to a high yield is an indicator that a source is over predicted. If a point-source discharge location was incorrect (for example, the location was assigned to discharge upstream of a calibration station but is actually located downstream of the calibration station), an error associated with a high yield prediction would be an indicator of that mismatch. Residuals of the TN and TP models were void of that mismatch indicator.

In absolute terms, the larger TN model residuals occurred mostly during summer low flows whereas the TP model residuals were largest during winter and fall high flows (fig. 7*C–H*). Most calibration stations had a mix of positive and negative residuals, indicating that homoscedasticity in error was achieved (figs. 8 and 9). The TP model typically underpredicted loads discharging from the headwaters of the Nooksack River during winter and fall yet tended to overpredict loads from agricultural streams in the lower Skagit River (figs. 1 and 9). At a few stations, while still capturing dynamic signals in loads, the model tended to underpredict in, for example, the Deschutes and Puyallup-White WRIAs and overpredict in the Skokomish-Dosewallips WRIA. Weighting of those stations was tested using the inverse of their squared residuals, but an improvement to prediction accuracy was not found. For the TN model, residuals at stations were also mostly a mix of positive and negative values with many stations nearly matching observations (fig. 8). However, both models consistently underrepresented load exported from the Deschutes River. The Deschutes River exported only 0.4 percent and 1.3 percent of the TP and TN load, respectively, to marine waters from the entire Puget Sound region (app. 2; tables 2.1 and 2.2); thus, smaller loads are likely to have higher uncertainty because they have less effect on the overall model calibration.

A slight seasonal pattern was found in the squared residuals of the models, and seasonal weights were applied. The highest weights were applied to spring, winter, fall, and lowest to summer. However, that weighting had only marginal improvements to the largest squared residuals of the TP model.

Table 2. Model statistics for the explanatory variables included in the dynamic Puget Sound region SPARROW (SPAtially Referenced Regressions on Watershed attributes) total nitrogen model.

[Abbreviations and definitions: VIF, variance inflation factor, a measure of collinearity. Symbols: —, not applicable; <, less than]

Explanatory variable	Variable unit	Coefficient unit	Coefficient mean value (90% confidence interval)[a]	Standard error	*t*-value	*p*-value	VIF	Standard error[b]	*t*-value[b]	*p*-value[b]
Source input variables										
Inflow from Canada	Kilograms per year	Fraction delivered	1.0	—	—	—	—	—	—	—
Permitted treated wastewater	Kilograms per year	Fraction delivered	1.0	—	—	—	—	—	—	—
Animal feeding operations	Number of animals	Kilograms per animal per year	8.37 (6.65 to 10.3)	1.43	5.86	<0.0001	2.5	2.40	3.49	0.0005
On-site treated wastewater	Number of households	Kilograms per household per year	4.47 (3.35 to 5.41)	0.480	9.32	<0.0001	3.7	0.82	5.43	<0.0001
Crop fertilizer	Kilograms per year	Fraction delivered	0.094 (0.064 to 0.118)	0.012	7.74	<0.0001	2.6	0.019	4.97	<0.0001
Atmospheric deposition	Kilograms per year	Fraction delivered	0.250 (0.217 to 0.278)	0.019	13.0	<0.0001	3.2	0.031	7.99	<0.0001
Urban land	Square kilometers	Kilograms per square kilometer per year	802 (653 to 909)	56.1	14.3	<0.0001	3.4	97.1	8.26	<0.0001
Red alder trees	Square meters	Kilograms per square meter per year	0.360 (0.306 to 0.403)	0.026	14.0	<0.0001	10.7	0.040	9.07	<0.0001
Storage lag	Kilograms per year	Fraction retained	0.245 (0.209 to 0.283)	0.017	14.3	<0.0001	8.5	0.018	13.3	<0.0001
Land-to-water delivery variables[c]										
ln(precipitation)	ln(millimeters)	1/ln(millimeters)	1.41 (1.33 to 1.52)	0.051	27.9	<0.0001	5.0	0.074	19.1	<0.0001
ln(organic matter content)	ln(fraction)	1/ln(fraction)	0.574 (0.464 to 0.690)	0.070	8.19	<0.0001	3.6	0.122	4.69	<0.0001
ln(clay content)	ln(fraction)	1/ln(fraction)	−0.485 (−0.566 to −0.423)	0.043	−11.2	<0.0001	3.3	0.075	−6.46	<0.0001
ln(storm outfall density × rainfall intensity)	ln(number per square kilometer)	1/ln(number per square kilometer)	−0.459 (−0.529 to −0.386)	0.036	−12.8	<0.0001	1.4	0.063	−7.31	<0.0001
Season-to-season change in ln(evapotranspiration)	ln(millimeters)	1/ln(millimeters)	−0.412 (−0.506 to −0.315)	0.050	−8.29	<0.0001	1.2	0.046	−9.01	<0.0001

Table 2. Model statistics for the explanatory variables included in the dynamic Puget Sound region SPARROW (SPAtially Referenced Regressions on Watershed attributes) total nitrogen model.—Continued

[Abbreviations and definitions: VIF, variance inflation factor, a measure of collinearity. Symbols: —, not applicable; <, less than]

Explanatory variable	Variable unit	Coefficient unit	Coefficient mean value (90% confidence interval)[a]	Standard error	*t*-value	*p*-value	VIF	Standard error[b]	*t*-value[b]	*p*-value[b]
			Aquatic decay variables							
Waterbody reciprocal hydraulic load	Years per meter	Meters per year	4.11 (3.47 to 4.60)	1.62	2.54	0.0112	1.5	2.39	1.72	0.0855
Stream reciprocal hydraulic load	Days per meter	Meters per day	0.309 (0.254 to 0.359)	0.026	11.7	<0.0001	12.6	0.040	7.63	<0.0001
ln(stream temperature)[c]	ln(degrees Celsius)	1/ln(degrees Celsius)	0.191 (0.123 to 0.247)	0.035	5.53	<0.0001	4.5	0.037	5.17	<0.0001

[a]90 percent confidence intervals estimated by bootstrap resampling (comparable to the adjusted standard error × 1.65).

[b]Adjusted to account for serial correlation effects.

[c]Mean-centered with positive and negative values; *p*-value is two-sided for land-to-water delivery variables and stream temperature.

Table 3. Serial correlation statistics for the dynamic Puget Sound region SPARROW (SPAtially Referenced Regressions on Watershed attributes) total nitrogen model.

[Symbol: <, less than]

Parameter	Estimate	Standard error	*t*-value	*p*-value
Previous period ln(residual)	0.543	0.016	34.9	<0.0001

Table 4. Summary statistics for the dynamic Puget Sound region SPARROW (SPAtially Referenced Regressions on Watershed attributes) total nitrogen model.

[Winter includes January, February, March; spring includes April, May, June; summer includes July, August, September; fall includes October, November, December. Abbreviations and symbols: %, percent; R^2, coefficient of determination; RMSE, root mean square error]

Parameter	Value
Root mean square error, in natural logarithm space	0.470
Root mean square error[a] percentage in real space	50%
Mean square error, in natural logarithm space	0.221
Mean exponentiated weighted error	1.148
Adjusted R^2	0.950
Yield R^2	0.822
Nash-Sutcliffe efficiency, in natural logarithm space	0.940
Nash-Sutcliffe efficiency, in real space	0.877
Model degrees of freedom	15
Number of observations	2,951
Number of stations	49
Mean square error, winter	0.179
Mean square error, spring	0.202
Mean square error, summer	0.352
Mean square error, fall	0.185

[a]Estimated as percentage in real space as: $100\times\sqrt{(\exp(RMSE^2) - 1)}$.

Table 5. Model statistics for the explanatory variables included in the dynamic Puget Sound region SPARROW (SPAtially Referenced Regressions on Watershed attributes) total phosphorus model.

[Abbreviations and definitions: VIF, variance inflation factor, a measure of collinearity. Symbols: —, not applicable; <, less than]

Explanatory variable	Variable unit	Coefficient unit	Coefficient mean value (90% confidence interval)[a]	Standard error	*t*-value	*p*-value	VIF	Standard error[b]	*t*-value[b]	*p*-value[b]
Source input variables										
Inflow from Canada	Kilograms per year	Fraction delivered	1.0	—	—	—	—	—	—	—
Permitted treated wastewater	Kilograms per year	Fraction delivered	1.0	—	—	—	—	—	—	—
Animal feeding operations	Number of animals	Kilograms per animal per year	2.29 (1.23 to 4.00)	0.341	6.71	<0.0001	2.8	0.557	4.10	<0.0001
On-site treated wastewater	Number of households	Kilograms per household per year	0.177 (0.094 to 0.353)	0.036	4.89	<0.0001	5.4	0.056	3.18	0.0015
Crop fertilizer	Kilograms per year	Fraction delivered	0.030 (0.014 to 0.047)	0.005	5.79	<0.0001	4.5	0.008	3.78	0.0002
Urban land	Square kilometers	Kilograms per square kilometer per year	78.7 (64.6 to 111)	6.00	13.1	<0.0001	7.9	9.05	8.69	<0.0001
Upland geologic material	Metric tons per year	Fraction delivered	0.0030 (−0.0092 to 0.0043)	0.0004	7.94	<0.0001	11.8	0.0006	8.69	<0.0001
Storage lag	Kilograms per year	Fraction retained	0.291 (0.240 to 0.333)	0.028	10.4	<0.0001	16.5	0.036	8.03	<0.0001
Land-to-water delivery variables[c]										
ln(precipitation)	ln(millimeters)	1/ln(millimeters)	1.49 (1.31 to 1.99)	0.078	19.0	<0.0001	7.5	0.105	14.2	<0.0001
ln(evapotranspiration)	ln(millimeters)	1/ln(millimeters)	−0.828 (−1.18 to 1.28)	0.234	−3.54	0.0004	1.9	0.238	−3.48	0.0003
√ (stream density)	√ (square kilometer per square kilometer)	1/√ (square kilometer per square kilometer)	10.1 (8.09 to 12.9)	1.64	6.19	<0.0001	3.7	2.81	3.60	0.0002
ln(soil erodibility upper horizon)	ln(K-factor)	1/ln(K-factor)	6.26 (5.44 to 7.09)	0.264	23.7	<0.0001	6.1	0.442	14.2	<0.0001
ln(clay content)	ln(fraction)	1/ln(fraction)	−1.75 (−2.05 to −1.34)	0.111	−15.7	<0.0001	5.2	0.189	−9.26	<0.0001
ln(catchment mean slope)	ln(meter per meter)	1/ln(meter per meter)	0.875 (0.741 to 1.31)	0.046	19.1	<0.0001	7.2	0.076	11.46	<0.0001
Previous period ln(precipitation)	ln(millimeters)	1/ln(millimeters)	−0.504 (−0.629 to −0.360)	0.076	−6.65	<0.0001	2.6	0.086	−5.83	<0.0001
Previous period ln(evapotranspiration)	ln(millimeters)	1/ln(millimeters)	−0.296 (−0.577 to −0.121)	0.094	−3.14	0.0009	2.0	0.099	−3.01	0.0014

Table 5. Model statistics for the explanatory variables included in the dynamic Puget Sound region SPARROW (SPAtially Referenced Regressions on Watershed attributes) total phosphorus model.—Continued

[Abbreviations and definitions: VIF, variance inflation factor, a measure of collinearity. Symbols: —, not applicable; <, less than]

Explanatory variable	Variable unit	Coefficient unit	Coefficient mean value (90% confidence interval)[a]	Standard error	*t*-value	*p*-value	VIF	Standard error[b]	*t*-value[b]	*p*-value[b]
Aquatic decay variables										
Waterbody reciprocal hydraulic load	Years per meter	Meters per year	30.6 (−247 to 45.7)	4.55	6.71	<0.0001	1.9	7.35	4.16	<0.0001
Stream reciprocal hydraulic load[d]	Days per meter	Meters per day	0.191 (0.086 to 0.234)	0.022	8.49	<0.0001	4.0	0.028	6.81	<0.0001

[a]90 percent confidence intervals estimated by bootstrap resampling (comparable to the adjusted standard error × 1.65).

[b]Adjusted to account for serial correlation effects.

[c]Mean-centered with positive and negative values; *p*-value is two-sided for land-to-water delivery variables.

[d]Streamflow below annual mean.

Table 6. Serial correlation statistics for the dynamic Puget Sound region SPARROW (SPAtially Referenced Regressions on Watershed attributes) total phosphorus model.

[Symbol: <, less than]

Parameter	Estimate	Standard error	*t*-value	*p*-value
Previous period ln(residual)	0.513	0.016	31.8	<0.0001

Table 7. Summary statistics for the dynamic Puget Sound region SPARROW (SPAtially Referenced Regressions on Watershed attributes) total phosphorus model.

[Winter includes January, February, March; spring includes April, May, June; summer includes July, August, September; fall includes October, November, December. Abbreviations and symbols: %, percent; R^2, coefficient of determination; RMSE, root mean square error]

Parameter	Value
Root mean square error, in natural logarithm space	0.648
Root mean square error[a] percentage in real space	72%
Mean square error, in natural logarithm space	0.420
Mean exponentiated weighted error	1.266
Adjusted R^2	0.933
Yield R^2	0.710
Nash-Sutcliffe efficiency, in natural logarithm space	0.921
Nash-Sutcliffe efficiency, in real space	0.448
Model degrees of freedom	16
Number of observations	2,834
Number of stations	47
Mean square error, winter	0.337
Mean square error, spring	0.293
Mean square error, summer	0.569
Mean square error, fall	0.443

[a]Estimated as percent in real space as: $100\times\sqrt{(\exp(RMSE^2) - 1)}$.

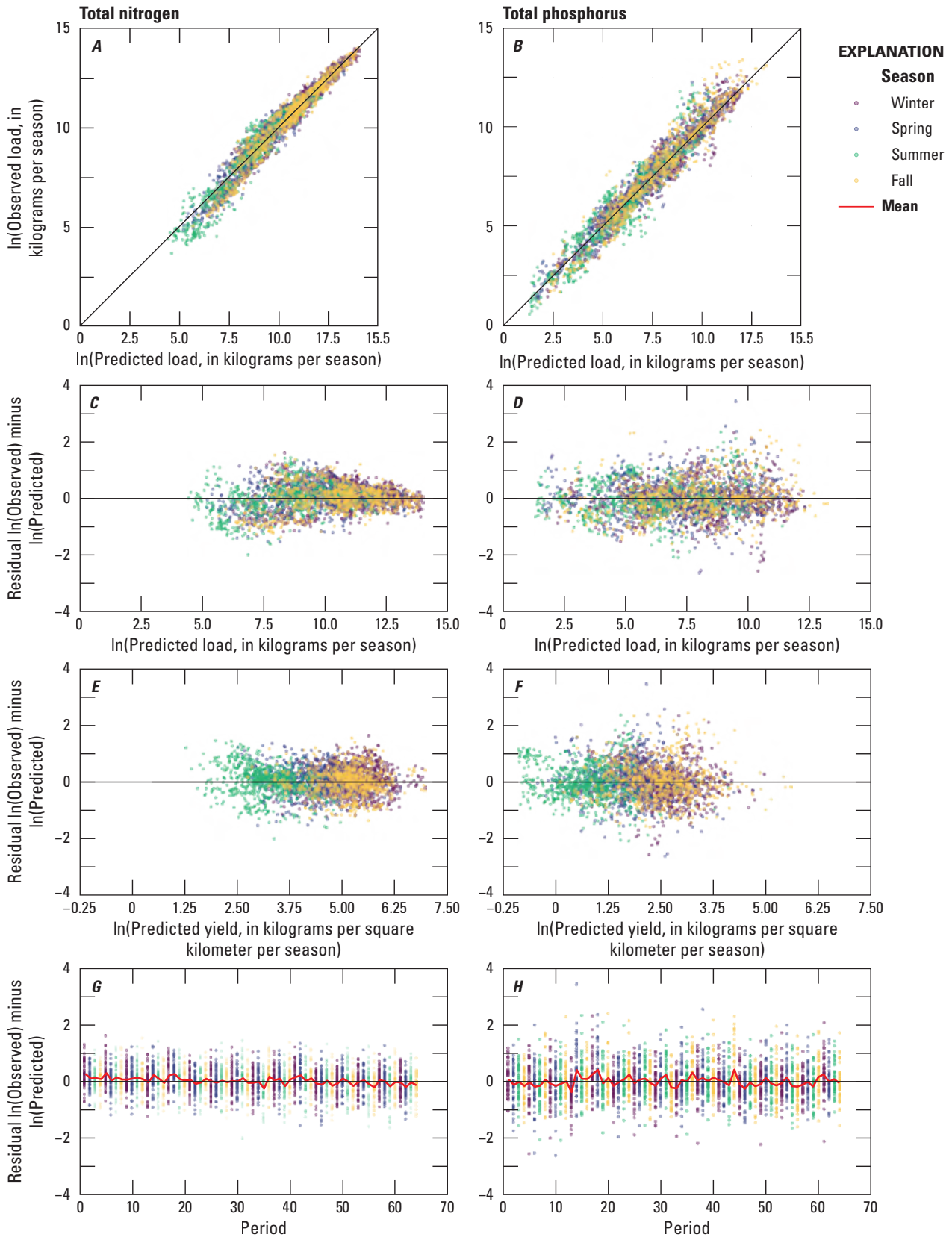

Figure 7. Graphs showing (*A*, *C*, *E*, *G*; left column) total nitrogen residuals and (*B*, *D*, *F*, *H*; right column) total phosphorus residuals from the dynamic Puget Sound region SPARROW (SPAtially Referenced Regressions On Watershed attributes) total nitrogen and total phosphorus models, 2005 through 2020. Residuals are expressed in natural logarithmic space as observed minus predicted load.

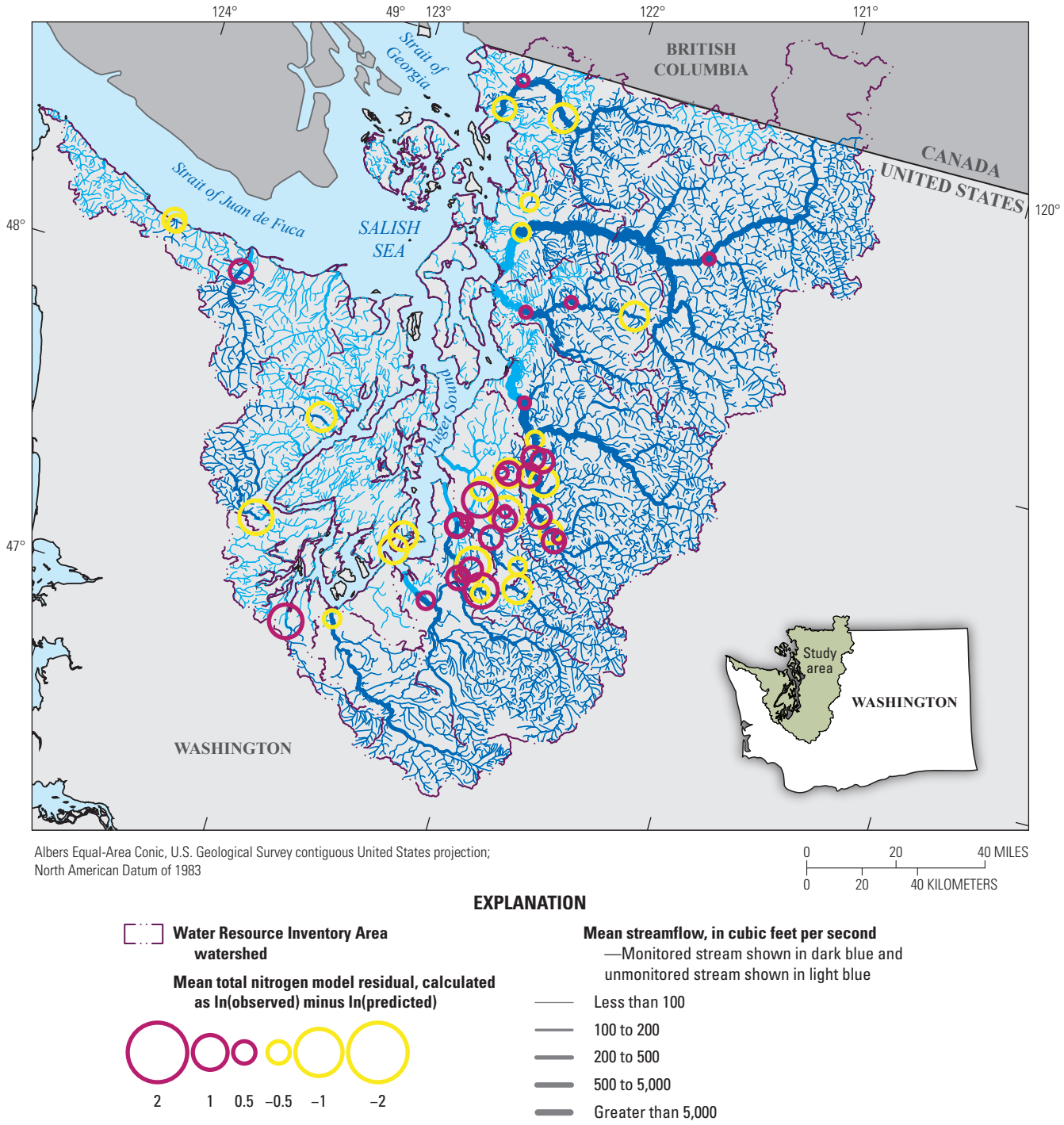

Figure 8. Mean of the total nitrogen model residuals, in natural logarithmic space, colored by positive (model underpredicts) and negative (model overpredicts) values. Each station has approximately 64 residuals representing the number of simulated seasons 2005 through 2020. Refer to figure 2.1 for all residuals.

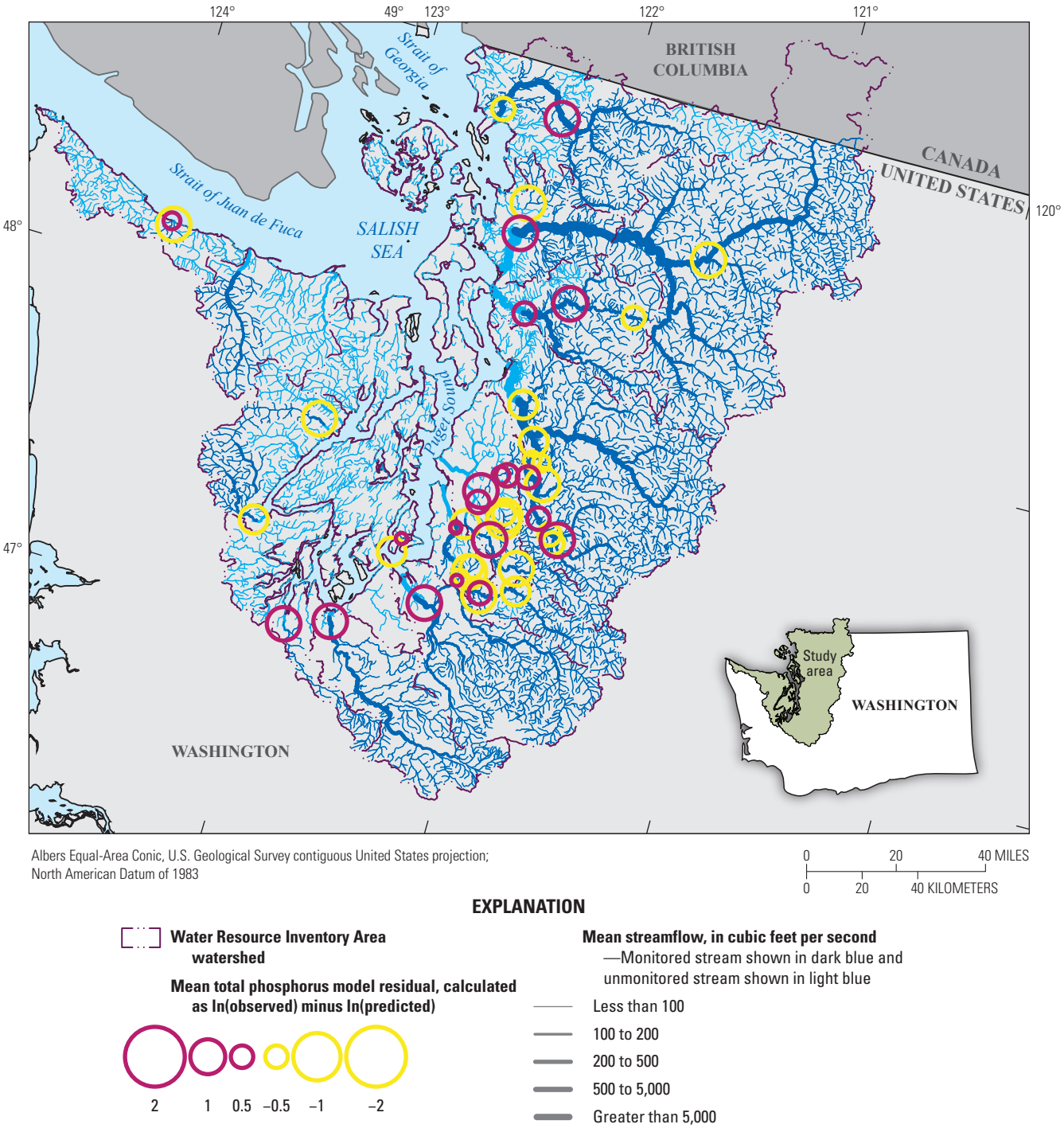

Figure 9. Mean of the total phosphorus model residuals in natural logarithmic space colored by positive (model underpredicts) and negative (model overpredicts) values. Each station has approximately 64 residuals representing the number of simulated seasons 2005 through 2020. Refer to figure 2.2 for all residuals.

Serial correlation had significant effects on artificially reducing the model coefficient standard errors, suggesting that a mean 51 to 54 percent of the current period residual can be explained by the previous period residual (tables 3 and 6). After correcting for serial correlation effects, the animal feeding operations source coefficient for the TN model increased in error and went from a *p*-value of less than (<) 0.0001 to 0.0005 (table 2). A *p*-value above 0.2 starts to become a concern in which the source coefficient may no longer be distinguishable from zero after accounting for serial correlation bias. It was interpreted that the animal feeding operations were still a TN source pathway, but the uncertainty in that pathway was instead estimated to be larger relative to other TN sources. For the TP model, serial correlation had a notable effect on more than one source coefficient. Coefficients for animal feeding operations and on-site wastewater treatment were still statistically different from zero and therefore considered representative of those source pathways, but adjusting for serial correlation provided a more representative estimate of error for those source coefficients. The largest effect was on the on-site treated wastewater coefficient, increasing the *p*-value from <0.0001 to 0.0015 (table 5). If an important source is not represented by the model, its contributing mass will shift to another source coefficient in model estimation to balance, potentially causing an overestimation of another source component. Therefore, while accounting for uncertainty, all source coefficients were kept, preventing any unfair assignment to any single source pathway.

Seasonal variability in observed load was represented by the TN and TP models. Model simulations were in agreement with observations at many stations as indicated by the observations falling within the estimated 90 percent confidence intervals of the simulations, and confidence intervals tended to be smaller for TN compared to TP (figs. 10 and 11). There were some cases, particularly for some TP stations, where the model simulation was generally close in magnitude to the observation, but with some disagreement between timing that tended to correct itself from upstream to downstream stations (for example, TP station 01A120 to 01A050; fig. 11).

As another general validation check, simulations were compared to annual load observations used in the previous annual SPARROW models (Wise, 2019), which were divided by four to convert units to kilograms per season for comparison. Magnitudes were in close agreement, yet annual estimates were on the higher end (horizontal lines in figs. 10 and 11). However, the seasonal load simulations produced a much larger range of extremes, oscillating by an order-of-magnitude each year—marine waters experienced their highest nutrient loading, in winter and fall.

Flow-weighted concentrations estimated from the model simulations (seasonal load divided by seasonal streamflow) were also compared to in situ continuous nitrate observations at three sites in the Nooksack WRIA (fig. 12*A*–*C*). Three locations in the Nooksack WRIA have records of continuous in situ observed nitrate, which were downloaded from NWIS under p-code 99133 (U.S. Geological Survey, 2022): 12211390 Kamm Creek at Kamm Road near Lynden, Washington (fig. 12*A*); 12212050 Fishtrap Creek at Front Street at Lynden, Washington (fig. 12*B*); and 12213100 Nooksack River at Ferndale, Washington (fig. 12*C*). The magnitude and timing of nitrate concentrations were comparable to the model simulations at Ferndale, Washington, near the mouth of the Nooksack River (fig. 12*C*)—high concentrations during winter followed by low summer concentrations indicated times of possible nitrogen depletion. Discretely measured concentrations at station 01A050 from 2009 through 2020 indicated that a mean 83 percent of the measured TN concentration was comprised of nitrate plus nitrite. The simulated seasonal TN concentrations were all slightly above the in situ nitrate concentrations, indicating agreement between simulated and observed at that station. However, a composition of mostly nitrate is less likely up toward forested headwaters as more organic and particulate forms of nitrogen are possible. Discrete observations further revealed that a pulse of ammonia plus ammonium occurred each winter (fig. 12*C*).

Moving upstream into tributaries affected by agriculture and urban development, concentration magnitudes were also comparable in Fishtrap Creek (fig. 12*B*). Generally comparable magnitudes indicated that source pathway representation was achieved in Fishtrap Creek; however, there was some mismatch in the timing of seasonal peaks and troughs that suggests that the model simulation was out of phase with TP source delivery from some headwater tributaries. In the adjacent Kamm Ditch tributary (referred to as Kamm Creek in the USGS site name), observed nitrate was consistently higher than the model simulations, yet timing appeared consistent. This indicated that, although dynamic drivers were perhaps well represented, the model likely under-represented or did not include a source pathway from Kamm Ditch. The TN and TP models would likely benefit from additional calibration stations in those tributaries.

Interpretation of Model Coefficients

The model coefficients can be interpreted as seasonal and annual flux rates (tables 2 and 5), which directly demonstrates the value of applying a statistical-physical approach for improved process and source pathway interpretation. The mean annual mass from animal feeding operations was estimated at a mean rate from 2005 through 2020 of about 8.4 kg of TN and 2.3 kg of TP delivered per animal per year (coefficients 8.37 and 2.29 in tables 2 and 5, respectively). Interactions with land-to-water delivery variables suggested that delivery was increased in winter and fall during higher precipitation (positive coefficient). Similarly, the models estimated that a mean rate of 4.5 kg of TN and 0.2 kg of TP leached from each household on a septic system each year, and leachate delivery also increased when catchments were wetter.

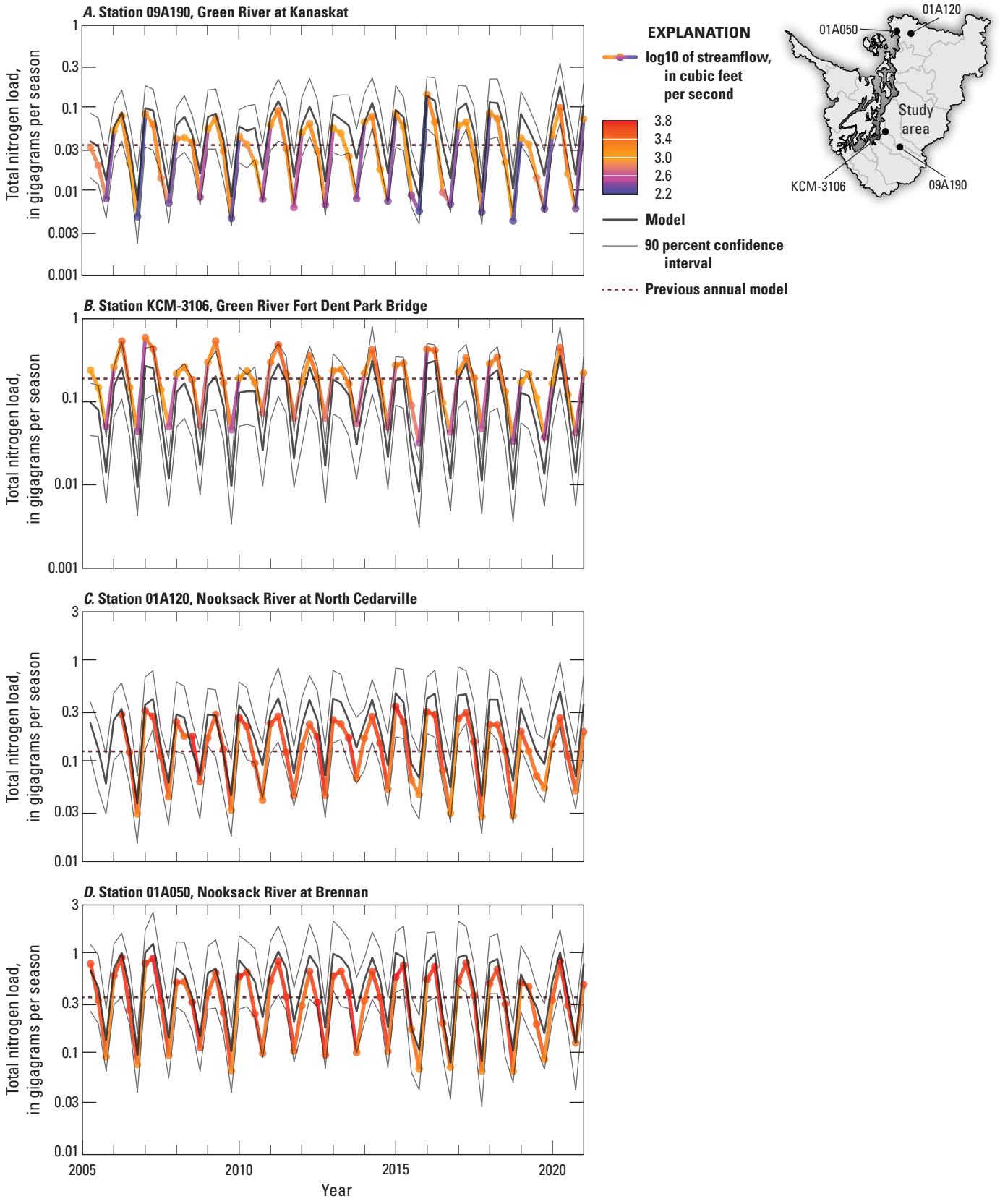

Figure 10. Example comparison of seasonal predicted versus observed total nitrogen load at calibration stations from upstream to downstream for the Green River at (*A*) Station 09A190 to (*B*) Station KCM-3106, and for the Nooksack River at (*C*) Station 01A120 to (*D*) Station 01A050, 2005 through 2020. The comparison includes 90 percent confidence intervals of predicted load and observed load colored by seasonal streamflow. The horizontal dashed line is the corresponding annual load observation (divided by four for seasonal comparison) detrended to 2012 and used by Wise (2020) in previous annual applications.

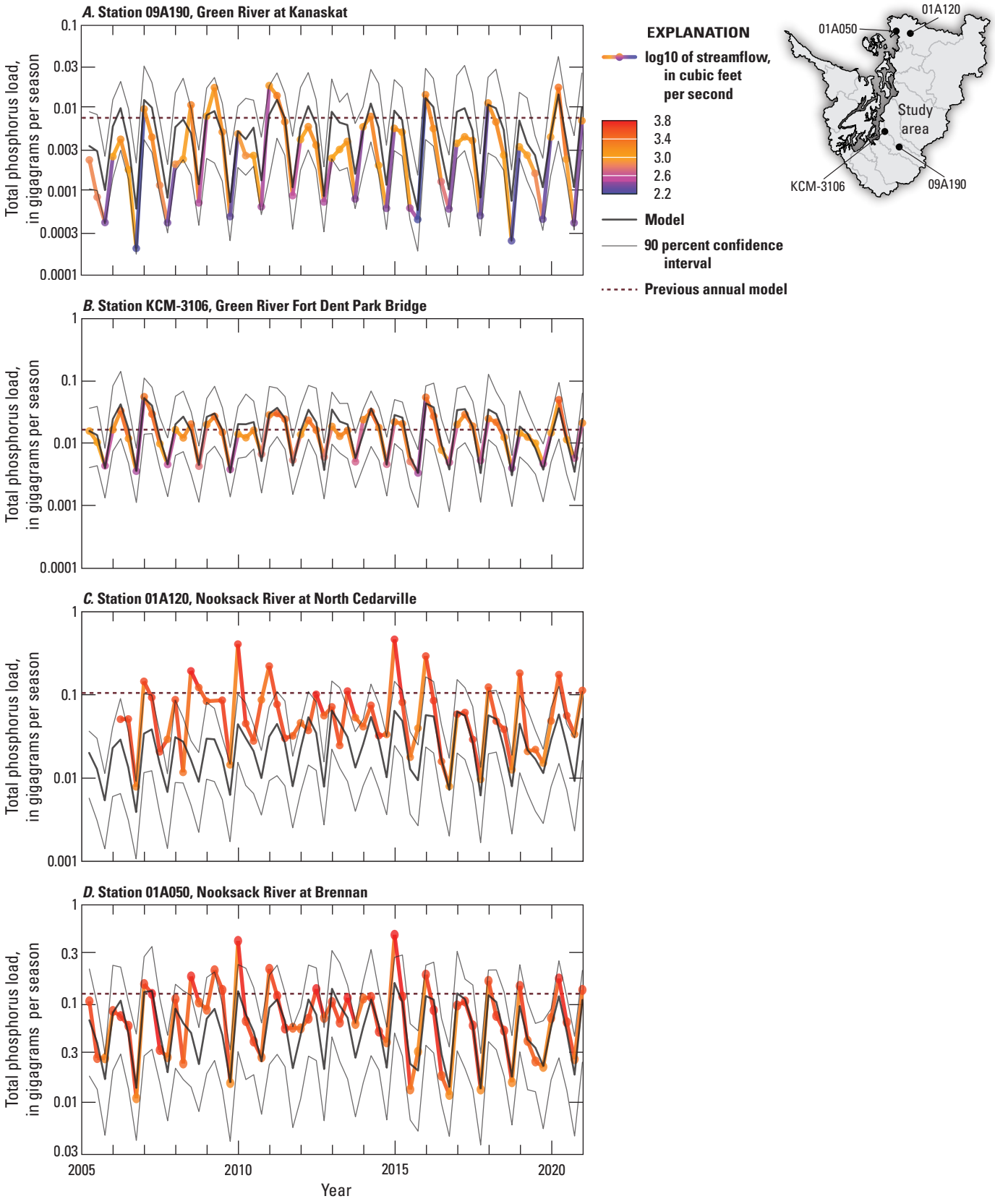

Figure 11. Example comparison of seasonal predicted versus observed total phosphorus load at calibration stations from upstream to downstream for the Green River at (*A*) Station 09A190 to (*B*) Station KCM-3106, and for the Nooksack River at (*C*) Station 01A120 to (*D*) Station 01A050, 2005 through 2020. The comparison includes 90 percent confidence intervals of predicted load and observed load colored by seasonal streamflow. The horizontal dashed line is the corresponding annual load observation (divided by four for seasonal comparison) detrended to 2012 and used by Wise (2020) in previous annual applications.

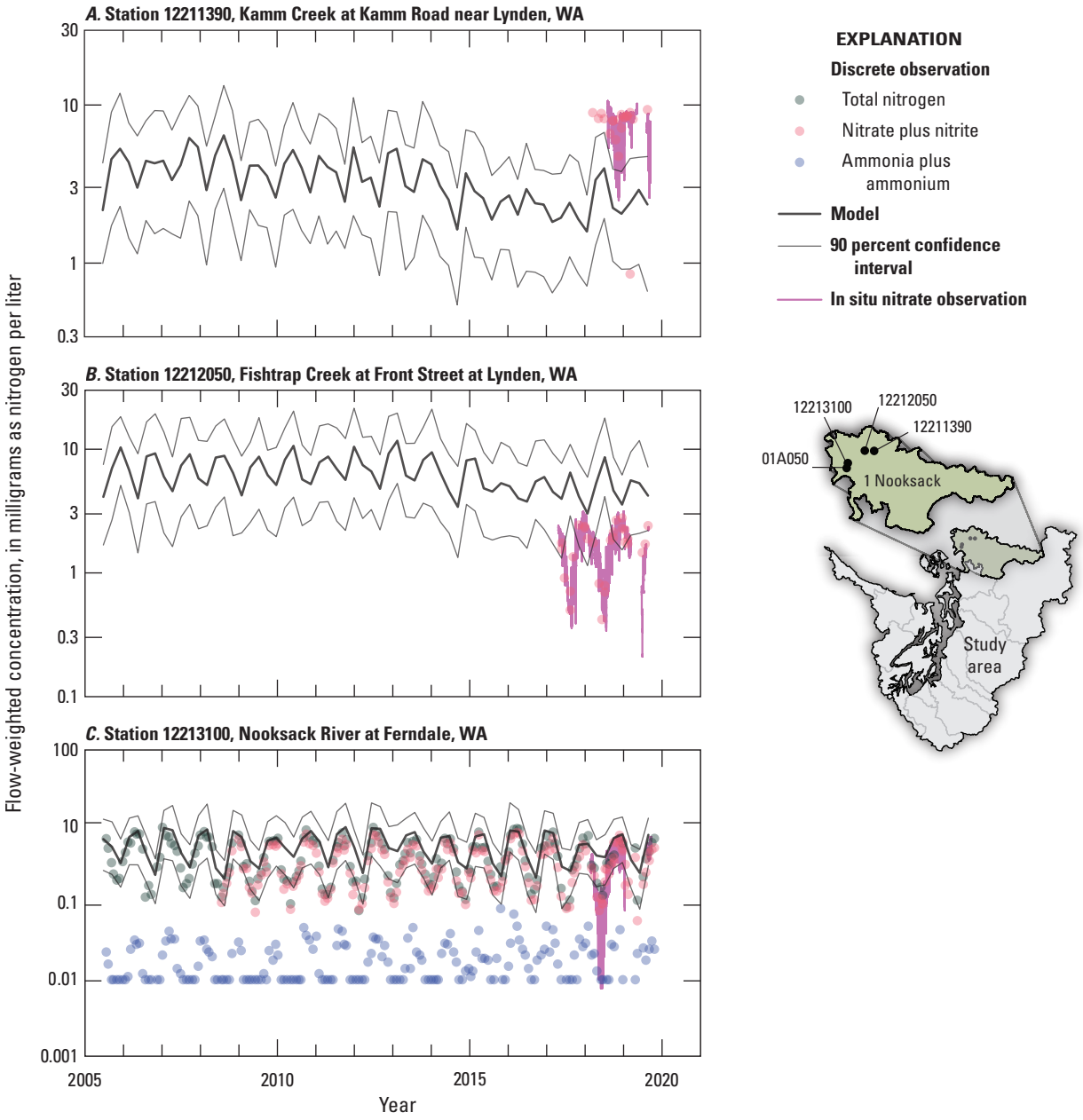

Figure 12. Comparison of seasonal predicted flow-weighted total nitrogen concentrations from three sites (*A*–*C*) in the Nooksack Water Resource Inventory Area, 2005 through 2020. Also shown are 90 percent confidence intervals, measured in situ continuous nitrate concentrations, discretely measured nitrate plus nitrite, ammonia plus ammonium from site 01A050, Nooksack at Brennan, and total nitrogen concentrations. [WA, Washington.]

Urban land was estimated to contribute 802 kg TN and 79 kg TP additional mass per square kilometer per year (tables 2 and 5). Based on the relative magnitudes of model coefficients, more TP came from urban land compared to TN while more TN came from septic systems compared to TP. In the TN model, the density of stormwater outfalls was found to inversely interact with urban land. During higher precipitation intensity, a negative interaction implies two possible pathways: (1) more diluted stormwater that went through the outfalls and (2) more mass that was carried from the atmospheric deposition pathway with precipitation falling on impervious surfaces. A significant coefficient identified for urban land and atmospheric deposition source pathways indicated that there were urban sources in addition to atmospheric—those urban sources not emitted into the atmosphere nor delivered from the atmosphere via impervious surfaces. The TN model further suggests that a mean annual 0.36 kg TN was produced by each square meter of red alder trees (table 2).

The storage lag coefficients for the TN and TP models were 0.25 and 0.29, respectively (tables 2 and 5). Those values represent the fractions of source inputs retained or lagged each season, which provided the mean strength of seasonal storage lag across the Puget Sound region for all predictions from 2005 through 2020. Model results suggest that nearly a quarter of contemporaneous nonpoint TN and TP source inputs were lagged in storage repositories each season and delivered to streams in later seasons, with a slightly larger storage effect estimated by the TP model. Nutrient load released from storage was highest during winter and fall. In the TN model, a positive change in ET from one season to the next was found to decrease the storage lag contribution (negative coefficient; table 2), indicating a loss of stored TN was represented by changes in ET where an increase in ET suggests a loss of stored TN. For the TP model, precipitation and ET from the previous season were found to inversely interact with the storage lag (negative coefficients, table 5). When the previous season had high precipitation or high ET, the model suggests that TP retained in storage was reduced. A negative ET coefficient may represent nutrient losses by processes including plant uptake and crop harvest.

The estimated net decay rate in streams was larger for TN compared to TP (0.31 compared to 0.19 m/d, respectively; tables 2 and 5). Stream decay in the TN model was found to have an additional interaction with water temperature. The mean TN uptake velocity in streams was 0.31 m/d but was estimated to increase when water temperature rose above the regional mean, and decreased when water temperature was below the mean, providing improved timing and spatial specificity, ranging from 0.20 m/d in the winter to 0.44 m/d in the summer (fig. 13*A*).

Waterbody decay was estimated for both models and had a larger effect on TP losses compared to TN. The estimated settling velocities of 4.1 meters per year (m/y) for TN and 31 m/y for TP (tables 2 and 5) were comparable to field values found in moderate size lakes and reservoirs (Cheng and Basu, 2017). However, after accounting for serial correlation, it was unclear whether an estimate of 4.1 m/y was statistically different from zero; thus, the TN model suggests that waterbodies were not a primary loss pathway, which is a consistent result with previous models (Wise, 2019). Waterbodies had a clearer effect on the TP model (table 5), but serial correlation affected their estimation, suggesting that there were additional seasonal changes to waterbodies not explicitly captured by seasonally changing streamflow.

Dominant Total Nitrogen and Total Phosphorus Source by Catchment and by Basin

Annual nutrient loads discharged from watersheds to marine waters from 2005 through 2020 were comprised of several different sources transported from different locations and times, but the dominant contributing individual source also varied by catchment (figs. 14 and 15). Moving downstream from the headwater catchments, the dominant source of TN load shifted from red alder trees and atmospheric deposition to urban and agricultural sources, with point sources from treated wastewater contributing the largest load in several coastal locations (fig. 14).

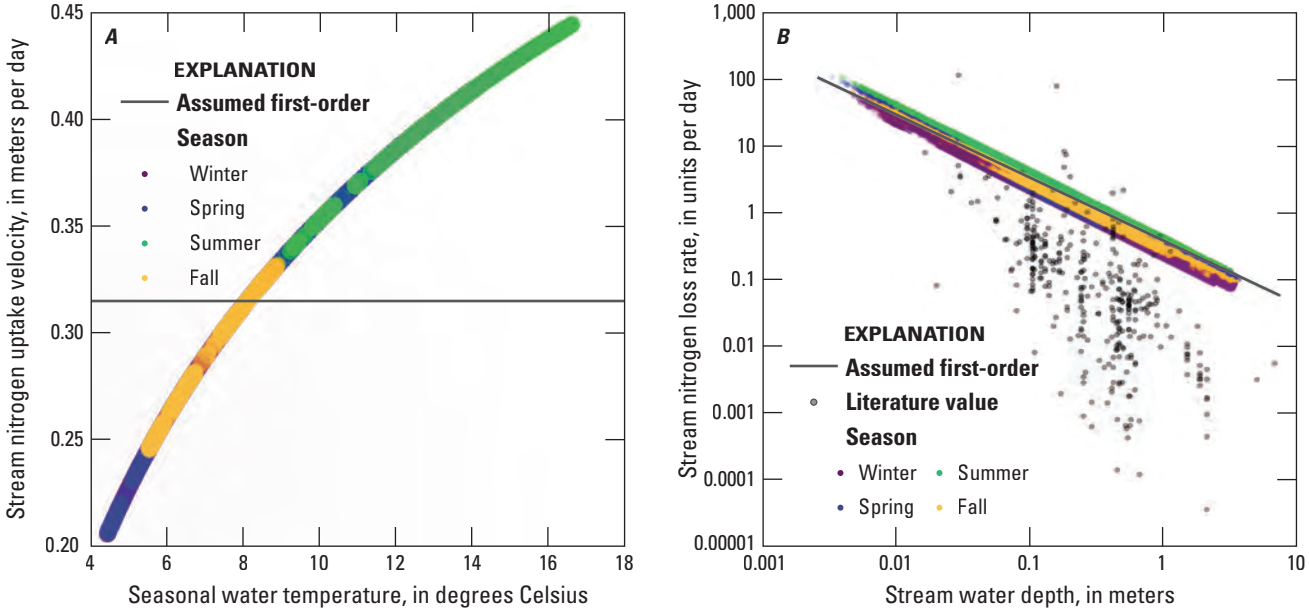

Figure 13. Total nitrogen removal estimates for streams of varying (*A*) water temperatures and (*B*) depths (refer to eqs. 3 and 4) and literature estimates (Mulholland and others, 2008; Böhlke and others, 2009). [Winter, January–March; Spring, April–June; Summer, July–September; Fall, October–December.]

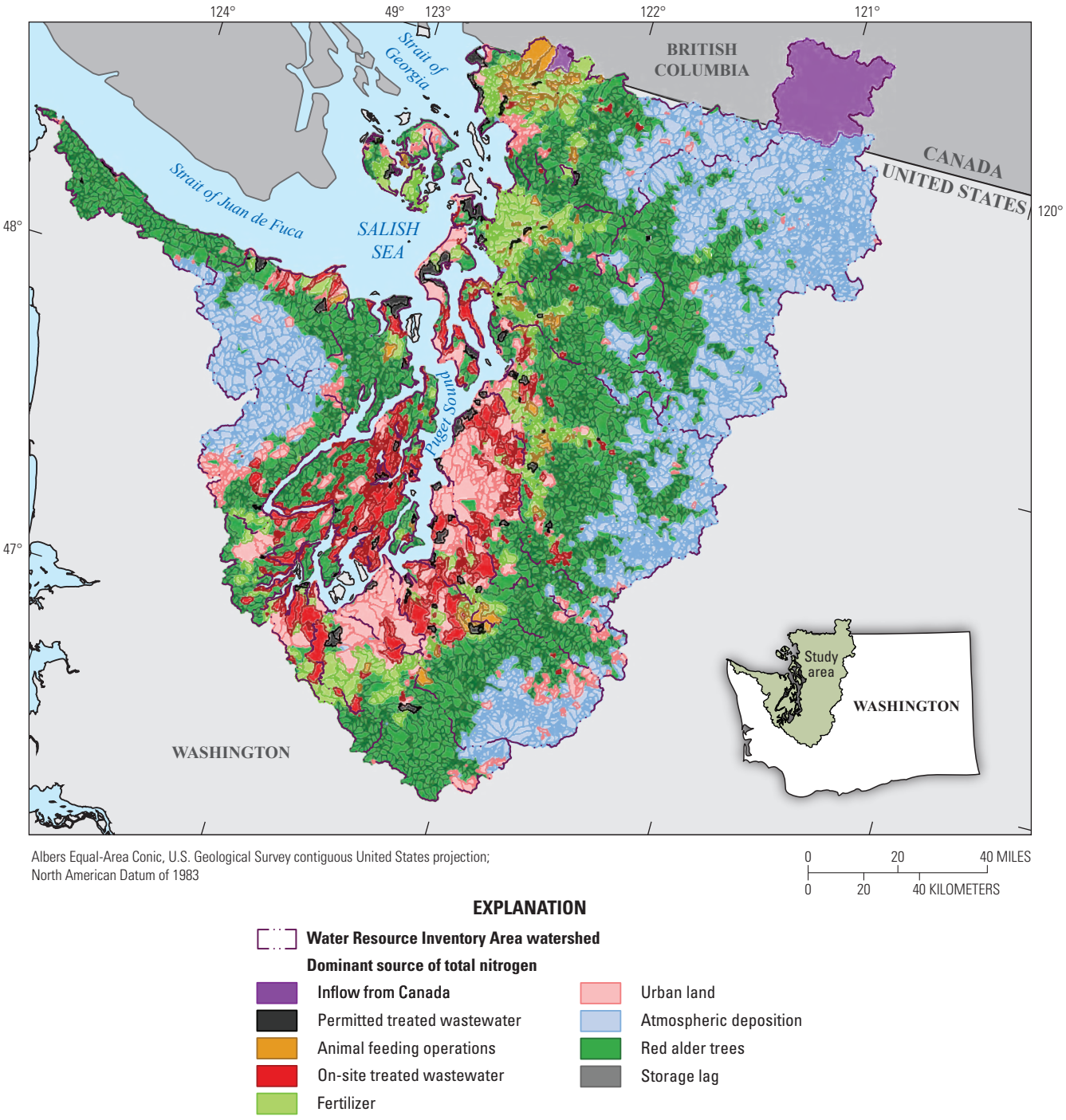

Figure 14. Dominant sources of total nitrogen incremental load, colored by NHDPlusV2 catchment, from the dynamic Puget Sound region SPARROW (SPAtially Referenced Regressions On Watershed attributes) total nitrogen model, 2005 through 2020.

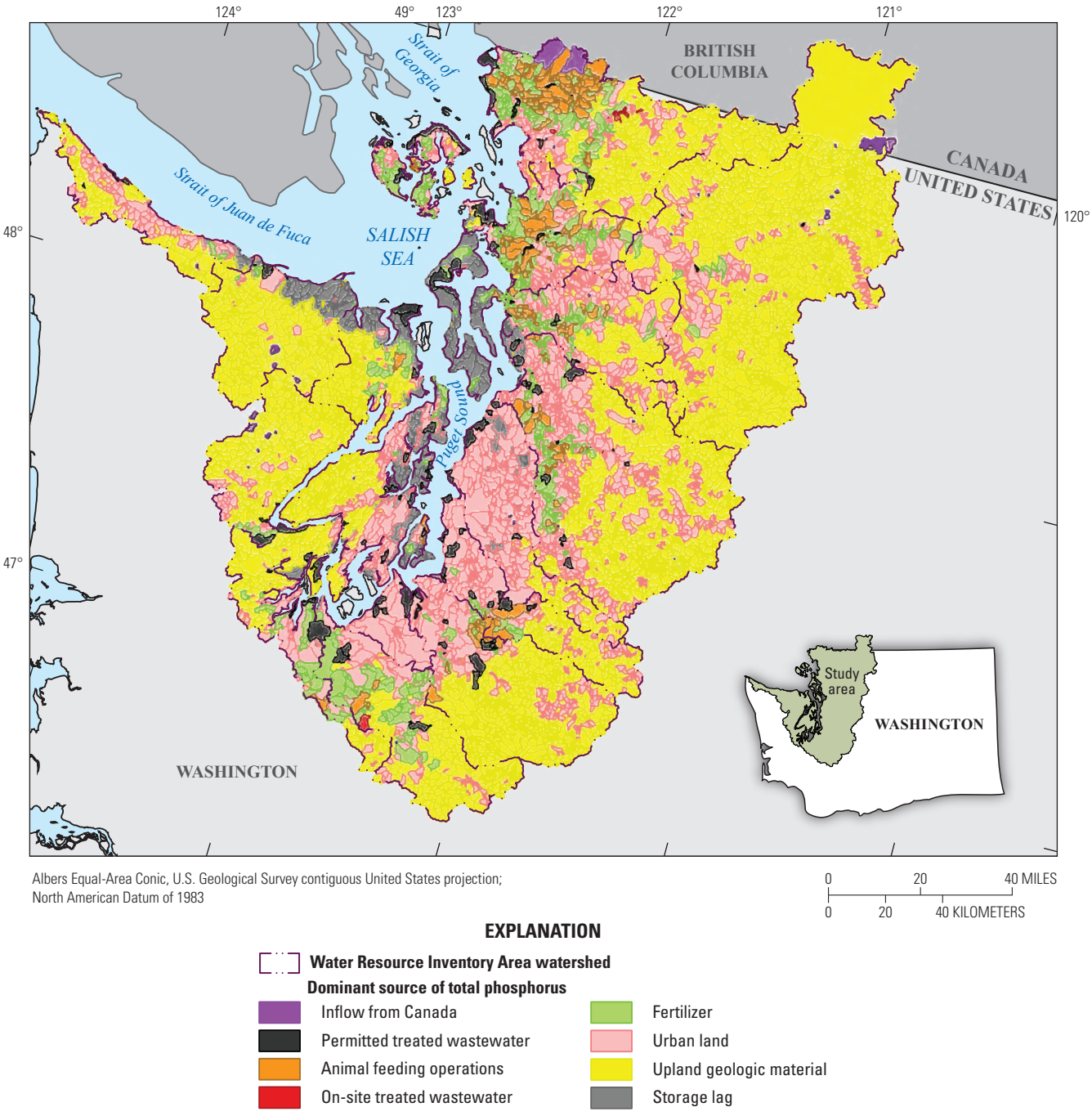

Figure 15. Dominant sources of total phosphorus incremental load, colored by NHDPlusV2 catchment, from the dynamic Puget Sound region SPARROW (SPAtially Referenced Regressions On Watershed attributes) total phosphorus model, 2005 through 2020. Refer to figure 2.3 excluding sources lagged in storage.

These findings are generally consistent with previous nutrient syntheses indicating large human effects near coastal areas (Ahmed and others, 2019; McCarthy, 2019). Dominant TP sources followed a similar pattern, shifting from predominantly non-human geologic sources in the headwaters, such as soil erosion, to predominantly human-driven sources, such as urban runoff, in valleys and coastal areas (fig. 15). However, in some areas where urban land was the dominant source pathway of TP, on-site treated wastewater systems were the dominant source pathway of TN (figs. 14 and 15).

Aggregated by WRIA, the average load and relative source composition varied by basin (figs. 16*A–C* and 17*A–C*). The largest overall TN load discharged to marine waters was from the Cedar-Sammamish, Duwamish-Green, Snohomish, and Nooksack WRIAs (>4 gigagrams per year (Gg/y)], WRIAs 1, 7, 8, and 9; fig. 16*A*). TN sources in the Nooksack WRIA, for example, were a mix of red alder trees, animal feeding operations, crop fertilizer, and the storage lag of those sources, but the Cedar-Sammamish and Duwamish-Green WRIAs were mostly comprised of permitted treated wastewater discharge. Yield, or load delivered per drainage area, further indicated that the Chambers-Clover WRIA (422 square kilometers (km^2), table 2.1) was one of the highest yielding WRIAs due to the outsized contribution of permitted treated wastewater (fig. 16*B*). For context, the Chambers-Clover WRIA is only a third of the size compared to the Cedar-Sammamish (1,688 km^2) and Duwamish-Green (1,361 km^2) WRIAs. The contribution of nitrogen fixed by red alder trees comprised a substantial portion of TN load in most watersheds; modeling results suggest that TN sources in the Lyre-Hoko WRIA were mostly from fixation of atmospheric nitrogen. In the Deschutes, Kennedy-Goldsborough, and Kitsap WRIAs, the larger sources of TN suggested by the model were from on-site treated wastewater combined with urban land (fig. 16*C*).

The largest mean TP load discharged to marine waters was estimated from the Snohomish WRIA (>0.6 Gg/y; fig. 17*A*)—a mix of permitted treated wastewater, upland geologic material, animal feeding operations, urban land, on-site treated wastewater, and fertilizer—yet the highest yields were again from the Cedar-Sammamish and Duwamish-Green WRIAs, mostly from permitted treated wastewater (fig. 17*B*). In the Nooksack and Lower Skagit-Samish WRIAs, animal feeding operations and crop fertilizer comprised almost half of the TP load discharged to marine waters (fig. 17*C*). Compared to TN, the relative contributions of TP from animal feeding operations were more while crop fertilizer was less (figs. 16 and 17).

Seasonality of Total Nitrogen and Total Phosphorus Load, Yield, and Concentration by Source

There was strong seasonal variation in the TN and TP yield across the Puget Sound region with the highest yields predicted during the winter and fall followed by spring and summer (figs. 18 and 19). High yields were dense near coastal areas but also extended to locations far upstream, especially for TP. TN and TP yields during the summer were mostly driven by pockets of crop fertilizer and animal feeding operations.

As the incremental loads accumulated downstream, the final TN and TP load discharged to marine waters at the mouths of 14 major rivers fluctuated by nearly an order-of-magnitude in each river each season from 2005 through 2020 (figs. 20*A* and 21*A*). The Snohomish and Skagit Rivers discharged the largest TN and TP loads, yet the Samish River was shown to have the highest TN and TP yields and concentrations (figs. 20*B*, *C* and 21*B*, *C*). The range in load, yield, and concentration varied by orders-of-magnitude across rivers, yet the seasonal trend appeared mostly stable throughout the 16-year period of record. The exception was the Green River, which had its highest TN and TP yields and concentrations in 2006 and 2007 (figs. 20*B*, *C* and 21*B*, *C*). A breakdown by source indicated that the main cause of seasonal fluctuations of load in the Duwamish-Green WRIA was permitted treated wastewater discharge with higher inputs in 2006 and 2007 (figs. 16*C* and 17*C*).

TN and TP yield by WRIA provided an indication of which watersheds may be most affected by seasonal variability in loads. The Samish River stands out; its seasonal loads, compared to the other 13 example rivers, lie somewhere in the middle, yet its yields and concentrations were some of the highest in the Puget Sound region, and they stayed high throughout the year (for example, concentrations approached 1 milligram per liter [mg/L] of TN and 0.3 mg/L of TP; figs. 20*C* and 21*C*). The TP model tended to overpredict load from the Samish River (figs. 9 and 21), and even after considering confidence bounds, the predicted yield and concentration were still high relative to other rivers. For context, a TN concentration threshold of 0.5 mg/L of TN has been noted in other locations as a level at which biogeochemical processes start to become saturated and stop decaying nitrogen (Schmadel and others, 2020). In the Puget Sound region, there is evidence that stream uptake rates of nutrients have been reduced in areas of high concentrations (Sheibley and others, 2015), but that concentration effect was not explicitly quantified in the TN and TP models.

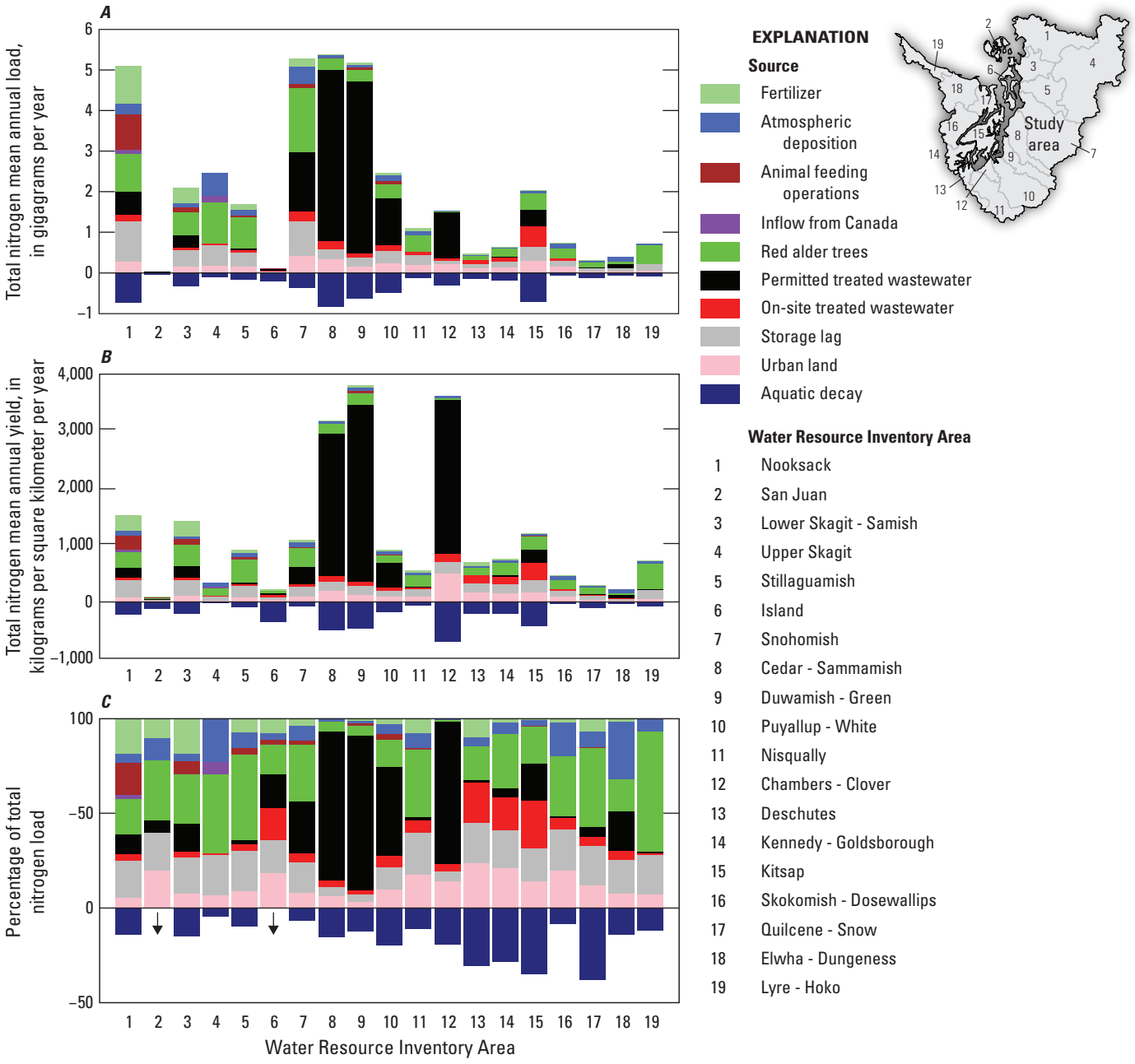

Figure 16. (*A*) Mean annual total nitrogen incremental load, (*B*) mean annual total nitrogen incremental yield, and (*C*) proportion of total nitrogen load discharged to streams and coasts, from the dynamic Puget Sound region SPARROW (SPAtially Referenced Regressions On Watershed attributes) total nitrogen model, 2005 through 2020. Results are summarized by source as the summation for each Water Resource Inventory Area. Arrows indicate values larger than displayed.

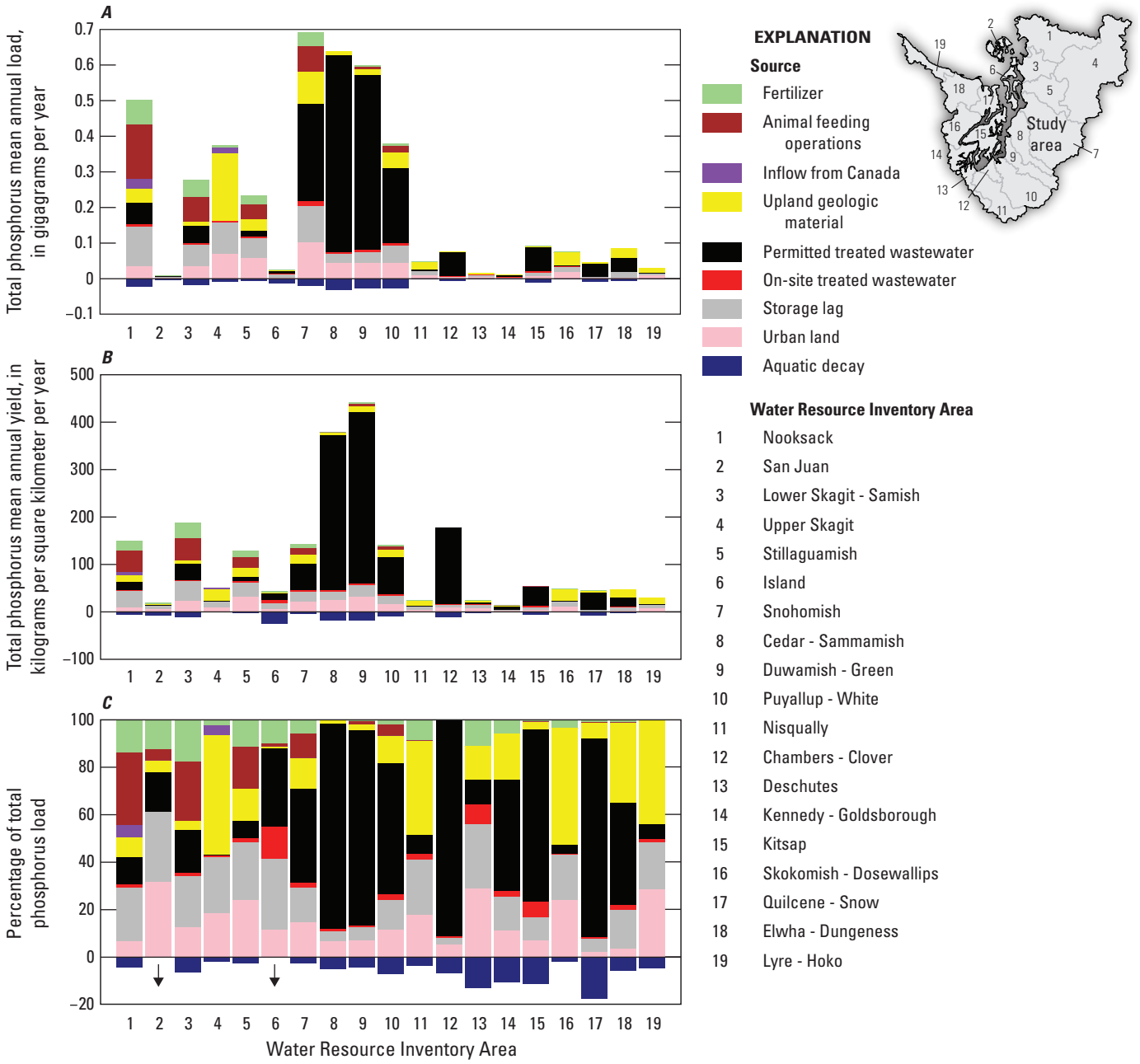

Figure 17. (*A*) Mean annual total phosphorus incremental load, (*B*) mean annual total phosphorus incremental yield, and (*C*) proportion of total phosphorus load discharged to streams and coasts, from the dynamic Puget Sound region SPARROW (SPAtially Referenced Regressions On Watershed attributes) total phosphorus model, 2005 through 2020. Results are summarized by source as the summation for each Water Resource Inventory Area. Arrows indicate values larger than displayed.

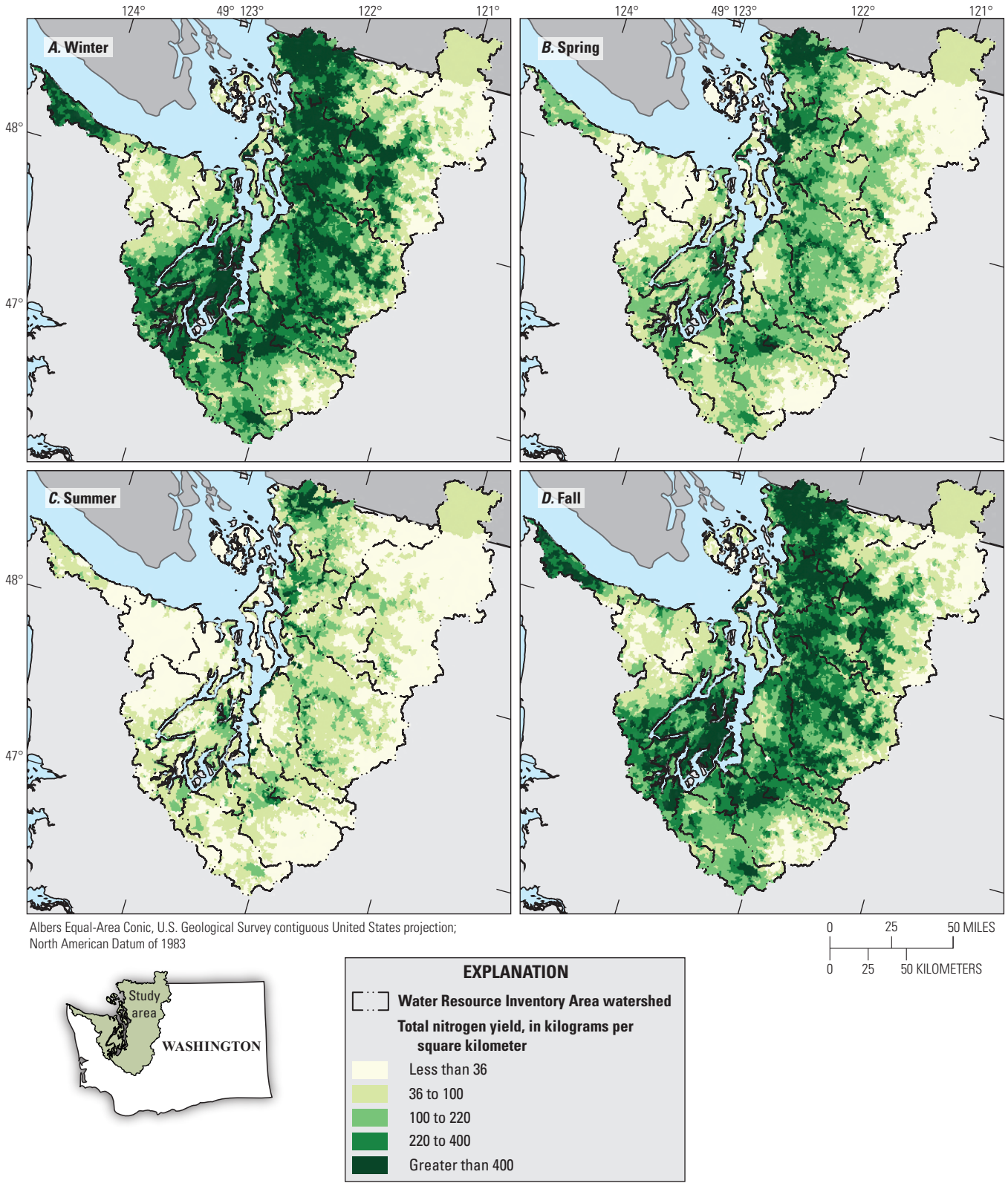

Figure 18. Mean seasonal total nitrogen incremental yield for (*A*) Winter, January–March; (*B*) Spring, April–June; (*C*) Summer, July–September; (*D*) Fall, October–December, from the dynamic Puget Sound region SPARROW (SPAtially Referenced Regressions On Watershed attributes) total nitrogen model, 2005 through 2020. Results are summarized by NHDPlusV2 catchment.

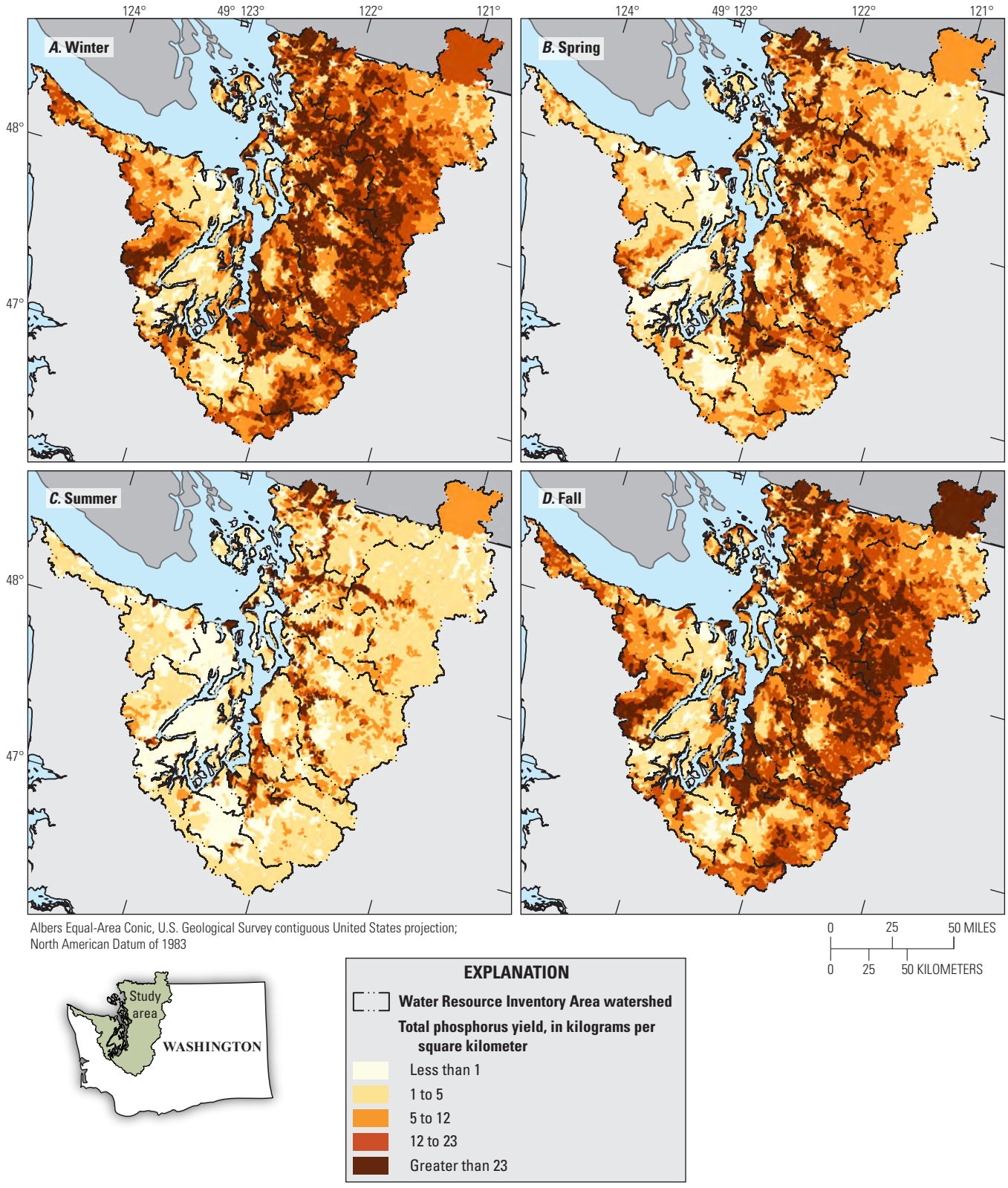

Figure 19. Mean seasonal total phosphorus incremental yield for (A) Winter, January–March; (*B*) Spring, April–June; (*C*) Summer, July–September; (*D*) Fall, October–December, from the dynamic Puget Sound region SPARROW (SPAtially Referenced Regressions On Watershed attributes) total phosphorus model, 2005 through 2020. Results are summarized by NHDPlusV2 catchment.

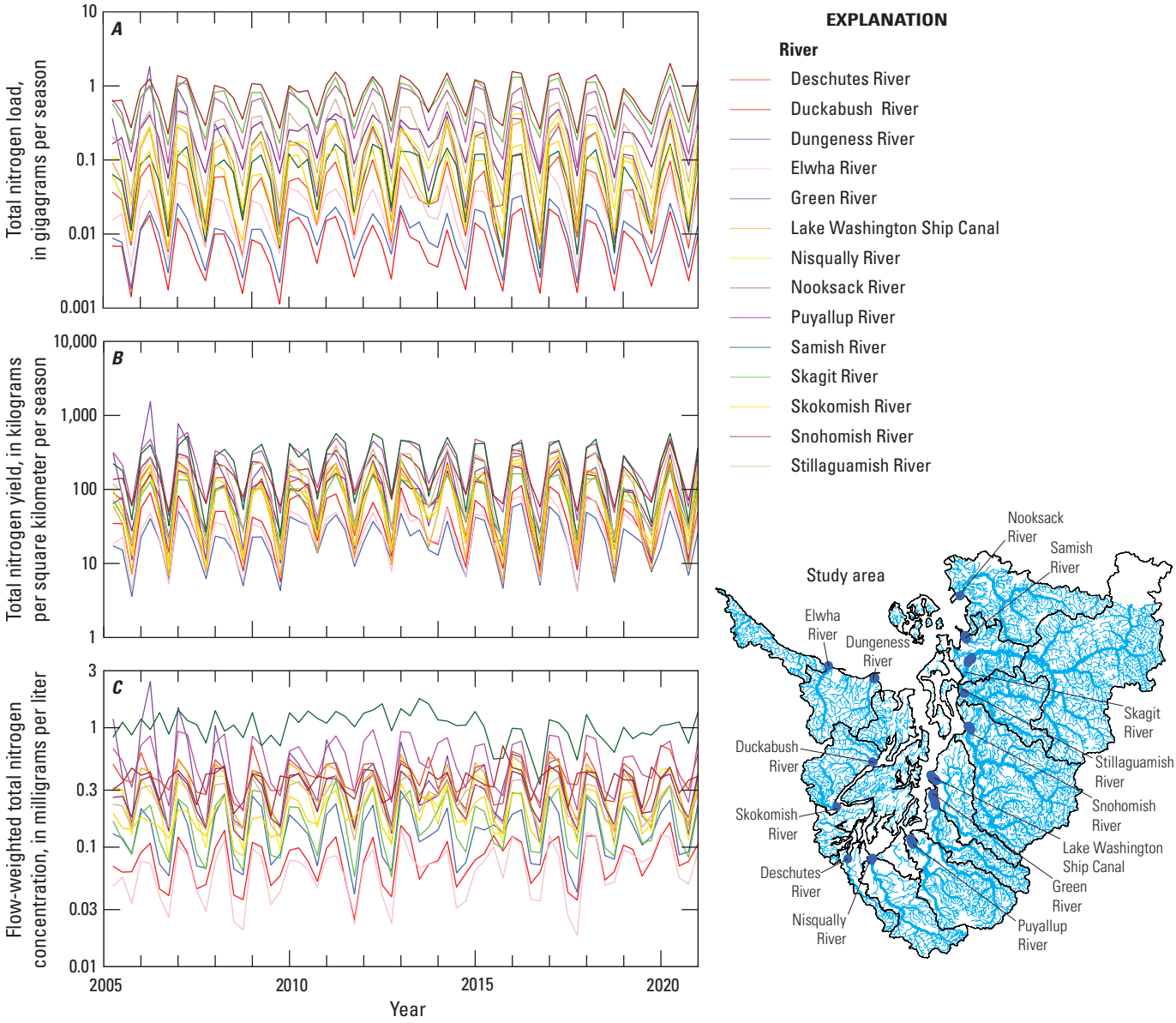

Figure 20. Predicted seasonal accumulated (*A*) total nitrogen load, (*B*) total nitrogen yield, and (*C*) flow-weighted total nitrogen concentration at the terminal outlet of 14 major rivers discharging to marine waters from the Puget Sound region, 2005 through 2020.

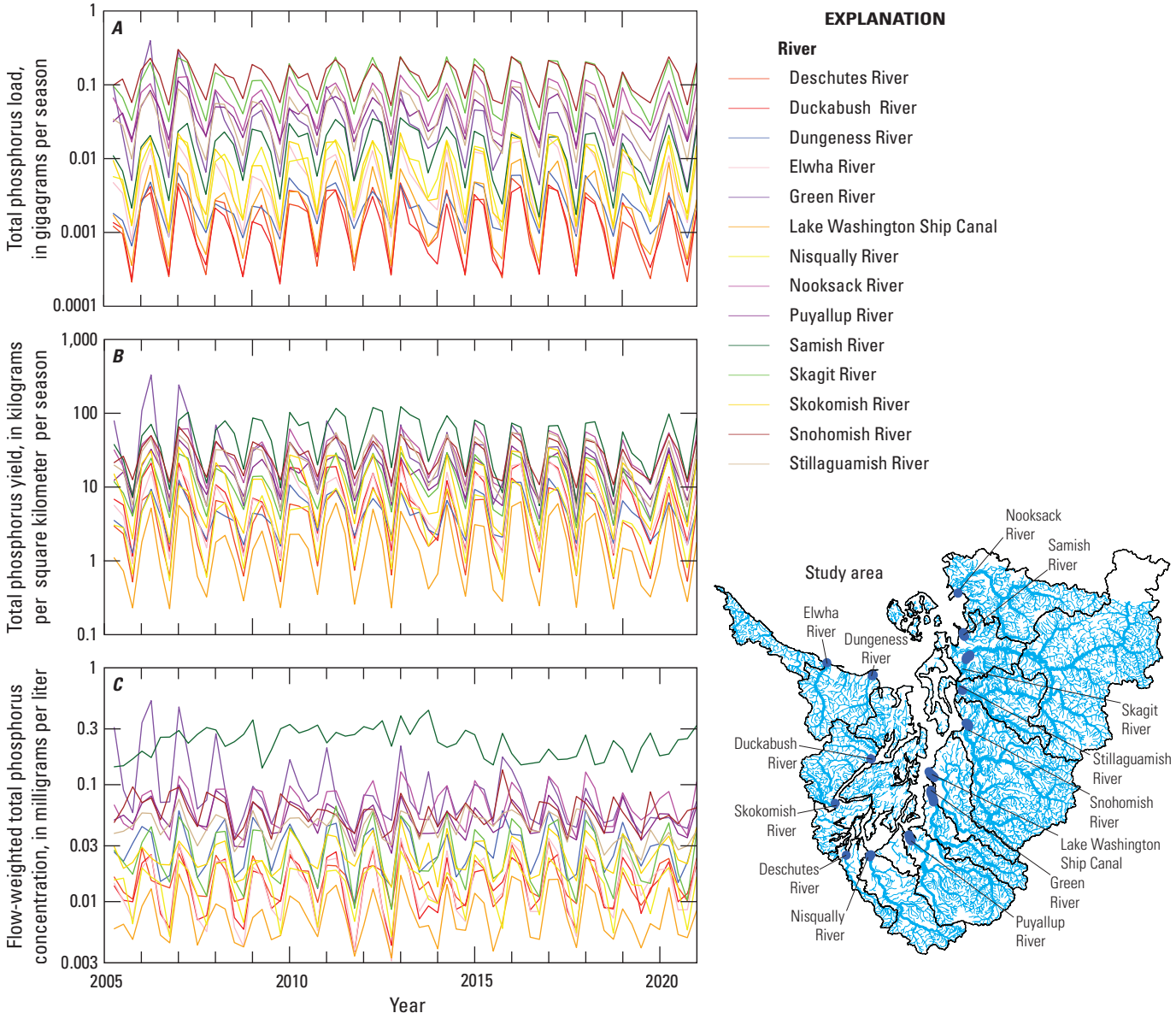

Figure 21. Predicted seasonal accumulated (*A*) total phosphorus load, (*B*) total phosphorus yield, and (*C*) flow-weighted total phosphorus concentration at the terminal outlet of 14 major rivers discharging to marine waters from the Puget Sound region, 2005 through 2020.

TN loads discharged to marine waters were consistently the largest during winter (fig. 22). Fall TN loads were also consistently large, but slightly lower compared to winter. In locations with high TN sources from red alder trees, the models suggest that leachate from fixed nitrogen was highest in winter and fall (for example, Nooksack and Skagit Rivers; fig. 22). The TN load from storage lag was highest during winter followed by fall, yet its relative contribution comprised half of the TN load during summer when loads were lowest. The largest relative TN aquatic losses also occurred during the summer when travel times and water temperature were highest.

TP load was also consistently highest in winter followed by fall; however, model results suggested that TP load from the Nooksack River was more often higher in fall than in winter (fig. 23). The seasonal lag of all nonpoint sources comprised 25–50 percent of total TP load with the highest relative contributions during spring and summer—a fraction of the larger magnitude fall and winter fluxes was lagged in delivery until the spring and summer seasons. In the Nooksack River, the components of storage lag were mostly from animal feeding operations, upland geologic material, and crop fertilizer. In the Skagit River, upland geologic material followed by urban land, and their lagged components, were the main contributors to TP load. The largest relative TP aquatic losses occurred during the summer when travel times were highest but were nearly four times lower than the relative losses of TN by aquatic decay (figs. 22 and 23).

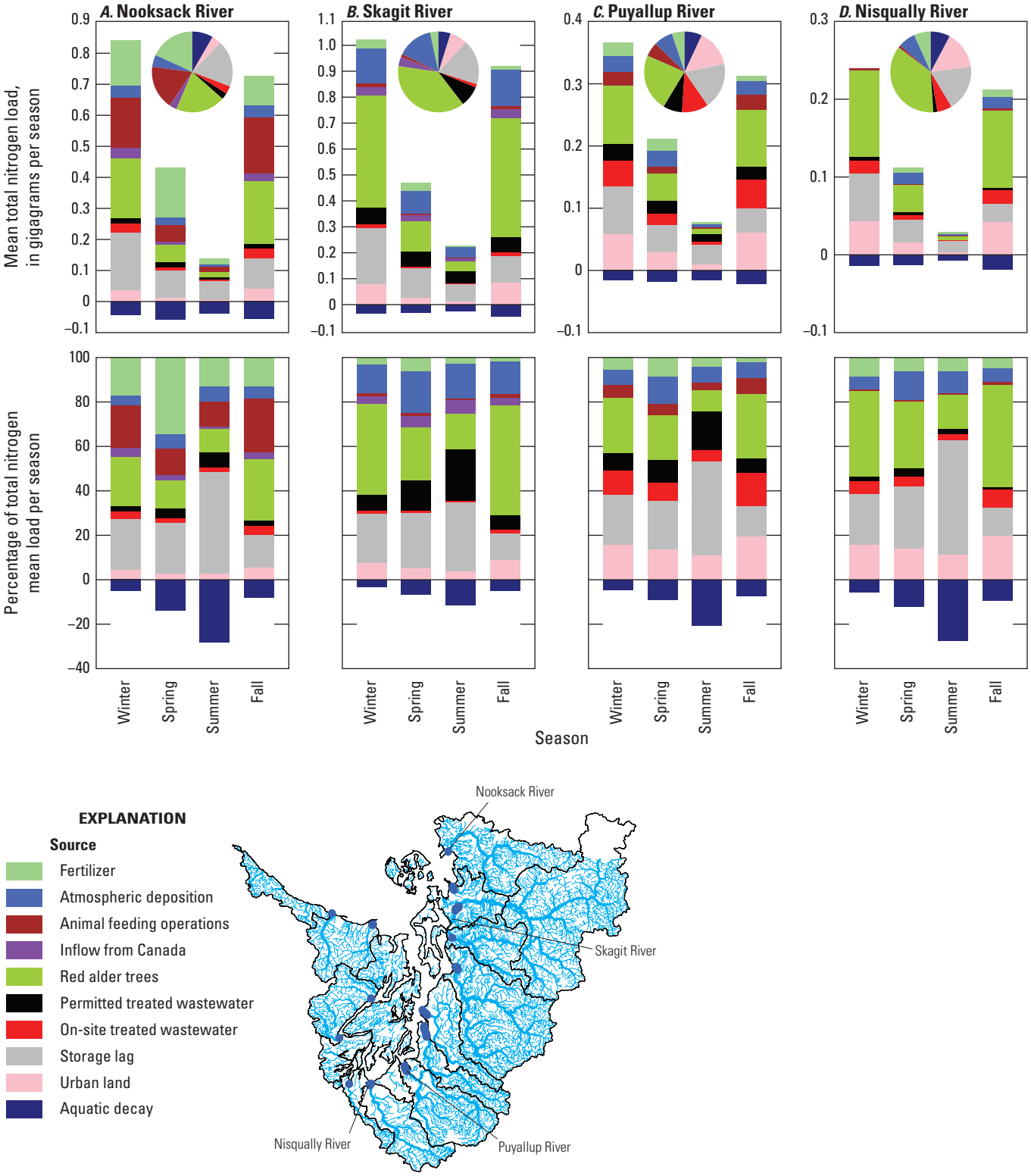

Figure 22. Predicted total nitrogen (top panel) mean seasonal accumulated load by source and as a (bottom panel) percentage for the (*A*) Nooksack River, (*B*) Skagit River, (*C*) Puyallup River, and (*D*) Nisqually River. Pie charts represent the mean source composition, 2005 through 2020. [Winter, January–March; Spring, April–June; Summer, July–September; Fall, October–December.]

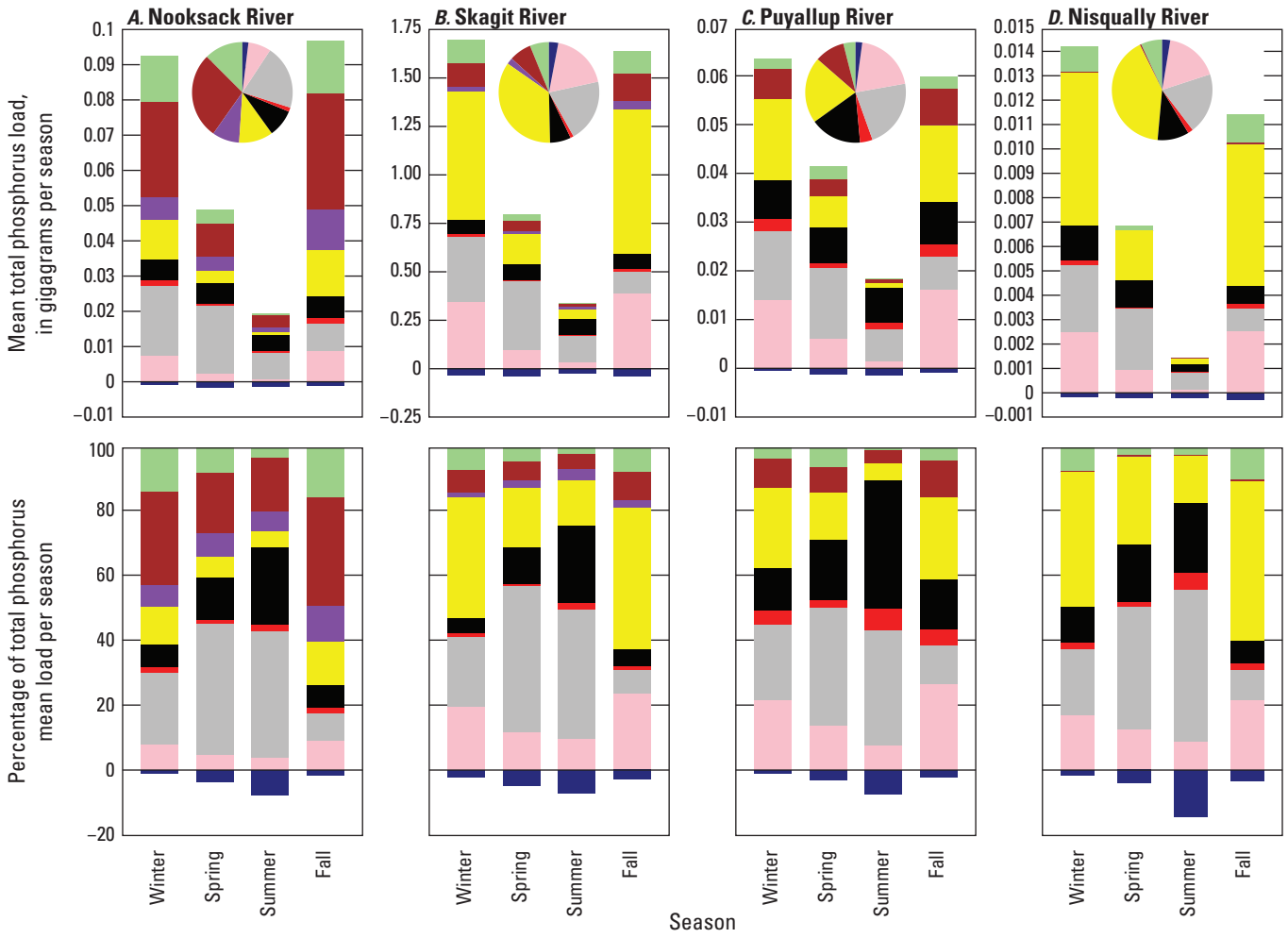

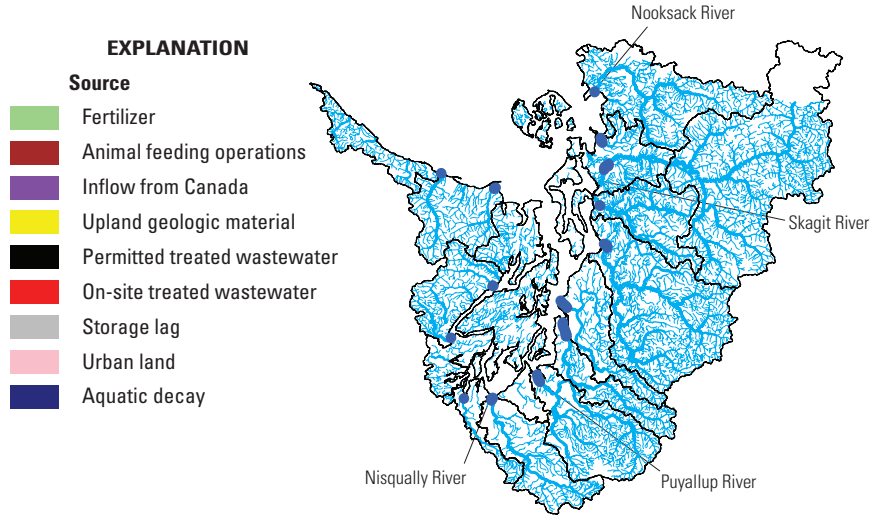

Figure 23. Predicted total phosphorus (top panel) mean seasonal accumulated load by source and as a (bottom panel) percentage for the (*A*) Nooksack River, (*B*) Skagit River, (*C*) Puyallup River, and (*D*) Nisqually River. Pie charts represent the mean source composition, 2005 through 2020. [Winter, January–March; Spring, April–June; Summer, July–September; Fall, October–December.]

Historical Red Alder and Wetland Reference Scenario

An understanding of pre-industrial nutrient reference conditions helps identify locations that may have increased in nutrient yield over time until present (defined by the study period-of-record, 2005 through 2020). Given reference datasets and appropriate assumptions, the calibrated models and coefficients could be used to run different scenarios to evaluate change. Ecology has developed datasets of pre-industrial (historical) red alder tree coverage along with historical wetland coverage (made available in Schmadel and others [2025]; figs. 24*A*, *B*). In the TN model, fixation by red alder trees was found to be a major source pathway whereas wetlands mostly do not exist today.

The shift in red alder tree coverage from historical conditions to present tended to decrease in higher elevations and increase in lower elevations (fig. 24*C*). The historical red alder tree and wetland coverages were produced using land coverages and assumptions from Collins and others (2003), Peter and Harrington (2010), and Stanley and others (2019). The historical red alder tree coverage was represented as a range to express uncertainty, and trees were assumed to exist below 762 meters in elevation (Deal and Harrington, 2006). Refer to Figueroa-Kaminsky and others (2022) and Schmadel and others (2025) for more details.

The TN model was used to run a scenario to estimate the net change in TN flux from historical conditions to the present. The present red alder tree coverage was replaced with the historical estimates, and contemporaneous anthropogenic sources were set to zero, including urban land, animal feeding operations, fertilizer, septic leachate, and point sources. Present atmospheric deposition likely contains urban influences (Conrad-Rooney and others, 2023); therefore, wet inorganic nitrogen atmospheric deposition was re-estimated following Schmadel and Peterman-Phipps (2023) using the present precipitation multiplied by an assumed spatially uniform monthly atmospheric concentration from NADP WA14 Olympic National Park-Hoh Ranger Station.

The Puget Sound region once contained many more wetlands than exist today (fig. 24*B*). In the TN scenario, reservoir waterbodies were excluded but wetlands were added to represent historical aquatic conditions. The TN model identified aquatic decay processes, but wetlands were not identified due to their present-day scarcity. Wetlands were added as an additional loss term in the scenario, assuming wetlands were a net sink in the region. However, because wetlands were not included in the calibrated model, additional assumptions were applied: based on a compilation of hundreds of literature values (Cheng and Basu, 2017), a mean TN uptake velocity of 18 m/y was assumed for wetlands. Reciprocal hydraulic load through wetlands was estimated based on the wetland area per catchment divided by a current estimate of seasonal streamflow at the outlet of that catchment. This scenario applied conditions based on a robust historical understanding of the region (Collins and others, 2003; Peter and Harrington, 2010; Stanley and others, 2019), but scenario conditions were outside of the calibration range of conditions and, therefore, caution in interpretation and use of results should be exercised. Scenario results should be further evaluated, scrutinized, and improved as new data become available.

The reference scenario results suggested an overall minor net decrease in TN flux from some headwaters but a much larger increase from valleys and coastal areas (present TN yield in many areas has increased >1,000 kilograms per square kilometer per year [kg/km^2/y] relative to historical conditions; fig. 24*D*). Aggregated by WRIA, the scenario suggests that the Cedar-Sammamish, Duwamish-Green, and Chambers-Clover WRIAs have seen the largest increases in TN flux from historical conditions to present (fig. 25), which are presently dominated by permitted treated wastewater discharge (fig. 16). The Elwha-Dungeness and Quilcene-Snow WRIAs were estimated to have the lowest increase in TN flux (figs. 24*D* and 25). Accounting for uncertainty in the historical red alder tree coverage, it was still unclear whether some WRIAs like the Upper Skagit and Skokomish-Dosewallips contributed more TN flux relative to historical conditions (fig. 25). The scenario also suggests that, even with a loss of wetlands, more TN was removed relative to historical conditions simply because TN flux has mostly increased across WRIAs—more TN delivered leads to more TN processed instream.

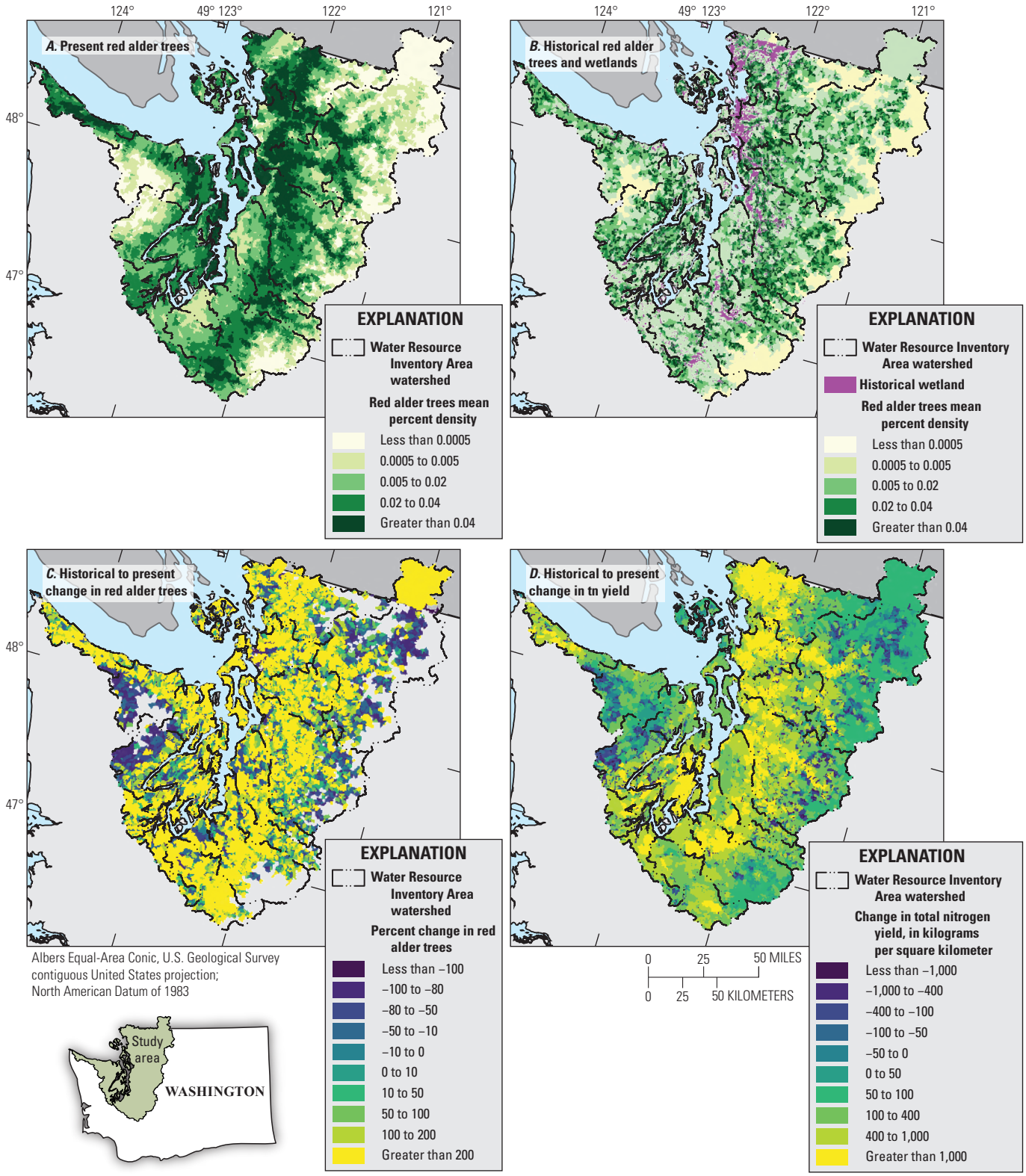

Figure 24. Maps showing (*A*) present (2005 through 2020) red alder tree density, (*B*) preindustrial historical red alder tree and wetland density, (*C*) percentage change in red alder tree coverage from historical to present conditions, and (*D*) simulated net change in total nitrogen yield from historical to current conditions.

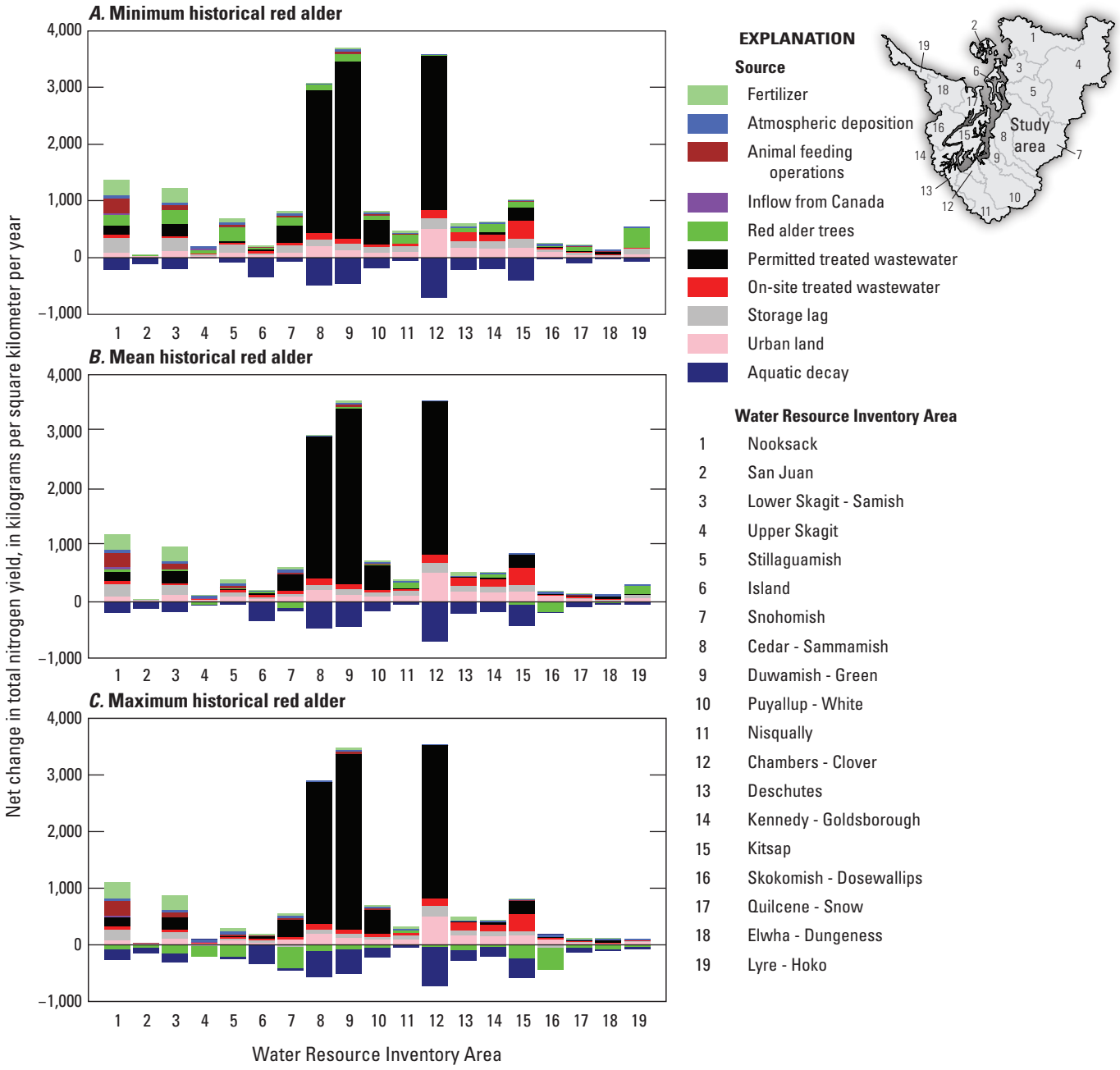

Figure 25. Reference scenario outcome of simulated net change in total nitrogen yield from pre-industrial historical to present delivered to streams and coasts within each Water Resource Inventory Area by running scenarios of (*A*) minimum, (*B*) mean, and (*C*) maximum possible estimated historical red alder tree coverage using the dynamic Puget Sound region SPARROW (SPAtially Referenced Regressions On Watershed attributes) total nitrogen model, 2005 through 2020.

Discussion

Advantages and Limitations to Modeling Approach in the Puget Sound Region

Compliance with DO standards in the bottom layers of marine waters depends on nutrient reductions to upstream freshwater sources. This includes reductions in discharge from wastewater treatment plants into marine waters and reductions from other sources of nutrient inputs from watersheds (Mohamedali and others, 2011; Ahmed and others, 2019). The SSM suggests that marine waters of the Salish Sea are TN limited whereas freshwaters are more typically TP limited—higher TP yield can result in increased primary productivity and thus higher delivery of organic carbon loads (Ahmed and others, 2019). Thus, any reduction of TN should be considered with TP and vice versa. Predicting the time of year marine inlets are most vulnerable to low marine DO concentrations requires information regarding when and where TN and TP loads are delivered from the Puget Sound region. In other words, representation of the temporal variability of nutrient delivery across the region may be more important to Ecology's PSNSRP than a mean spatial distribution of loads previously provided at annual timesteps when dynamic loads are likely to contribute to low marine DO. The seasonal TN and TP models developed here help inform the regional assessment of major sources, demonstrate how loads and concentrations varied seasonally and spatially, and define the primary drivers of those loads, including lagged components beyond what was capable from previous annual approaches (figs. 22 and 23). The dynamic SPARROW models are useful for evaluation and implementation of nitrogen reduction actions initiated in the PSNSRP, and perhaps more broadly for watershed management to meet approved freshwater DO TMDLs. The U.S. Environmental Protection Agency's River Basin Export Reduction Optimization Support Tool (RBEROST; Chamberlin and others, 2022) is an example of a tool that can incorporate the dynamic SPARROW output to help managers identify best management practices (BMPs) to reduce nutrient loading from the Puget Sound region on a seasonal basis.

The dynamic modeling approach described in this report linked many unique datasets to physically based equations through statistical coefficients that provided useful interpretation of nutrient source pathways and processes accumulating throughout the stream network (tables 2 and 5). For example, the TN model quantified mass delivery rates estimated from animal feeding operations and on-site treated wastewater systems at 8.4 kg of TN per animal per year and 4.5 kg of TN per household per year, respectively (table 2). For TP, the rate of mass from animal feeding was relatively higher than for septic systems (2.3 kg of TP per animal and 0.2 kg TP per household per year, respectively; table 5), suggesting that more TN comes from septic compared to TP while more TP comes from animal feeding operations compared to TN, which is similar to patterns found in other locations in the Cascade Range (Anderson, 2002).

Urban land was treated as a lumped coverage source pathway, estimated to yield an additional 802 kilograms per square kilometer per year (kg/km^2/y) TN and 79 kg/km^2/y TP (tables 2 and 5). Compared to previous approaches, those urban values were generally higher (246 kilograms per year [kg/y] TN and 12 kg/y TP in the Pacific region model by Wise [2019]; 122 kg/y TN and 64 kg/y TP in the Midwest model by Robertson and Saad [2019]; and 150 kg/y TN and 24 kg/y TP in the Illinois model by Schmadel and others [2024]). Differences in urban coefficients could reflect some regional variation; the models developed for the Puget Sound region were much smaller in spatial size than previously attempted. Urban land comprised 12 percent of the Puget Sound region where coefficients represent the relative mean contributions for this region. Additionally, in the TN model, a new variable that represents stormwater outfall density interacted with the urban source variable, which caused the mean urban TN yield to nearly double from around 400 to over 800 kg/km^2/y. The larger coefficient value suggests that, during higher precipitation intensity, more diluted stormwater went through the outfalls. It also suggests that additional source pathways are represented from atmospheric deposition with precipitation falling on impervious surfaces. A negative coefficient identified for stormwater outfall density indicated that sources from urban areas were reduced during higher precipitation, and other sources like atmospheric deposition were more dominant, but it also indicated that urban areas may be a dominant source during drier periods. A negative coefficient also suggests that there may be some potential effects of recently implemented BMPs in the stormwater conveyance systems (Figueroa-Kaminsky and others, 2022) but were not explicitly represented by the model.

TN leachate from red alder tree nitrogen fixation was estimated as 0.36 kg of TN fixed and produced by each square meter of trees per year (table 2), a value comparable to previous SPARROW applications (0.27 kilograms per square meter per year [kg/m^2/y TN], Wise [2019]) and field estimates of fixation rates (0.31 kg/m^2/y of nitrogen [N], Compton and others [2003]). However, that value does not directly translate to the TN flux exported from a watershed—fixed TN is accumulated and decomposed in the soils and later leached out. Therefore, across all WRIAs, the mean yield estimated by the TN model was 200 kg/km^2/y N produced by red alder trees (fig. 16). For watersheds dominated by red alders, the mean yield increased to over 2,000 kg/km^2/y N. Likewise, Compton and others (2003) further estimated that the fixation rate of 0.31 kg/m^2/y N in watersheds dominated by red alder trees could yield between 2,600 and 3,900 kg/km^2/y N from a watershed. The TN model's representation of red alder tree fixation compared well to field measurements, but it is possible that the correlation to the coverage dataset represented more than just red alder trees and included additional nitrogen-fixing species such

as lichens and maples (Compton and others, 2003). Further tests with the TN model using other vegetation datasets could be fruitful toward improved source pathway representation. However, inclusion of red alder tree coverage as a source input dataset greatly improved the TN model performance and was far better compared to other similar datasets such as NLCD forested cover.

The storage lag coefficients for the TN and TP models were 0.25 and 0.29, respectively (tables 2 and 5), indicating that 25 percent and 29 percent of contemporaneous nonpoint TN and TP source inputs were lagged in storage repositories each season and delivered to streams in later seasons, respectively. That estimate suggests that mean seasonal flux of nutrients was relatively fast in which a large portion of any source input passing through the storage repository got flushed through each year. Likewise, the relative contribution of storage lag was lowest during high load and streamflow conditions, yet retention caused an increased lagged contribution of mass as watersheds dried out. Models quantify a bulk retention rate and thus caution should still be exercised if used to interpret lagged timescales as that retention rate currently lumps many timescales. For example, urban nonpoint sources may be stored very briefly (a lower α_S with a faster timescale and lower lag effect [eq. 6]) compared to agricultural sources more connected to groundwater (a larger α_S with a slower timescale). If the stream or waterbody was also contributing to temporary storage instead of operating solely as a sink, α_S could be further biased toward faster timescales. Additional parsing or representation of different types of storage retention may be an area for improved nutrient prediction.

The relative net aquatic decay of TN and TP in streams was highest in summer during the longest travel times (figs. 22 and 23). TN and TP instream decay rates were comparable to the empirical estimates by Sheibley and others (2015) for nitrate (0.59 m/d) and orthophosphate (0.36 m/d) in the Puget Sound region. Consistent with field studies elsewhere (Miller and others, 2016), instream decay of nitrogen increased with water temperature, mostly during summer (fig. 13*A*). Sheibley and others (2015) found additional loss explanation with channel attributes. For example, they noted higher decay with higher sinuosity yet lower decay in channels with higher slopes, particularly for phosphorus. The SPARROW models are flexible in that more terms could be added and tested (refer to eq. 4). For example, adding slope in the TP model stream decay expression could improve explanation. However, slope has already been factored into the estimate of TP loss with Jobson velocity and depth derived from streamflow. Likewise, higher streamflow did not return significant instream TP decay (table 5).

Aquatic nitrogen and phosphorus storage may be temporary (Valett and others, 2022), especially in spring and summer associated with seasonal stratification in reservoirs and uptake by algae and aquatic vegetation or permanently removed through processes such as denitrification (Harvey and others, 2013). In addition, particulate phosphorus is often stored seasonally or longer in reservoirs, especially after dam construction, which at later times becomes susceptible to releases with increased sediment infill or following summer stratification and changes in sediment from reduction-oxidation processes (Posch and others, 2012). Processes related to dam removal were not explicitly represented by the TN and TP models. For example, a dam was removed on the Elwha River in 2013, and the downstream calibration station reflected a large increase in downstream TP load while TN load was less affected. That increase in TP load was likely mass previously stored in the reservoir and not explicitly accounted for in the model. Therefore, that downstream calibration station was excluded from the TP model—another dataset or process such as suspended sediment could improve representation of mass stored and released. Both models tended to over predict load from the Skokomish-Dosewallips WRIA, which is an indication that upstream influences from, for example, Lake Cushman, perhaps were not well represented (figs. 8, 9, and 1.1).

The modeling approach described in this report has proven useful for quantifying seasonal sources and drivers of nutrient load across the region but also identified challenges, limitations, and possible areas for improvement. Across the Puget Sound region, the overall mean error was 50 percent for the TN simulated load and 72 percent for the TP simulated load (tables 4 and 7). Although those results are considered promising, compared to the TN model, the TP model source pathways were more challenging to identify—possibly due to a lack of representation of erosion caused by human activity and high precipitation—and coefficients still contained large levels of uncertainty after adjusting for effects of serial correlation. There may be additional processes like mass stored and released by reservoirs not explicitly represented. Likewise, load estimation of the calibration data consistently returned higher errors for TP compared to TN, especially using the WRTDS_K approach. Also compared to the TP model, calibration of the TN model seemed more straightforward where most of the variation in calibration load data could be explained using only the source pathway variables interacting only with seasonal precipitation.

If error is large in any one source pathway, an option is sometimes to lump that pathway with another or altogether exclude one of the pathways. If a pathway is excluded, error in other coefficients might decrease, but the model will likely inaccurately assign mass to a defined pathway. For example, excluding the septic source pathway from the TP model could cause the animal feeding pathway coefficient to increase, sometimes by ten-fold; that animal feeding pathway coefficient would have a smaller standard error and *p*-value by excluding the septic source pathway, but it would not necessarily produce a better model if septic systems are in reality an independent source pathway—a higher animal feeding coefficient may increase just to compensate for the model missing septic contributions.

Regional-scale modeling is an efficient way to simulate water quality in streams but requires simplifications of processes and thus that may not account for specific conditions at unique locations. Likewise, a model can lack process representation if a key dataset is missed, or if data are not sufficient to separate and track a unique source pathway. For example, a mismatch in timing between simulation and observation at a few locations indicated a potential missing source pathway or land-to-water delivery information such as erosion rates during high precipitation. At the TP stations 01A120 and 01A050, for example, the TP model mostly missed the timing of observed load for 2007 through 2009 and then again in 2013 and 2014, but the model was nearly representative of instream load for 2017 through 2020 (fig. 11). It could be that some process or change in land use or management in the Nooksack WRIA occurred during the modeling period that affected TP load more so than TN load but was not explicitly represented by data and model coefficients. Management activities and BMPs not explicitly represented with data and coefficients, such as the inclusion of a dataset representing stormwater detention ponds, are areas to look for improvements. Similarly, as dam removal on the Elwha River caused large effects on instream TP load, sudden release of stored TP in reservoirs was not a process explicitly represented. Sediment transport processes are likely candidates for improving the TP load representation, but dam removal on the Elwha River was unprecedented and unlikely to represent any viable management actions for the region. Although independence in data is a limiting assumption, the SPARROW framework is uniquely suited for improvements to process representation and model error by its ability to include new interactions, processes, or datasets. Data representing the amount of stored mass in a reservoir, the age of the stored mass, together with dam release rates, potentially could improve model representation of TP load. However, the Elwha River contributed a smaller fraction of TP mass relative to some of the other WRIAs (1.5 percent of regional total; fig. 17; table 2.2), and thus additional data added to the Elwha-Dungeness WRIA may improve local accuracy but not necessarily improve overall model performance across the region.

Potential Model Improvements in the Puget Sound Region

A comprehensive quantification of source attribution and accumulation across space and time is helpful to assess where and how nutrient reductions could be most effective, but several limitations in the TN and TP models were identified. Although the models are useful to identify where error is low and high, and perhaps identify where other data are needed, the lumped process representation and seasonal timestep could be improved through further parsing of the lumped storage lag into more bins of different timescales (for example, nutrients lagged in groundwater versus in soils; Miller and others, 2024), integration of other data (for example, estimates of groundwater discharge), integration with other models (for example, transit time distribution of the subsurface or machine learning techniques), and with updated expressions of aquatic decay and wetland losses to potentially allow for estimation of any net sources from streams and waterbodies.

Better data integration, improvements to data processing and assumptions, or simply considering more data to test in calibration could improve process representation and quantification of source pathways. A first step could be increasing the number of calibration stations. The goal for the Puget Sound region, which is consistent with most water-quality models, was to include as many calibration stations as possible to reduce the weight of any single station used to explain error and comprehensively represent observed instream mass across space and time (in other words, represent gradients of the region). Coverage of calibration stations for the Puget Sound region was considered sufficient to represent variability across the region, but a few smaller WRIAs did not contain monitored data and half of the WRIAs contained only one or two stations mostly located low in the basin far away from headwaters (fig. 3). A few more calibration stations located more toward headwaters could improve process representation by explaining more variability and thus accuracy of simulation timing and magnitude or could further indicate if and where source pathway data may be missing or even misleading. There was consideration of expanding the model domain size to include more calibration stations and gradients. However, there is value in having Puget Sound region-specific models for faster simulations and more focused data collection and compilation efforts, which may allow for identification of source pathways unique to the region that might not otherwise be identified with a larger scale model. There were just enough stations to cover most of the region; a larger scale model may better represent variability in climatic and atmospheric drivers, but in exchange it may provide less isolated source information.

The effort to compile data for the TN and TP models was comprehensive yet there were still many datasets not used in the TN and TP models for a variety of reasons. While there are many other areas of potential data improvements to consider, more data do not always indicate that a better model is possible. For example, other data types may contain strong serial correlation—adding more constant variables can increase noise or cause issues with multicollinearity if also correlated with similar datasets. Other data types considered in the models included permeability, historical wildfire extent, mean percentage snow cover, and tile drainage, yet none were found significant or to improve models. There may be additional sources from springs (Rohde and others, 2024), but the springs dataset correlated well in space with urban cover. It is possible the urban source pathway contains a spring component, but it also may be coincidence that urban development falls closely where springs discharge into valleys at mountain fronts. Therefore, more exploration into

those possible source pathways, and whether they would be considered separate or interacting pathways, could improve interpretation of the urban pathway.

Likewise for stormwater outfalls as both dilution and source delivery pathways, the explicit collection area for each outfall was not directly mapped or estimated. More data processing, and perhaps collection, would be needed to better isolate and represent the outfall component, but outfall size and collection area variables established consistently across the region could improve outfall representation in the models. Concentrations have been collected in some outfalls and such data would help quantify fluxes (Figueroa-Kaminsky and others, 2022), but those data would be needed consistently and comprehensively to represent outfall effects in the models. It is possible that the TN model is also picking up BMPs in the stormwater conveyance systems and it could be useful to separate and quantify the effects of BMPs, but that also would require additional data and further testing to establish a clear and significant statistical interaction to be a consistent variable used to represent a particular BMP (Detenbeck and others, 2018). Inconsistencies in datasets like BMPs or stormwater outfalls instead could be expressed as noise error and thus further limit model interpretation.

Near-term improvements to aquatic decay functions could be made using datasets such as reservoir volumes and operations, showing possible stratification, and improved local streamflow estimated through better dynamic estimation of water use and diversions. Net aquatic TN losses were occurring in streams with additional evidence that rates increased with water temperature (table 2; fig. 13*A*). Net TN losses in waterbodies, however, were not as clearly identified, suggesting that waterbodies were not removing much TN relative to streams. TP decay coefficients were difficult to identify for streams—if the overall net effect of streams was near zero, even if gross aquatic losses and sources are present, it is unlikely to identify a model coefficient different than zero. However, once the TP stream decay coefficient was set to estimate a loss for streamflow conditions below the annual mean, which assumes losses are occurring during lower streamflow, a significant stream decay process was quantified. Differences in net decay rates during different hydrologic conditions suggest that some temporary storage of mass in streams and waterbodies was likely occurring, particularly for TP. Although a net decay assumption is a model limitation, some reality in varying decay rates was still mimicked based on adjustments with streamflow and water temperature.

The seasonal mass balance representation of streams from headwaters to marine-water discharge points by source is important information to support Ecology's nutrient reduction plan. Certainly, there are limitations with process representation and simulation accuracy, but the modeling approach directly provided real, interpretable values. A mass balance has been a cornerstone upon which interpretation depends. Although model uncertainty can be high when zoomed into unique reaches (50–72 percent mean error), an ability to quantify uncertainty in space and time is a strength—the models and their residuals can be useful toward identifying locations where data and understanding are lacking. The seasonal mass balance simulations also provide a dataset for further analyses or modeling. For example, seasonal loads could provide boundary conditions, or a point of comparison, for more localized and detailed water-quality studies.

Improvements to simulation accuracy and resolution of nutrient conditions may be possible with a machine learning (ML) modeling approach, capable of producing results at a daily timestep (Basu and others, 2023). Common critiques of ML models, however, are limited process interpretability and possible overparameterization as sometimes hundreds of variables are used (Maier and others, 2024). If the most important information is daily simulations of instream nutrient concentrations entering marine waters, an ML model might be favorable. However, some type of ML-mechanistic hybrid modeling framework may be the most useful approach to support Ecology's needs of dynamic knowledge of nutrient delivery to marine waters by major source pathway. Next steps that build on the models developed here need to retain interpretable mass-balance information that include estimation of aquatic processes.

Summary

Watershed models were developed to simulate seasonal load of total nitrogen (TN) and total phosphorus (TP) discharging into the Washington State waters of the Salish Sea from 2005 through 2020. The modeling approach used was dynamic SPARROW (SPAtially Referenced Regressions On Watershed attributes), a statistical-physical watershed modeling technique that provided interpretation of sources and pathways, evaluation of sub-watershed contributions throughout the stream network, and estimation of loads delivered to marine waters at surface confluences along the shoreline. Seasonal models comprehensively tracked nine different TN and eight different TP source pathways. Treated wastewater discharge and hatchery point sources and nonpoint sources from crop fertilizer, animal feeding operations, septic systems, urban land, atmosphere deposition (TN only), nitrogen fixation by *Alnus rubra* Bong. (red alder) trees (TN only), background geologic material (TP only), and the seasonal storage lag component of those nonpoint sources were identified and quantified. The nutrient load magnitudes and source composition varied by watershed, and even within each watershed, yet the largest loads discharged to marine waters typically occurred in winter and fall, with the largest sources being from treated wastewater followed by nitrogen-fixing red alder trees, animal feeding operations, upland geologic material, crop fertilizer, urban land, and storage lag. TN and TP loads were typically lowest in summer when relative instream losses were highest. Considering the influence of upstream watershed contributions of nutrients

to their marine-discharge points, a few hundred locations modeled here, is a key aspect of Ecology's current Puget Sound Nutrient Source Reduction Project (PSNSRP). The estimated seasonal TN and TP loads across the Puget Sound region from 2005 through 2020 help clarify contributions from discernible point and nonpoint sources and when, where, and why they are high. The Snohomish and Skagit Rivers discharged the largest TN and TP loads, yet the Samish River was shown to have the highest TN and TP yields and concentrations. Additionally, a reference scenario was developed to provide an estimate of the pre-industrial local and regional loads, which indicated that the largest increases in TN yield from historical conditions to present (2005 through 2020) were from the Cedar and Green Rivers and from the Chambers-Clover Creeks watershed in Pierce County, Washington. With appropriate datasets and assumptions, the models could be used to evaluate other scenarios or used to forecast loads.

References Cited

Ahmed, A., Figueroa-Kaminsky, C., Gala, J., Mohamedali, T., Pelletier, G., and McCarthy, S., 2019, Puget Sound nutrient source reduction project, volume 1—Model updates and bounding scenarios: Olympia, Wash., Washington State Department of Ecology, publication 19-03-001, 102 p. accessed January, 2022, at https://apps.ecology.wa.gov/publications/SummaryPages/1903001.html.

Alexander, R.B., Smith, R.A., and Schwarz, G.E., 2000, Effect of stream channel size on the delivery of nitrogen to the Gulf of Mexico: Nature, v. 403, no. 6771, p. 758–761, accessed July, 2021, at https://doi.org/10.1038/35001562.

Anderson, C.W., 2002, Ecological effects on streams from forest fertilization—Literature review and conceptual framework for future study in the western Cascades: U.S. Geological Survey Water Resources Investigations Report 01–4047, 49 p., accessed March, 2022, at https://pubs.usgs.gov/wri/2001/4047/wri01-4047.pdf.

Basu, N.B., Dony, J., Van Meter, K.J., Johnston, S.J., and Layton, A.T., 2023, A random forest in the Great Lakes—Stream nutrient concentrations across the transboundary Great Lakes Basin: Earth's Future, v. 11, no. 4, article e2021EF002571, accessed August, 2024, at https://doi.org/10.1029/2021EF002571.

Böhlke, J.K., Antweiler, R.C., Harvey, J.W., Laursen, A.E., Smith, L.K., Smith, R.L., and Voytek, M.A., 2009, Multi-scale measurements and modeling of denitrification in streams with varying flow and nitrate concentration in the upper Mississippi River Basin: Biogeochemistry, v. 93, nos. 1–2, p. 117–141, accessed January, 2022, at https://doi.org/10.1007/s10533-008-9282-8.

Chamberlin, C., Detenbeck, N., ten Brink, M., Le, A., Munson, K., Morin, I., Marks, M., and Li, Y., 2022, River Basin Export Reduction Optimization Support Tool (RBEROST) user guide (ver. 1.15): U.S. Environmental Protection Agency, accessed June, 2024, at: https://github.com/USEPA/RBEROST.

Cheng, F.Y., and Basu, N.B., 2017, Biogeochemical hotspots—Role of small water bodies in landscape nutrient processing: Water Resources Research, v. 53, no. 6, p. 5038–5056, accessed January, 2022, at https://doi.org/10.1002/2016WR020102.

Collins, B.D., Montgomery, D.R., and Sheikh, A.J., 2003, Reconstructing the historical riverine landscape of the Puget Lowland, *in* Montgomery, D.R., Bolton, S.M., Booth, D.B., and Wall, L., eds., Restoration of Puget Sound rivers: Seattle, Wash., University of Washington Press, p. 79–128., accessed May, 2022, at https://faculty.washington.edu/bcollins/publications_pdfs/Collins_et_al_2003_Reconstructing_the_historical_riverine_landscape_of_the_Puget_Lowland.pdf.

Compton, J.E., Church, M.R., Larned, S.T., and Hogsett, W.E., 2003, Nitrogen export from forested watersheds in the Oregon Coast Range—The role of N2-fixing red alder: Ecosystems, v. 6, no. 8, p. 773–785., accessed June, 2022, at https://doi.org/10.1007/s10021-002-0207-4.

Conrad-Rooney, E., Gewirtzman, J., Pappas, Y., Pasquarella, V.J., Hutyra, L.R., and Templer, P.H., 2023, Atmospheric wet deposition in urban and suburban sites across the United States: Atmospheric Environment, v. 305, p. 119783, accessed September, 2024, at https://doi.org/10.1016/j.atmosenv.2023.119783.

Deal, R.L., and Harrington, C.A., 2006, Red alder—A state of knowledge: Portland, Oreg., U.S. Department of Agriculture Pacific Northwest Research Station, General Technical Report PNWGTR-669, 150 p., accessed January, 2022, at https://www.fs.usda.gov/pnw/olympia/silv/publications/opt/531_DealHarrington2006-PartA.pdf. [Also available at https://doi.org/10.2737/PNW-GTR-669.]

Detenbeck, N., Piscopo, A., Tenbrink, M., Weaver, C., Morrison, A., Stagnitta, T., Abele, R., Leclair, J., Garrigan, T., Zoltay, V., Brown, A., Le, A., Stein, J., and Morin, I., 2018, Watershed management optimization support tool v3: Washington, DC, U.S. Environmental Protection Agency, EPA/600/C-18/001, accessed January, 2022, at https://www.epa.gov/hydrowq/wmost.

Dewitz, J., and U.S. Geological Survey, 2021, National Land Cover Database (NLCD) 2019 products: U.S. Geological Survey data release, accessed January, 2022, at https://doi.org/10.5066/P9KZCM54.

Figueroa-Kaminsky, C., Wasielewski, J., Schmadel, N., McCarthy, S., Wise, D., Johnson, Z., and Black, R., 2022, Quality assurance project plan—Puget Sound Spatially Referenced Regression on Watershed attributes (SPARROW): Olympia, Wash., Washington State Department of Ecology publication 22-03-109, 76 p., accessed August, 2024, at https://apps.ecology.wa.gov/publications/SummaryPages/2203109.html.

Harvey, J.W., Böhlke, J.K., Voytek, M.A., Scott, D., and Tobias, C.R., 2013, Hyporheic zone denitrification—Controls on effective reaction depth and contribution to whole-stream mass balance: Water Resources Research, v. 49, no. 10, p. 6298–6316, accessed January, 2022, at https://doi.org/10.1002/wrcr.20492.

Hirsch, R.M., Archfield, S.A., and De Cicco, L.A., 2015, A bootstrap method for estimating uncertainty of water quality trends: Environmental Modelling & Software, v. 73, p. 148–166, accessed January, 2022, at https://doi.org/10.1016/j.envsoft.2015.07.017.

Hirsch, R.M., Moyer, D.L., and Archfield, S.A., 2010, Weighted Regressions on Time, Discharge, and Season (WRTDS), with an application to Chesapeake Bay River inputs: Journal of the American Water Resources Association, v. 46, no. 5, p. 857–880, accessed January, 2022, at https://doi.org/10.1111/j.1752-1688.2010.00482.x.

Jobson, H.E., 1996, Prediction of traveltime and longitudinal dispersion in rivers and streams: U.S. Geological Survey Water-Resources Investigations Report 96–4013, 69 p., accessed October, 2021, at https://pubs.usgs.gov/wri/1996/4013/documents/dispersion.pdf.

King County, 2024, Hydrologic information center data download: King County, Wash. Water and Land Resource Division database, accessed May, 22, 2022, at https://green2.kingcounty.gov/hydrology/Data.aspx.

Konrad, C.P., 2019, Seasonal precipitation influences streamflow vulnerability to the 2015 drought in the western United States: Journal of Hydrometeorology, v. 20, no. 7, p. 1261–1274, accessed July, 2022, at https://doi.org/10.1175/JHM-D-18-0121.1.

Konrad, C.P., and Voss, F.D., 2012, Analysis of streamflow-gaging network for monitoring stormwater in small streams in the Puget Sound Basin, Washington: U.S. Geological Survey Scientific Investigations Report 2012–5020, 16 p., accessed July, 2022, at https://pubs.usgs.gov/sir/2012/5020/pdf/sir20125020.pdf. [Also available at https://doi.org/10.3133/sir20125020.]

Lee, C.J., Hirsch, R.M., and Crawford, C.G., 2019, An evaluation of methods for computing annual water-quality loads: U.S. Geological Survey Scientific Investigations Report 2019–5084, 59 p., accessed August, 2022, at https://doi.org/10.3133/sir20195084.

Lee, C.J., Hirsch, R.M., Schwarz, G.E., Holtschlag, D.J., Preston, S.D., Crawford, C.G., and Vecchia, A.V., 2016, An evaluation of methods for estimating decadal stream loads: Journal of Hydrology, v. 542, p. 185–203.

Leopold, L.B., and Maddock, T., 1953, The hydraulic geometry of stream channel and some physiographic implications: U.S. Geological Survey Professional Paper 252, 64 p.

Maier, H.R., Taghikhah, F.R., Nabavi, E., Razavi, S., Gupta, H., Wu, W., Radford, D.A.G., and Huang, J., 2024, How much X is in XAI—Responsible use of "explainable" artificial intelligence in hydrology and water resources: Journal of Hydrology X, v. 25, p. 100185., accessed September, 2024, at https://doi.org/10.1016/j.hydroa.2024.100185.

McCabe, G.J., and Wolock, D.M., 2011, Independent effects of temperature and precipitation on modeled runoff in the conterminous United States: Water Resources Research, v. 47, no. 11, p. 2011WR010630., accessed January, 2022, at https://doi.org/10.1029/2011WR010630.

McCarthy, S., 2019, Puget Sound nutrient synthesis report, part 2—Comparison of nutrient watershed load estimates: Olympia, Wash., Washington State Department of Ecology publication 19-03-019, 76 p., accessed June, 2022, at https://apps.ecology.wa.gov/publications/documents/1903019.pdf.

McMahon, G., Alexander, R.B., and Qian, S., 2003, Support of total maximum daily load programs using spatially referenced regression models: Journal of Water Resources Planning and Management, v. 129, no. 4, p. 315–329.

Miller, M.P., Tesoriero, A.J., Capel, P.D., Pellerin, B.A., Hyer, K.E., and Burns, D.A., 2016, Quantifying watershed-scale groundwater loading and in-stream fate of nitrate using high-frequency water quality data: Water Resources Research, v. 52, no. 1, p. 330–347, accessed May, 2022, at https://doi.org/10.1002/2015WR017753.

Miller, O.L., Putman, A.L., Smith, R.A., Schwarz, G.E., Hess, M.D., McDonnell, M.C., and Jones, D.K., 2024, Temporal variability in irrigated land and climate influences on salinity loading across the upper Colorado River Basin, 1986–2017: Environmental Research Letters, v. 19, no. 2, p. 024008, accessed August, 2024, at https://doi.org/10.1088/1748-9326/ad18dd.

Mohamedali, T., Roberts, M., Sackmann, B., and Kolosseus, A., 2011, Puget Sound dissolved oxygen model nutrient load summary for 1999–2008: Olympia, Wash., Washington State Department of Ecology publication 11-03-057, 172 p., accessed July, 2022, at https://apps.ecology.wa.gov/publications/summarypages/1103057.html.

Moriasi, D., Arnold, J., Van Liew, R., Bingner, R., Harmel, R., and Veith, T., 2007, Model evaluation guidelines for systematic quantification of accuracy in watershed simulations: American Society of Agricultural and Biological Engineers, v. 50, no. 3, p. 885−900.

Mulholland, P.J., Helton, A.M., Poole, G.C., Hall, R.O., Hamilton, S.K., Peterson, B.J., Tank, J.L., Ashkenas, L.R., Cooper, L.W., Dahm, C.N., Dodds, W.K., Findlay, S.E.G., Gregory, S.V., Grimm, N.B., Johnson, S.L., McDowell, W.H., Meyer, J.L., Valett, H.M., Webster, J.R., Arango, C.P., Beaulieu, J.J., Bernot, M.J., Burgin, A.J., Crenshaw, C.L., Johnson, L.T., Niederlehner, B.R., O'Brien, J.M., Potter, J.D., Sheibley, R.W., Sobota, D.J., and Thomas, S.M., 2008, Stream denitrification across biomes and its response to anthropogenic nitrate loading: Nature, v. 452, no. 7184, p. 202–205, accessed April, 2022, at https://doi.org/10.1038/nature06686.

National Atmospheric Deposition Program, 2022, National Atmospheric Deposition Program, National Trends Network: Monthly concentrations, accessed March 3, 2023, at https://nadp.slh.wisc.edu/networks/national-trends-network/.

National Oceanic and Atmospheric Administration, 2022a, National Water Model, 2022, CONUS Retrospective Dataset: National Oceanic and Atmospheric Administration [NOAA] CONUS retrospective dataset webpage, accessed December 1, 2022, at https://registry.opendata.aws/nwm-archive/.

National Oceanic and Atmospheric Administration, 2022b, Monthly Precipitation ClimGrid Data, National Centers for Environmental Information, accessed on December 1, 2022, at https://www.ncei.noaa.gov/data/nclimgrid-monthly/access/nclimgrid_prcp.nc.

Peter, D., and Harrington, C., 2010, Reconstructed old-growth forest stand structure and composition of two stands on the Olympic Peninsula, Washington State: USDA Forest Service research paper PNW-RP, 22 p., accessed February, 2022, at https://www.govinfo.gov/content/pkg/GOVPUB-A13-PURL-LPS122305/pdf/GOVPUB-A13-PURL-LPS122305.pdf.

Posch, T., Köster, O., Salcher, M.M., and Pernthaler, J., 2012, Harmful filamentous cyanobacteria favoured by reduced water turnover with lake warming: Nature Climate Change, v. 2, no. 11, p. 809–813, accessed May, 2022, at https://doi.org/10.1038/nclimate1581.

Preston, S.D., Alexander, R.B., Woodside, M.D., and Hamilton, P.A., 2009, SPARROW modeling—Enhancing understanding of the Nation's water quality: U.S. Geological Survey Fact Sheet 2009–3019, 6 p. [Also available at https://pubs.usgs.gov/fs/2009/3019/.]

Robertson, D.M., and Saad, D.A., 2019, Spatially referenced models of streamflow and nitrogen, phosphorus, and suspended-sediment transport in streams of the midwestern United States: U.S. Geological Survey Scientific Investigations Report 2019–5114, 74 p., accessed November, 2021, at https://doi.org/10.3133/sir20195114.

Rohde, M.M., Albano, C.M., Huggins, X., Klausmeyer, K.R., Morton, C., Sharman, A., Zaveri, E., Saito, L., Freed, Z., Howard, J.K., Job, N., Richter, H., Toderich, K., Rodella, A.-S., Gleeson, T., Huntington, J., Chandanpurkar, H.A., Purdy, A.J., Famiglietti, J.S., Singer, M.B., Roberts, D.A., Caylor, K., and Stella, J.C., 2024, Groundwater-dependent ecosystem map exposes global dryland protection needs: Nature, v. 632, no. 8023, p. 101–107, accessed August, 2024, at https://doi.org/10.1038/s41586-024-07702-8.

Schmadel, N.M., Figueroa-Kaminsky, C., Wise, D.R., Wasielewski, J.K., Gala, J., and Johnson, Z.C., 2025, Model application and calibration load data for seasonally dynamic total nitrogen and total phosphorus SPARROW models developed for watersheds draining to Washington waters of the Salish Sea, 2005 through 2020: U.S Geological Survey data release, https://doi.org/10.5066/P9LY1PQF.

Schmadel, N.M., Harvey, J.W., Alexander, R.B., Boyer, E., Schwarz, G., Gomez-Velez, J., Scott, D., and Konrad, C., 2020, Low threshold for nitrogen concentration saturation in headwaters increases regional and coastal delivery: Environmental Research Letters, v. 15, no. 4, p. 044018, accessed June, 2022, at https://doi.org/10.1088/1748-9326/ab751b.

Schmadel, N.M., Harvey, J.W., and Schwarz, G.E., 2021, Seasonally dynamic nutrient modeling quantifies storage lags and time-varying reactivity across large river basins: Environmental Research Letters, v. 16, no. 9, p. 095004, accessed January, 2022, at https://iopscience.iop.org/article/10.1088/1748-9326/ac1af4. [Also available at https://doi.org/10.1088/1748-9326/ac1af4.]

Schmadel, N.M., Miller, O.M., Ator, S.W., Miller, M.P., Schwarz, G.E., Robertson, D.M., Sekellick, A.J., Skinner, K.D., and Saad, D.A., 2024, Seasonally varying contributions of contemporaneous and lagged sources of instream total nitrogen and phosphorus load across the Illinois River Basin: Science of the Total Environment, v. 955, p. 176816, accessed September, 2024, at https://doi.org/10.1016/j.scitotenv.2024.176816.

Schmadel, N.M., and Peterman-Phipps, C.L., 2023, Monthly inorganic nitrogen atmospheric wet deposition estimates for the conterminous United States, 1999 through 2020: U.S. Geological Survey data release, accessed August, 2023, at https://doi.org/10.5066/P9ZLKCD2.

Schwarz, G.E., 2019, E2NHDPlusV2_us—Database of ancillary hydrologic attributes and modified routing for NHDPlus version 2.1 flowlines: U.S. Geological Survey data release, accessed February, 2022, at https://doi.org/10.5066/P986KZEM.

Schwarz, G.E., Hoos, A.B., Alexander, R.B., and Smith, R.A., 2006, The SPARROW surface water-quality model—Theory, applications and user documentation: U.S. Geological Survey Techniques and Methods, book 6, chap. B3, 248 p., accessed January, 2022, at https://doi.org/10.3133/tm6B3 [Also available on CD-ROM and at https://pubs.usgs.gov/tm/2006/tm6b3/.]

Sheibley, R.W., Konrad, C.P., and Black, R.W., 2015, Nutrient attenuation in rivers and streams, Puget Sound Basin, Washington (ver. 1.1, February 2016): U.S. Geological Survey Scientific Investigations Report 2015–5074, 67 p., accessed March, 2022, at https://doi.org/10.3133/sir20155074.

Stanley, S., Grigsby, S., Booth, D., Hartley, D., Horner, R., Hruby, T., Thomas, J., Bissonnette, P., Fuerstenberg, R., Lee, J., Olson, P., and Wilhere, G., 2019, Puget Sound characterization volume 1—The water resources assessments (water flow and water quality): Washington Department of Ecology publication 11-06-016, 75 p., accessed January, 2022, at https://apps.ecology.wa.gov/publications/SummaryPages/1106016.html.

U.S. Department of Agriculture, 2024, NorWEST Stream Temp: U.S. Department of Agriculture webpage, accessed December 1, 2023, at https://www.fs.usda.gov/rm/boise/AWAE/projects/NorWeST.html.

U.S. Environmental Protection Agency, 2019, NHDPlus national data: U.S. Environmental Protection Agency webpage, accessed December 1, 2023, at https://www.epa.gov/waterdata/nhdplus-national-data.

U.S. Geological Survey, 2025, SPARROW Puget Sound Seasonal Comparison Application: U.S. Geological Survey web page, accessed March 20, 2025, at https://apps.usgs.gov/sparrow/sparrow-puget-sound/.

U.S. Geological Survey, 2022, USGS water data for the Nation: U.S. Geological Survey National Water Information System database, accessed December 1, 2023, at https://doi.org/10.5066/F7P55KJN.

Valayamkunnath, P., Barlage, M., Chen, F., Gochis, D., and Franz, K., 2020, Mapping of 30-meter resolution tile-drained croplands using a geospatial modeling approach: Scientific Data, v. 7, article 257, accessed August, 10, 2022, at https://doi.org/10.1038/s41597-020-00596-x.

Valett, H.M., Peipoch, M., and Poole, G.C., 2022, Nutrient processing domains—Spatial and temporal patterns of material retention in running waters: Freshwater Science, v. 41, no. 2, p. 195–214, accessed May, 2023, at https://doi.org/10.1086/719991.

Washington State Department of Ecology, 2019a, River and Stream Water Quality Monitoring. Environmental Assessment Program: Washington State Department of Ecology river and stream monitoring web page, accessed December, 21, 2023, at https://ecology.wa.gov/Research-Data/Monitoring-assessment/River-stream-monitoring.

Washington State Department of Ecology, 2019b, EIM — Environmental monitoring data: Washington State Department of Ecology Environmental Information Management System (EIM) database web page, accessed June, 28, 2022, at https://ecology.wa.gov/Research-Data/Data-resources/Environmental-Information-Management-database.

Wasielewski, J.K., Wise, D.R., Ahmed, A., and Zulmuthi, H., 2024, Monthly point-source nutrient loads within the watersheds draining to Puget Sound and the Strait of Juan de Fuca, Washington, 2005 – 2020: U.S. Geological Survey data release, accessed August, 2024, at https://doi.org/10.5066/P9U49AWR.

Water Quality Portal, 2022, Download Water Quality Data: National Water Quality Monitoring Council, accessed June 28, 2022, at https://www.waterqualitydata.us/.

Wieczorek, M.E., Jackson, S.E., and Schwarz, G.E., 2018, Select attributes for NHDPlus version 2.1 reach catchments and modified network routed upstream watersheds for the conterminous United States (ver. 4.0, August 2023): U.S. Geological Survey data release, accessed September, 2023, at https://doi.org/10.5066/F7765D7V.

Wieczorek, M.E., Jackson, S.E., and Schwarz, G.E., 2023, Attributes for NHDPlus version 2.1 catchments and modified routing of upstream watersheds for the conterminous United States—National Land Cover Database 2019 versions for the years 2001, 2004, 2006, 2008, 2011, 2013, 2016, and 2019: U.S. Geological Survey data release, accessed September, 2023, at https://doi.org/10.5066/F7765D7V.

Wieczorek, M.E., Signell, R.P., McCabe, G.J., and Wolock, D.M., 2022, USGS monthly water balance model inputs and outputs for the conterminous United States, 1895-2020, based on ClimGrid data: U.S. Geological Survey data release, accessed September, 2023, at https://doi.org/10.5066/P9JTV1T6.

Wise, D.R., 2019, Spatially referenced models of streamflow and nitrogen, phosphorus, and suspended-sediment loads in streams of the Pacific region of the United States: U.S. Geological Survey Scientific Investigations Report 2019–5112, 64 p., accessed April, 2022, at https://doi.org/10.3133/sir20195112.

Wise, D.R., 2020, SPARROW model inputs and simulated streamflow, nutrient and suspended-sediment loads in streams of the Pacific Region of the United States, 2012 base year (ver 1.1, June 2020): U.S. Geological Survey data release, accessed May, 2022, at https://doi.org/10.5066/P9AXLOSM.

Wise, D.R., and Johnson, H.M., 2013, Application of the SPARROW model to assess surface-water nutrient conditions and sources in the United States Pacific Northwest: U.S. Geological Survey Scientific Investigations Report 2013–5103, 32 p., accessed March, 2022, at https://pubs.usgs.gov/sir/2013/5103/. [Also available at https://doi.org/10.3133/sir20135103.]

Wise, D.R., Johnson, H.M., and Stonewall, A.J., 2021, Surface-water transfers and removals in the Pacific drainages of the United States: U.S. Geological Survey data release, accessed September, 2023, at https://doi.org/10.5066/P94XV0J3.

Wise, D.R., Schmadel, N.M., and Wasielewski, J.K., 2025, Watershed landscape data used in the dynamic total nitrogen and total phosphorus SPARROW models developed for watersheds draining to Puget Sound and the Strait of Juan de Fuca, Washington, 2005 – 2020: U.S. Geological Survey data release, https://doi.org/10.5066/P9MTK0OB.

Wolock, D.M., and McCabe, G.J., 2018, Water balance model inputs and outputs for the conterminous United States, 1900-2015: U.S. Geological Survey data release, accessed July, 2022, at https://doi.org/10.5066/F71V5CWN.

Yearsley, J., 2009, A semi-Lagrangian water temperature model for advection-dominated river systems: Water Resources Research, v. 45, no. 12, 19 p., accessed July, 2022, at http://dx.doi.org/doi:10.1029/2008WR007629.

Appendix 1. Additional Model Inputs

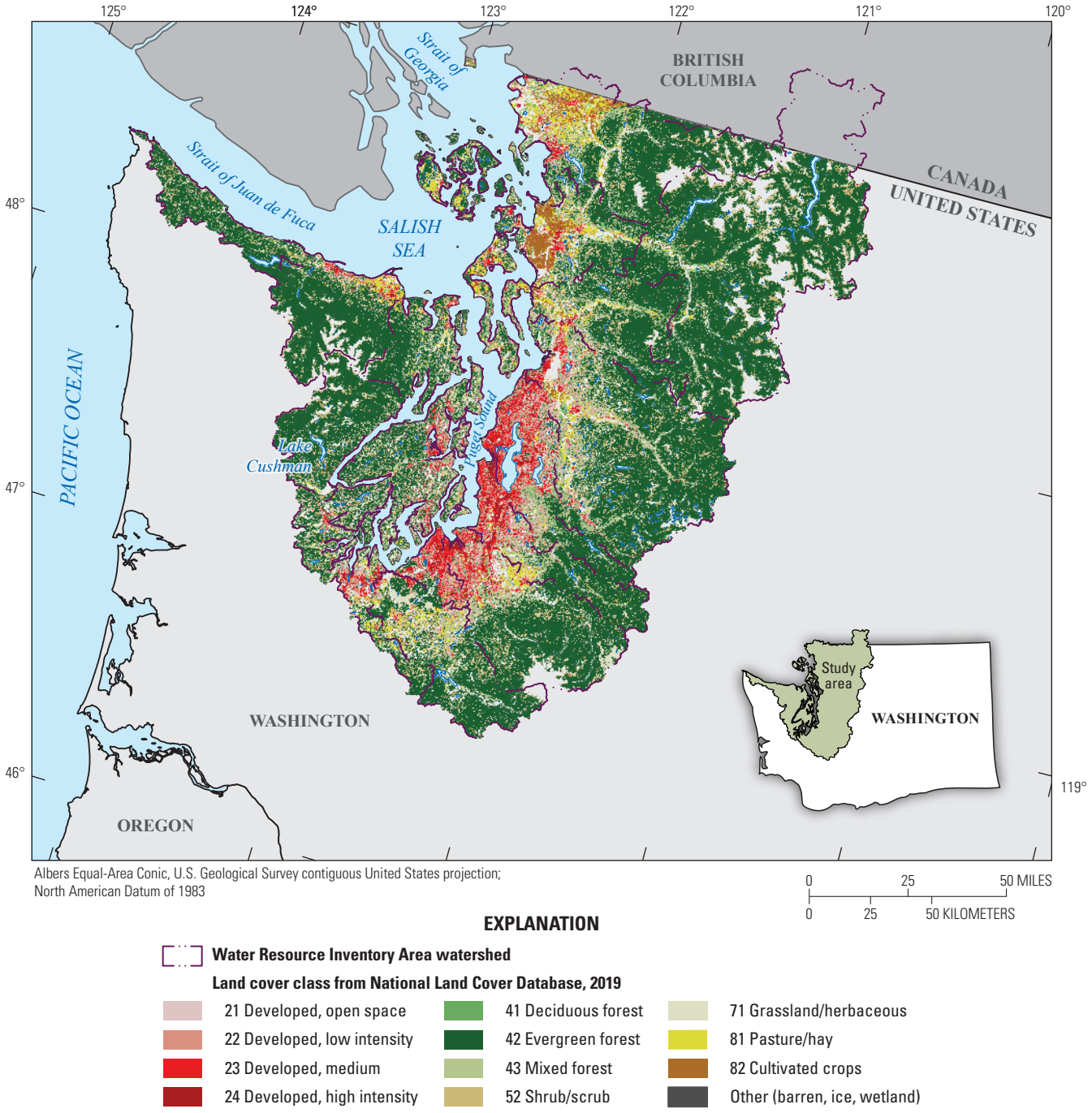

Figure 1.1. National Land Cover Database 2019 land cover in Puget Sound region watersheds (Dewitz and U.S. Geological Survey, 2021).

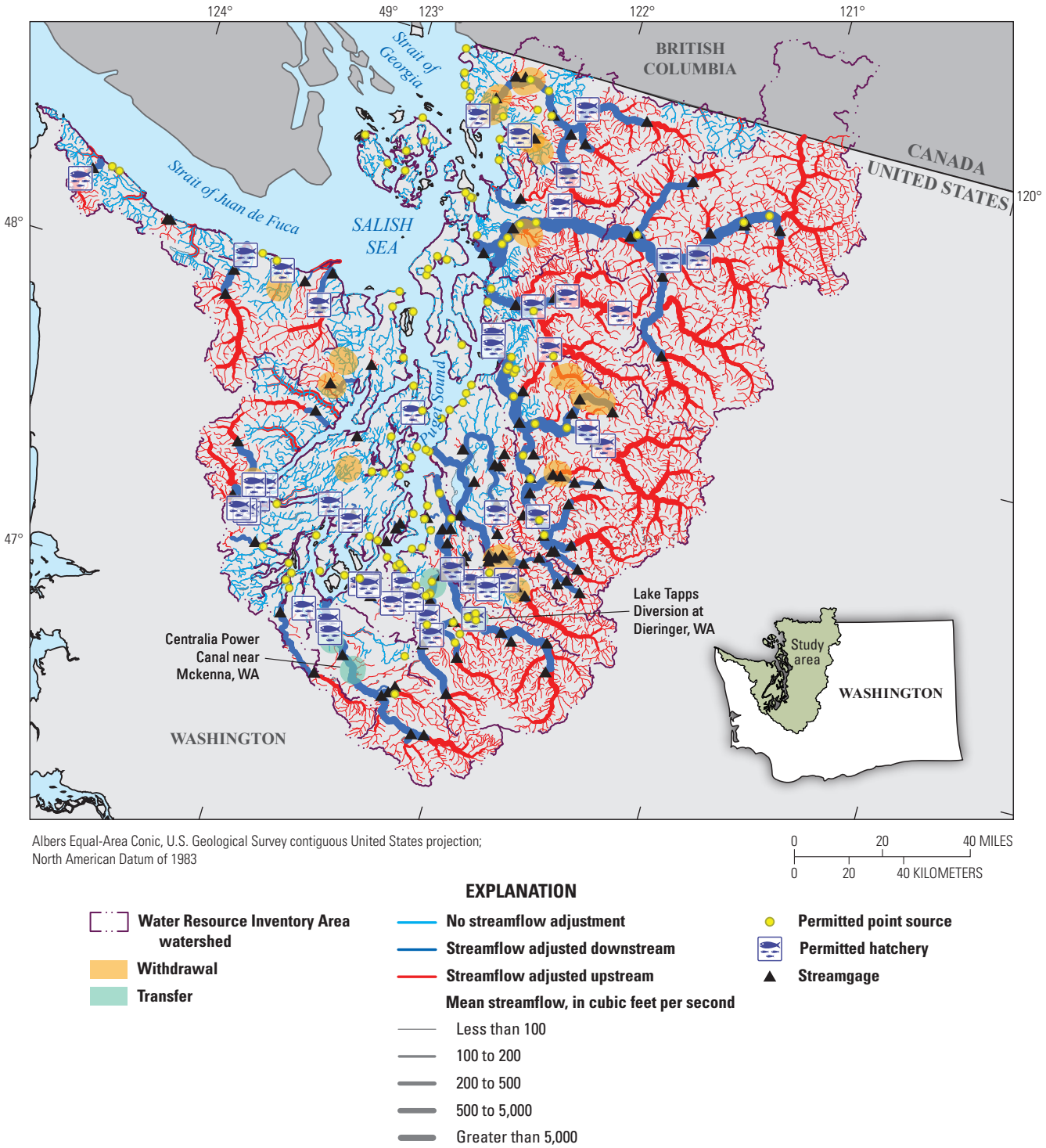

Figure 1.2. Locations of streamflow gaging stations, withdrawals for irrigation and municipal water uses, and water transfers throughout the Puget Sound region. The stream network is colored according to whether the streamflow was adjusted downstream, upstream, or not adjusted.

Table 1.1. Model statistics for the explanatory variables of a simple water balance model used to adjust streamflow downstream and upstream of each gaging station (refer to figure 1.2).

[Abbreviation: VIF, variance inflation factor. Symbols: —, not applicable; <, less than]

Explanatory variable	Variable unit	Coefficient unit	Coefficient mean value	Standard error	*t*-value	*p*-value	VIF
Source							
Inflow from Canada	cubic feet per second	Fraction delivered	1.0	—	—	—	—
Permitted treated wastewater inflow	cubic feet per second	Fraction delivered	1.0	—	—	—	—
Precipitation minus evapotranspiration	cubic feet per second	Fraction delivered	0.460	0.007	66.0	<0.0001	3.0
Storage lag	cubic feet per second	Fraction retained	0.404	0.005	75.1	<0.0001	3.2
Land-to-water delivery							
Previous period ln(aridity[a])	ln(cubic feet per second)	1/ln(cubic feet per second)	−0.082	0.006	−14.3	<0.0001	1.2

[a]Aridity = Potential evapotranspiration minus actual evapotranspiration.

Table 1.2. Summary statistics for the explanatory variables of a simple water balance model used to adjust streamflow downstream and upstream of each gaging station.

[Winter includes January, February, March; spring includes April, May, June; summer includes July, August, September; fall includes October, November, December. Abbreviation: R^2, coefficient of determination]

Parameter	Value
Root mean square error, in natural logarithm space	0.548
Mean square error, in natural logarithm space	0.301
Mean exponentiated weighted error	1.178
Adjusted R^2	0.929
Yield R^2	0.679
Model degrees of freedom	3
Number of observations	6,099
Number of stations	99
Mean square error, winter	0.1432
Mean square error, spring	0.2861
Mean square error, summer	0.5578
Mean square error, fall	0.2157

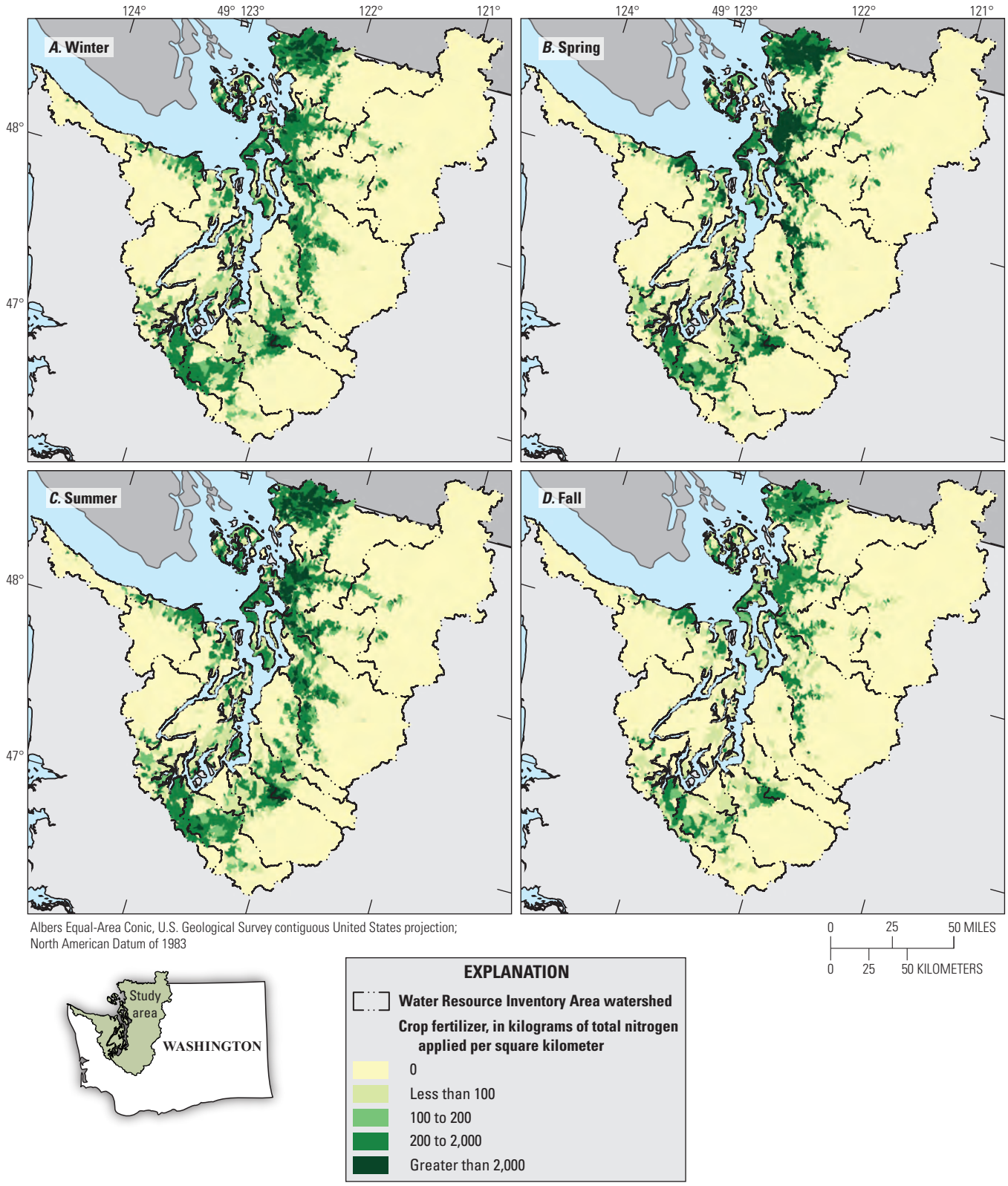

Figure 1.3. Mean seasonal (from 2005 through 2020) estimates of total nitrogen from crop fertilizer applied to NHDPlusV2 catchments throughout the Puget Sound region for (*A*) Winter, January–March; (*B*) Spring, April–June; (*C*) Summer, July–September; and (*D*) Fall, October–December, .

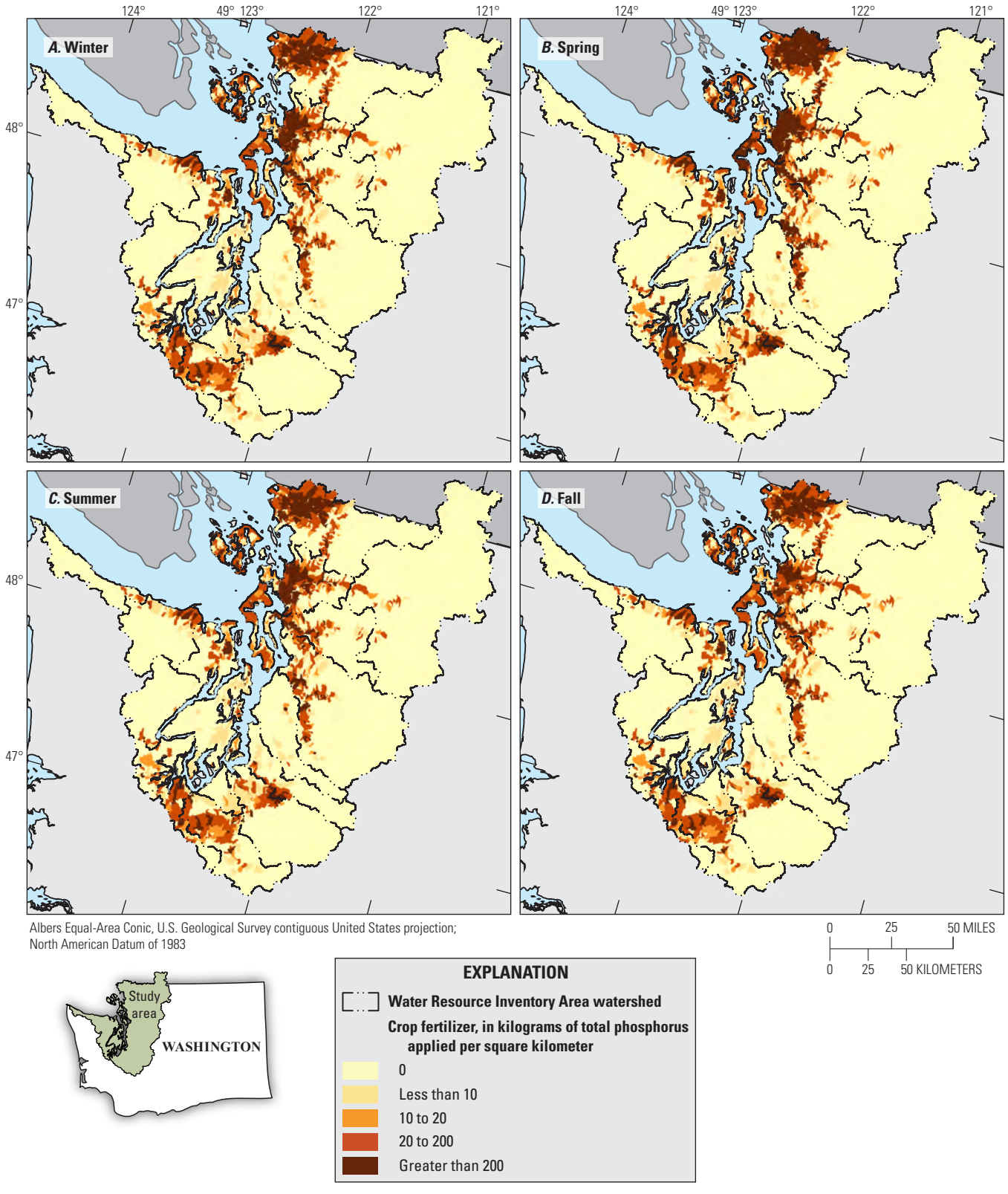

Figure 1.4. Mean seasonal (from 2005 through 2020) estimates of total phosphorus from crop fertilizer applied to NHDPlusV2 catchments throughout the Puget Sound region for (*A*) Winter, January–March; (*B*) Spring, April–June; (*C*) Summer, July–September; and (*D*) Fall, October–December.

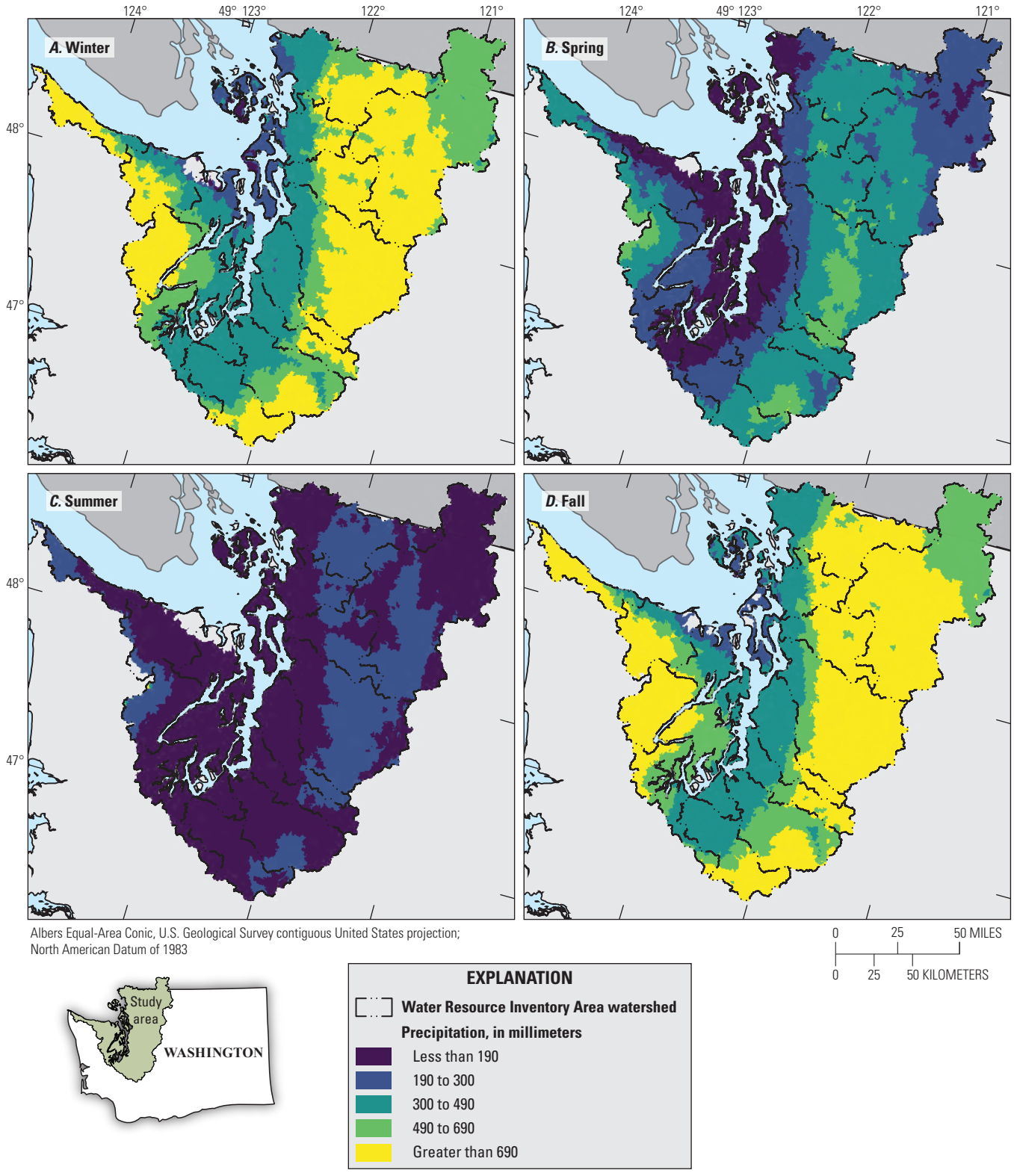

Figure 1.5. Mean seasonal (from 2005 through 2020) precipitation throughout the Puget Sound region for (*A*) Winter, January–March; (*B*) Spring, April–June; (*C*) Summer, July–September; and (*D*) Fall, October–December.

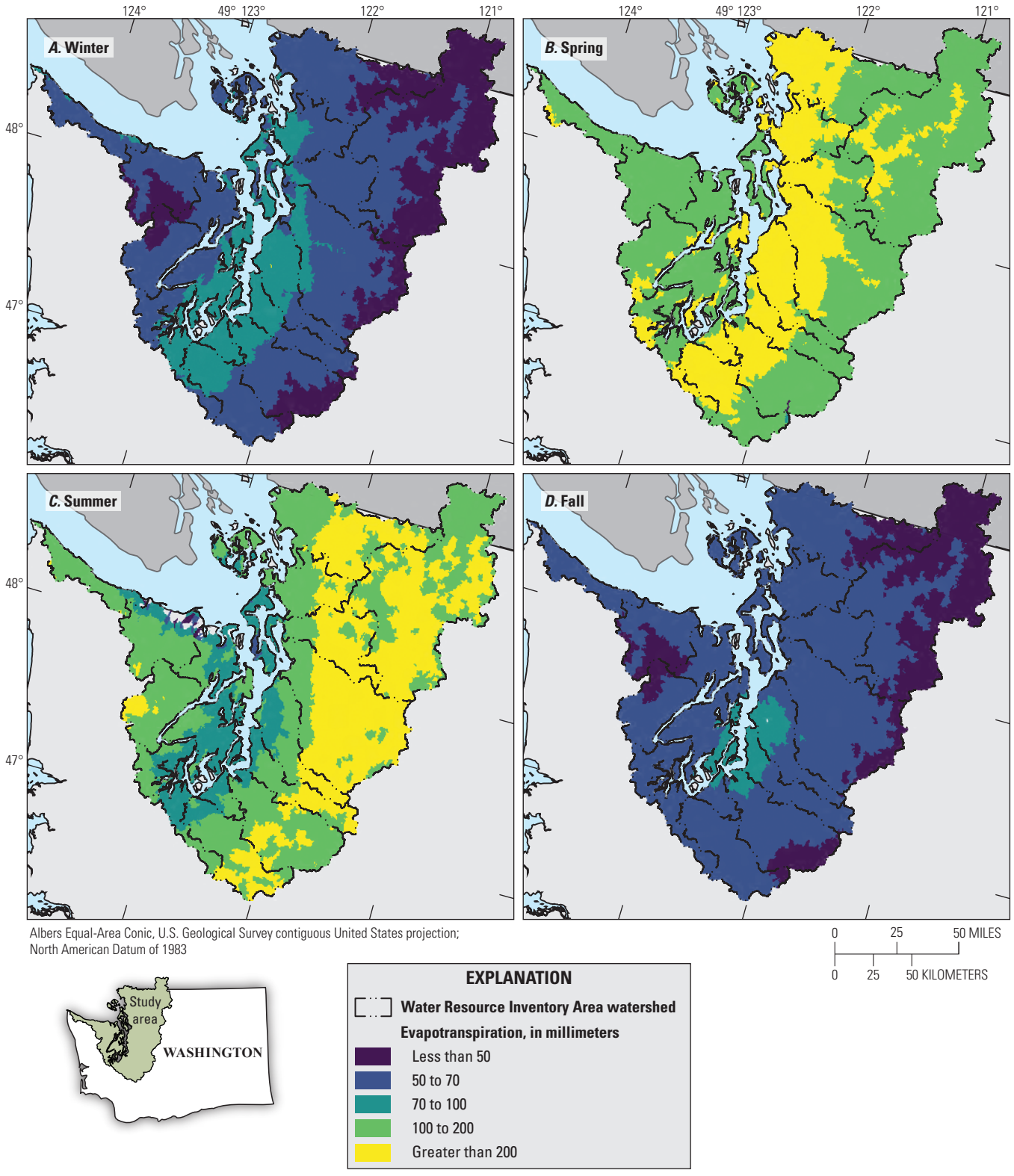

Figure 1.6. Mean seasonal (from 2005 through 2020) evapotranspiration throughout the Puget Sound region for (*A*) Winter, January–March; (*B*) Spring, April–June; (*C*) Summer, July–September; and (*D*) Fall, October–December.

Appendix 2. Results Summary

Table 2.1. Summary of total nitrogen load discharged to marine waters as a summation of incremental loads by Water Resource Inventory Area watershed, estimated with the dynamic Puget Sound Region SPARROW (SPAtially Referenced Regressions On Watershed attributes) total nitrogen model, 2005 through 2020.

[Drainage area is rounded to nearest square kilometer. Winter includes January, February, March; spring includes April, May, June; summer includes July, August, September; fall includes October, November, December. Abbreviations: WRIA: Water Resource Inventory Area; TN, total nitrogen]

WRIA number	WRIA name	Drainage area (square kilometers)	Total TN load discharged from 2005 through 2020 (gigagrams)	Mean annual TN yield discharged (kilograms per square kilometer)	Mean percentage seasonal contributions			
					Winter	Spring	Summer	Fall
1	Nooksack	3,351	81.54	1,520.8	34	22	11	33
2	San Juan	417	0.567	85.15	46	13	6	36
3 and 4	Skagit - Samish	8,861	72.83	513.7	35	21	11	33
5	Stillaguamish	1,819	26.83	922.0	38	19	9	35
6	Island	553	1.90	214.3	47	16	4	33
7	Snohomish	4,836	84.24	1,088.7	33	22	12	33
8	Cedar - Sammamish	1,688	85.84	3,178.6	28	23	19	30
9	Duwamish - Green	1,361	82.80	3,803.5	33	23	17	27
10	Puyallup - White	2,703	39.29	908.4	31	23	15	31
11	Nisqually	1,980	17.54	553.6	38	20	9	34
12	Chambers - Clover	422	24.34	3,607.6	30	24	18	28
13	Deschutes	680	7.61	698.9	41	16	7	35
14	Kennedy - Goldsborough	856	10.21	745.7	43	14	6	38
15	Kitsap	1,690	32.45	1,200.3	40	15	8	37
16	Skokomish - Dosewallips	1,572	11.72	466.3	40	15	7	38
17	Quilcene - Snow	1,020	4.84	296.5	39	17	7	37
18	Elwha - Dungeness	1,824	6.36	217.9	34	19	11	35
19	Lyre - Hoko	999	11.48	718.1	42	14	6	38
All WRIA watersheds		36,630[a]	602.4[a]	1,027.8[a]	34[b]	21[b]	13[b]	32[b]

[a]Summation of WRIAs.

[b]Mean of WRIAs.

Table 2.2. Summary of total phosphorus load discharged to marine waters as a summation of incremental loads by Water Resource Inventory Area watershed, estimated with the dynamic Puget Sound Region SPARROW (SPAtially Referenced Regressions On Watersheds) total phosphorus model, 2005 through 2020.

[Drainage area is rounded to nearest square kilometer. Winter includes January, February, March; spring includes April, May, June; summer includes July, August, September; fall includes October, November, December. Abbreviations: WRIA: Water Resource Inventory Area; TP, total phosphorus]

WRIA number	WRIA name	Drainage area (square kilometers)	Total TP load discharged from 2005 through 2020 (gigagrams)	Mean annual TP yield discharged (kilograms per square kilometer)	Mean percentage seasonal contributions			
					Winter	Spring	Summer	Fall
1	Nooksack	3,351	8.037	149.9	35	20	10	35
2	San Juan	417	0.128	19.23	41	12	4	43
3 and 4	Skagit - Samish	8,861	10.46	73.80	36	19	10	35
5	Stillaguamish	1,819	3.758	129.1	35	20	9	36
6	Island	553	0.393	44.36	40	17	6	37
7	Snohomish	4,836	11.08	143.2	31	22	16	31
8	Cedar - Sammamish	1,688	10.22	378.3	26	23	21	29
9	Duwamish - Green	1,361	9.605	441.2	31	22	19	28
10	Puyallup - White	2,703	6.074	140.4	29	23	17	30
11	Nisqually	1,980	0.792	25.00	37	20	8	34
12	Chambers - Clover	422	1.197	177.4	28	23	25	23
13	Deschutes	680	0.276	25.38	38	17	8	37
14	Kennedy - Goldsborough	856	0.195	14.25	37	14	16	33
15	Kitsap	1,690	1.459	53.96	29	20	19	32
16	Skokomish - Dosewallips	1,572	1.220	48.51	39	15	6	40
17	Quilcene - Snow	1,020	0.729	44.66	30	24	20	27
18	Elwha - Dungeness	1,824	1.384	47.41	33	19	13	35
19	Lyre - Hoko	999	0.468	29.30	40	15	7	39
All WRIA watersheds		36,630[a]	67.47[a]	115.1[a]	32[b]	21[b]	15[b]	32[b]

[a]Summation of WRIAs.

[b]Mean of WRIAs.

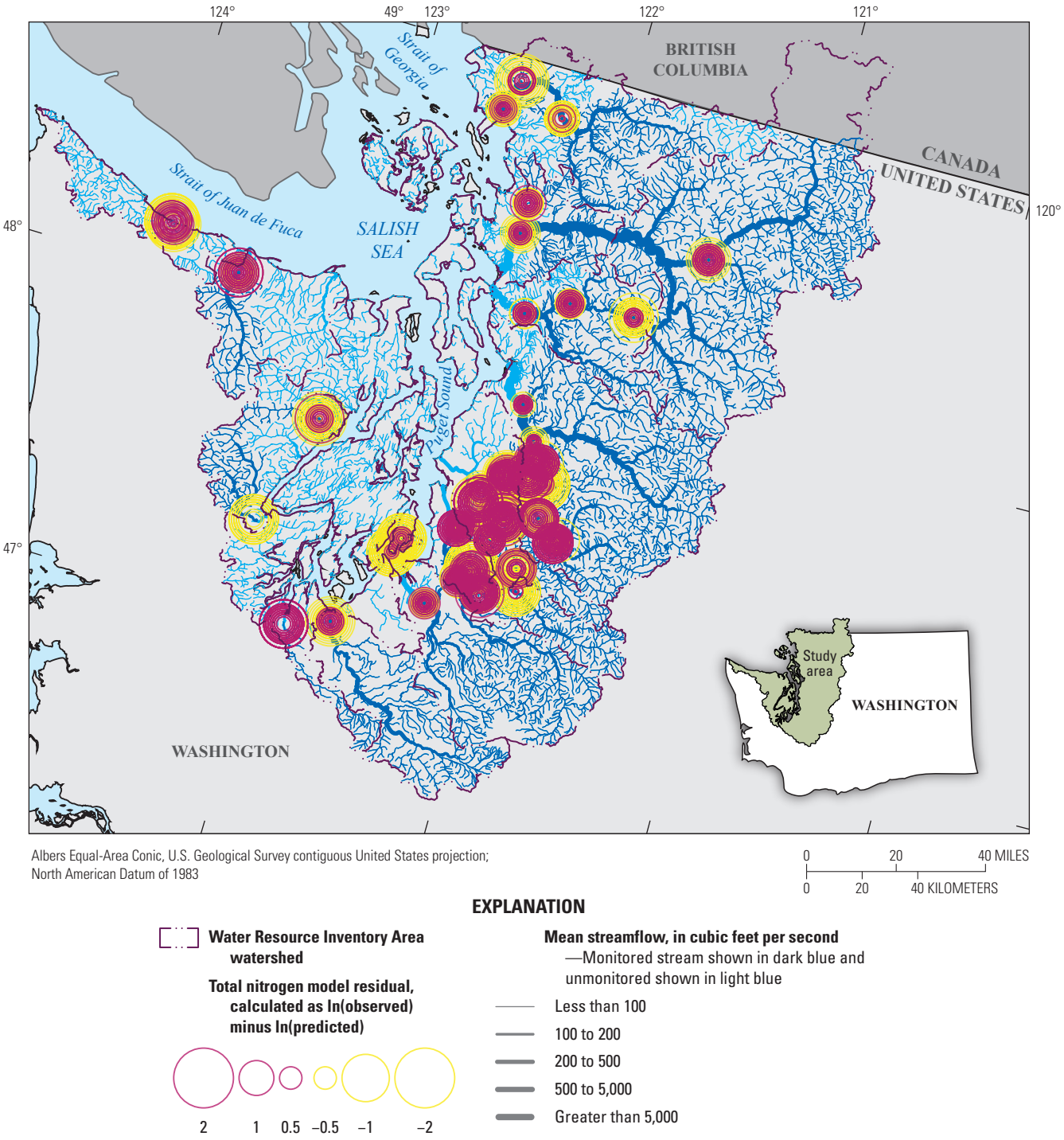

Figure 2.1. Total nitrogen model residuals in natural logarithmic space colored by positive (model underpredicts) and negative (model overpredicts) values, from the dynamic Puget Sound region SPARROW (SPAtially Referenced Regressions On Watersheds) total nitrogen model, 2005 through 2020. Each station has approximately 64 residuals representing the number of simulated seasons.

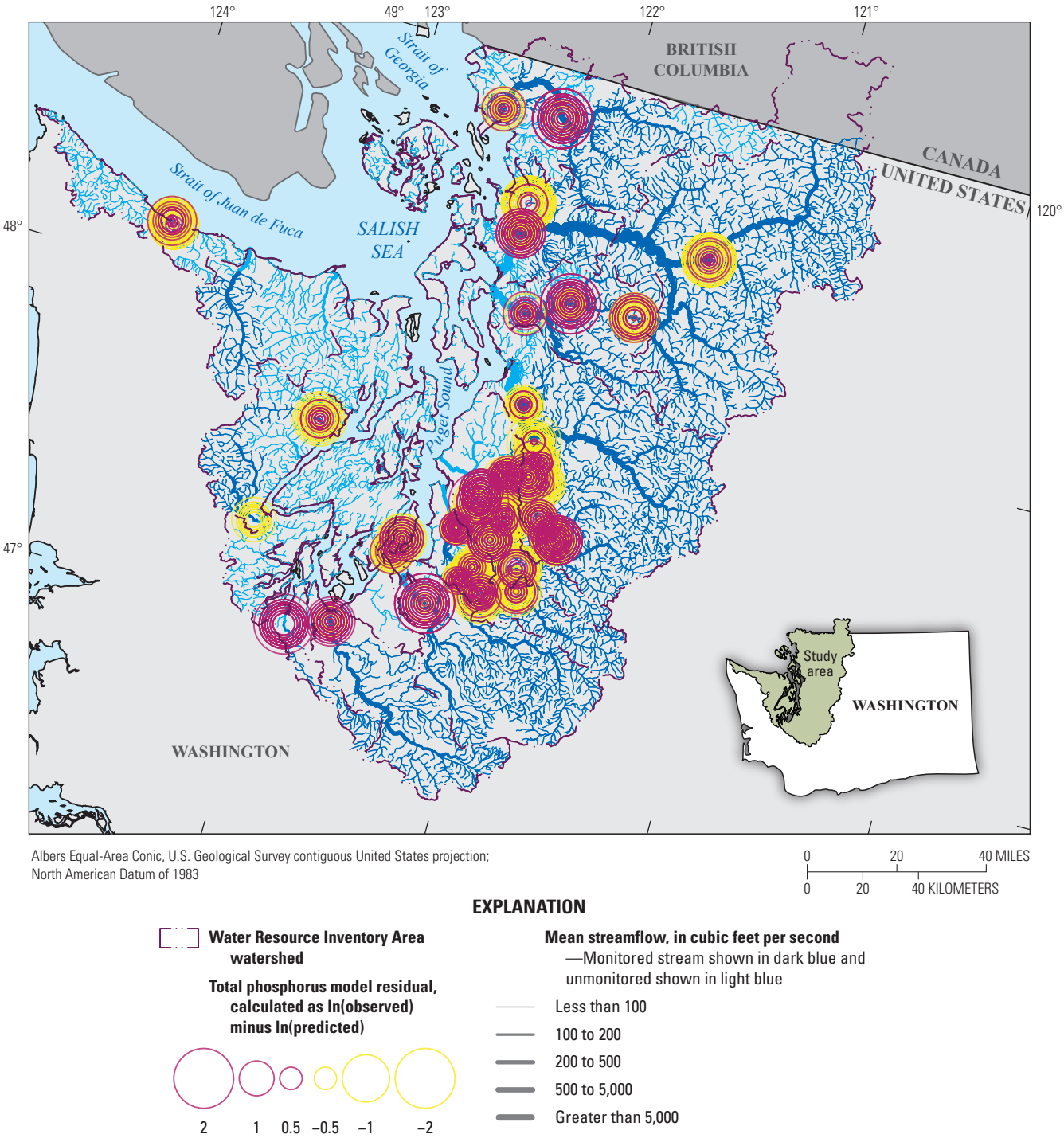

Figure 2.2. Total phosphorus model residuals in natural logarithmic space colored by positive (model underpredicts) and negative (model overpredicts) values, from the dynamic Puget Sound region SPARROW (SPAtially Referenced Regressions On Watersheds) total phosphorus model, 2005 through 2020. Each station has approximately 64 residuals representing the number of simulated seasons.

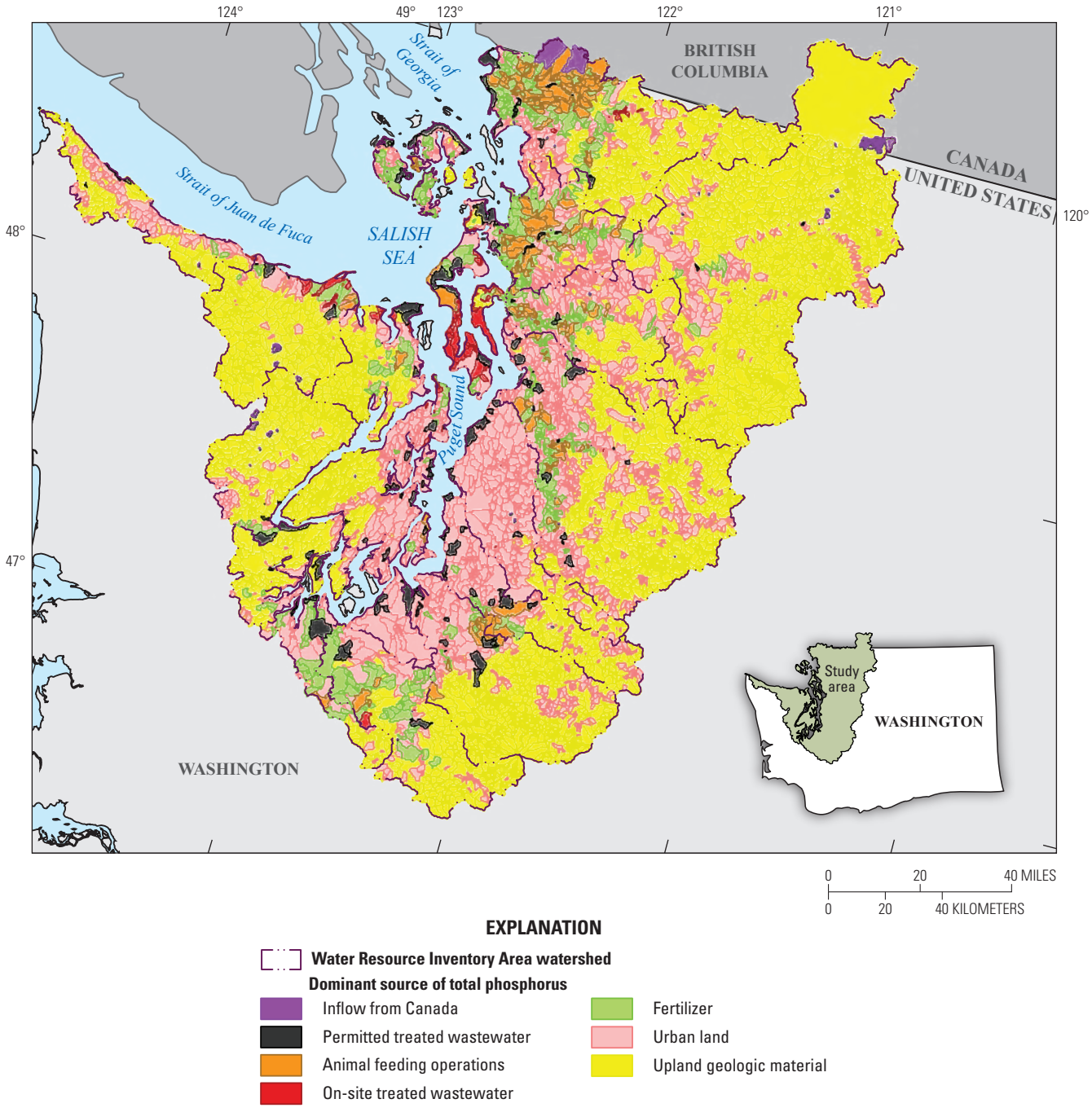

Figure 2.3. The dominant source of total phosphorus, other than storage lag, in NHDPlusV2 catchments throughout the 16-year modeling period of the dynamic Puget Sound region SPARROW (SPAtially Referenced Regressions On Watersheds) total phosphorus model, 2005 through 2020. Refer to figure 15 with storage lag.

For information about the research in this report, contact the
Director, Oregon Water Science Center
U.S. Geological Survey
601 SW 2nd Avenue, Suite 1950
Portland, Oregon 97204

Manuscript approved on March 2, 2026

Publishing support provided by the U.S. Geological Survey
Science Publishing Network, Tacoma Publishing Service Center
Edited by Esther Pischel
Illustration support by Teresa A. Lewis
Layout, cover, and design by Yanis X. Castillo

ISSN 2328-0328 (online)
https://doi.org/10.3133/sir20265001
Supersedes preprint https://doi.org/10.22541/essoar.173878059.92247480/v1